PROCESSING, CHARACTERIZATION AND WEAR RESPONSE OF PARTICULATE FILLED EPOXY BASED HYBRID COMPOSITES

A THESIS SUBMITTED

IN PARTIAL FULFILLMENT OF THE REQUIREMENT FOR THE DEGREE OF

Doctor of Philosophy

in

Mechanical Engineering

By

Sandhyarani Biswas

Department of Mechanical Engineering
National Institute of Technology
Rourkela, India

September, 2010

PROCESSING, CHARACTERIZATION AND WEAR RESPONSE OF PARTICULATE FILLED EPOXY BASED HYBRID COMPOSITES

A THESIS SUBMITTED IN PARTIAL FULFILLMENT OF THE REQUIREMENTS FOR THE DEGREE OF

Doctor of Philosophy

in

Mechanical Engineering

Submitted to

National Institute of Technology, Rourkela

By

Sandhyarani Biswas

(Roll No. 508ME406)

Under the supervision of

Prof. Alok Satapathy

Department of Mechanical Engineering
National Institute of Technology
Rourkela, India

September, 2010

Dedicated to

My Grand Father & Grand Mother

DEPARTMENT OF MECHANICAL ENGINEERING

NATIONAL INSTITUTE OF TECHNOLOGY

ROURKELA 769008

C E RT I F I C A T E

This is to certify that the thesis entitled **Processing, Characterization and Wear Response of Particulate Filled Epoxy Based Hybrid Composites**, submitted by **Sandhyarani Biswas** (Roll No: 508ME406) in partial fulfillment of the requirements for the award of **Doctor of Philosophy** in Mechanical Engineering to the National Institute of Technology, Rourkela is an authentic record of research work carried out by her under my supervision and guidance.

To the best of my knowledge, the work incorporated in this thesis has not been submitted elsewhere for the award of any degree.

Place: Rourkela
Date:

Prof. Alok Satapathy
Associate Professor
Department of Mechanical Engineering
National Institute of Technology, Rourkela
India 769008

ACKNOWLEDGEMENT

It gives me immense pleasure to express my deep sense of gratitude to my supervisor **Prof. Alok Satapathy** for his invaluable guidance, motivation, constant inspiration and above all for his ever co-operating attitude that enabled me in bringing up this thesis in the present form.

I am grateful to **Prof. S. K. Sarangi**, Director, National Institute of Technology, Rourkela who has been a constant source of inspiration for me. I am equally grateful to **Prof. R. K. Sahoo**, Head of the Department of Mechanical Engineering for his help and cooperation. I also appreciate the encouragement from faculty members of the Mechanical Engineering Dept. of N.I.T. Rourkela.

I would like to record my sincere thanks to **Prof. B. C. Ray**, **Prof. M. K. Mishra** and **Prof. R. K. Behera**, learned members of my doctoral scrutiny committee for being helpful and generous during the entire course of this work.

My very special thanks go to all my family members. Their love, affection and patience made this work possible and the blessings and encouragement of my beloved parents greatly helped me in carrying out this research work. I am also extremely thankful to my friends and relatives for their kind support.

Finally, but most importantly, I thank Almighty God, my Lord for giving me the will power and strength to make it this far when I didn't see a light.

Place: Rourkela
Date:

Sandhyarani Biswas
Department of Mechanical Engineering
National Institute of Technology, Rourkela
India 769008

LIST OF FIGURES

*****

LIST OF TABLES

*****

ABSTRACT

Solid particle erosion of polymer composites is a complex surface damage process, strongly affected by material properties and operational conditions. The present research work is undertaken to study the development, characterization and erosion wear performance of bamboo fiber reinforced epoxy composites with and without particulate fillers. Attempts have been made to explore the possible use of some industrial wastes such as copper slag and red mud as filler materials in these composites. To make an assessment of their reinforcing potential in terms of wear performance and mechanical properties, two other conventional ceramic fillers such as alumina (Al_2O_3) and silicon carbide (SiC) are also considered for comparison. The mechanical properties and erosion wear characteristics of bamboo based hybrid composites are compared with those of a similar set of composites reinforced with the most commonly used synthetic fiber (E-glass). A theoretical model has been proposed for estimation of erosion damage caused by solid particle impact on bamboo fiber reinforced epoxy composites. The experimental results are found to be in good agreement with the theoretical values. This study indicates that erosion wear performance of bamboo based composites is better than that of the glass fiber reinforced composites. The morphology of eroded surfaces is examined by using scanning electron microscopy (SEM) and possible erosion mechanisms are discussed.

CONTENTS

Chapter 1

INTRODUCTION

1.1 Background and Motivation

In recent years, the concept of 'eco-materials' has gained key importance due to the need to preserve our environment. The meaning of eco-material includes 'safe' material systems for human and other life forms at all times. Past experiences have shown that it is necessary to characterize materials and determine those which are safe for both short and long-term utilization. Selection of a material system that satisfies not only industrial requirements but also this wider definition of eco-materials, as described above, is an urgent necessity. Here, the most appropriate concept for material selection is composite materials with natural fiber reinforcement. The interest in natural fiber reinforced composites is growing rapidly both in terms of their industrial applications and fundamental research. Their availability, renewability, low density and price as well as satisfactory mechanical properties make them an attractive ecological alternative to glass, carbon and other man-made fibers used for the manufacturing of composites.

Basically, composites are materials consisting of two or more chemically distinct constituents, on a macro-scale, having a distinct interface separating them. One or more discontinuous phases are, therefore, embedded in a continuous phase to form a composite [1]. The discontinuous phase is usually harder and stronger than the continuous phase and is called the *reinforcement*, whereas, the continuous phase is termed as the *matrix*. The matrix material can be metallic, polymeric or can even be ceramic. When the matrix is a polymer, the composite is called polymer matrix composite (PMC).

Over the past few decades, it is found that polymers have replaced many of the conventional metals/materials in various applications. This is possible because of the advantages such as ease of processing, productivity, cost reduction etc.

offered by polymers over conventional materials. In most of these applications, the properties of polymers are modified by using fibers to suit the high strength/high modulus requirements. Fiber reinforced composite materials consist of fibers embedded in or bonded to a matrix with distinct interfaces (boundaries) between them. In this form, both fibers and matrix retain their physical and chemical identities, yet they produce a combination of properties that cannot be achieved with either of the constituents acting alone. In general, fibers are the principal load-carrying members, while the surrounding matrix keeps them in the desired location and orientation. The matrix also acts as a load transfer medium between them and protects the fibers from environmental damages due to elevated temperatures, humidity etc.[1]. Thus, even though the fibers provide reinforcement for the matrix, the latter also serves a number of useful functions in a composite material. Many fiber reinforced polymers (FRPs) offer a combination of strength and modulus that are either comparable to or better than many traditional metallic materials. In addition, fatigue strength as well as fatigue damage tolerance of many composite laminates are excellent. For these reasons, FRPs have emerged as a major class of structural materials and find applications in almost all material domains such as house furnishing, packaging, sports, leisure and in many other weight-critical components in aerospace, automotive and other industries.

All synthetic polymers (thermoplastics, thermosets and elastomers) can be used as matrices in PMCs. As far as the reinforcement is concerned, extensive use has been made of inorganic man-made fibers such as glass and organic fibers such as carbon and aramid. As all these reinforcing fibers are expensive, various fibers like cellulose, wool, silk etc. abundantly available in nature are also used in composites. Cellulosic fibers like henequen, sisal, coconut fiber (coir), jute, palm, bamboo and wood, in their natural conditions and several waste cellulosic products such as shell flour, wood flour and pulp have also been used as reinforcing agents of different thermosetting and thermoplastic resins. It is well known that natural fibers impart high specific stiffness, strength and

biodegradability to polymer matrix composites. Also, cellulosic fibers are readily available from natural sources and most importantly, they have low cost per unit volume.

Historically, the origin of the concept of composite material is based on natural resources such as bamboo and wood. These are good examples of natural composites where cellulosic fibers are in close association with hemi-celluloses to reinforce the lignin matrix. Our ancestors have also used this concept in building houses that consisted of bamboo, straw and clay in building walls. Being a conventional construction material since ancient times, bamboo fiber is a good candidate for use as natural fibers in composite materials. As the development of modern material science progresses, a large amount of masonry, concrete and steel are used in the building structure, but bamboo and some other non-conventional natural materials still exist and are being used due to their natural characteristics and good mechanical properties. Bamboo is available everywhere around the world and is an abundant natural resource. It is a giant grass-like plant and not a tree as commonly believed, belonging to the family of the *Bambusoideae*. Besides, bamboo is one of the fastest renewable plants with a maturity cycle of 3 to 4 years. It has excellent mechanical properties in comparison with its weight due to its longitudinally aligned fibers. Although the utilization potential of this material for a number of applications has been explored, such superior mechanical properties have not been adequately well drawn for polymer-based composites. The use of bamboo fiber can also help to reduce the demand for wood fibers and environmental impacts associated with wood fiber harvesting [2]. In view of this, the present research work is undertaken to study the reinforcement potential of bamboo fibers in polymer composites.

Major constituents in a natural fiber reinforced composite are the reinforcing fibers and a matrix, which acts as a binder for the fibers. In addition, particulate fillers can also be used with some polymeric matrices primarily to reduce cost

and improve their dimensional stability. So, although a judicious selection of matrix and the reinforcing phase can lead to a composite with a combination of strength and modulus comparable to or even better than those of conventional metallic materials [3], the physical and mechanical characteristics can further be modified by adding a solid filler phase to the matrix body during the composite preparation. The fillers play a major role in determining the properties and behaviour of particulate reinforced composites. The term 'filler' is very broad and encompasses a very wide range of materials. It is arbitrarily defined as a variety of natural or synthetic solid particulates (inorganic, organic) that may be irregular, acicular, fibrous or flakey. The improved performance of polymers and their composites in industrial and structural applications by the addition of particulate fillers has shown a great promise and so has lately been a subject of considerable interest.

Hard particulate fillers consisting of ceramic or metal particles and fiber-fillers made of glass are being used these days to dramatically improve the mechanical and wear properties of many composites. But in this context, the potential of ceramic-rich industrial wastes for such use in polymeric matrices has rarely been explored. Rapid industrial development over the last decades has led to the generation of large amounts of solid wastes in the form of ash, mud or slag, which has now come to a stage of environmental threat and needs disposal and/or utilization. Most of these wastes are buried in landfills, which is costly and environmentally unsatisfactory. Therefore, it is essential to seek new options to recycle or reuse these inorganic residues. It is evident from the characteristics of some of these wastes, generated from different processes, that they have good potential for recycling and for utilization in developing various value-added products. To this end, an attempt has been made in this research work to effectively utilize a couple of industrial wastes as particulate fillers for making composites.

Another possibility that the incorporation of both particulates and fibers in polymer could provide a synergism in terms of improved properties and wear performance has not been adequately explored so far. However, some recent reports suggest that by incorporating filler particles into the matrix of fibre reinforced composites, synergistic effects may be achieved in the form of higher modulus and reduced material cost, yet accompanied with decreased strength and impact toughness [4, 5]. Such multi-component composites consisting of a matrix phase reinforced with a fiber and filled with particulates are termed as *hybrid* composites.

Polymer composites are often used as engineering as well as structural components functioning in hostile workplaces where they are subjected to different wear situations. *Wear* is defined as the damage to a solid surface usually involving progressive loss of materials, owing to relative motion between the surface and a contacting substance or substances [6]. It is a material response to the external stimulus and can be mechanical or chemical in nature. The effect of wear on the reliability of industrial components is recognised widely and the cost of wear has also been recognised to be very high. Systematic efforts in wear research were started in 1960s in industrialized countries. The direct costs of wear failures (i.e. wear part replacements), increased work and time, loss of productivity as well as indirect losses of energy and the increased environmental burden are real problems in everyday work and business. In catastrophic failures, there is also the possibility of human losses. Although wear has been extensively studied scientifically, still wear problems persist in industrial applications. This actually reveals the complexity of the wear phenomenon [7].

There are quite a few terms to describe various wear modes which can be clubbed into four principal categories viz. abrasion, adhesion, erosion and surface fatigue [8]. Generally, abrasive wear occurs when two surfaces in contact move against each other and the harder particle in one cut through the

other. This form of wear comes into play when a tangential motion causes the material removal by the simultaneous micro-ploughing and micro-cutting [6]. However, wear due to localised bonding between contacting solid surfaces leading to material transfer between the two surfaces or the loss from either surface is termed as adhesive wear. Similarly, surface fatigue is another wear process that takes place when tiny wear particles are dislodged from a surface by fracture on repeated rolling or sliding on the surface. Owing to a repeated loading action subsurface cracks grow from pre-existing defects, join hands with other vicinal cracks and finally come to the surface removing a small chunk of material [8]. Finally in the erosion wear mode, a progressive loss of material occurs from a solid surface due to mechanical interaction between that surface and a fluid, a multi-component fluid, or impinging liquid or solid particles [9].

Solid particle erosion (SPE), a typical erosion wear mode, is the loss of material that results from repeated impact of small, solid particles. In some cases SPE is a useful phenomenon, as in sandblasting and high-speed abrasive water jet cutting but it is a serious problem in many engineering systems including steam and jet turbines, pipelines and valves carrying particulate matter and fluidized bed combustion systems. Solid particle erosion is to be expected whenever hard particles are entrained in a gas or liquid medium impinging on a solid at any significant velocity. In both cases, particles can be accelerated or decelerated and their directions of motion can be changed by the fluid.

Polymers and their composites form a very important class of tribo-engineering materials and are invariably used in mechanical components, where wear performance in non-lubricated condition is a key parameter for the material selection. Nowadays much attention is devoted towards the study of solid particle erosion behaviour of polymer composites due to the high potential use of these materials in many mechanical and structural applications. Hence, erosion resistance of polymer composites has become an important material property, particularly in selection of alternative materials and therefore the study of solid

particle erosion characteristics of the polymeric composites has become highly relevant. Differences in the erosion behaviour of various types of composite materials are caused by the amount, type, orientation and properties of the reinforcement on one hand and by the type and properties of the matrix and its adhesion to the fibers/fillers on the other hand. A full understanding of the effects of all system variables on the wear rate is necessary in order to undertake appropriate steps in the design of machine or structural component and in the choice of materials to reduce/control wear [10].

Statistical methods have commonly been used for analysis, prediction and/or optimization of a number of engineering processes. Such methods enable the user to define and study the effect of every single condition possible in an experiment where numerous factors are involved. Solid particle erosion is a complex wear phenomenon in which a number of control factors collectively determine the performance output (i.e. the erosion rate) and there is enormous scope in it for implementation of appropriate statistical techniques for process optimization. But unfortunately, such studies have not been adequately reported so far. The present research work addresses to this aspect by adopting a statistical approach called Taguchi experimental design. This technique provides a simple, systematic and efficient methodology for the analysis of the control factors.

The present research work thus is undertaken to study the processing, characterization and erosion wear performance of bamboo fibre reinforced epoxy composites with and without particulate fillers. Attempts have also been made to explore the possible use of some industrial wastes such as copper slag and red mud as filler materials in these composites. The specific objectives of this work are clearly outlined in the next chapter.

1.2 Thesis Outline

The remainder of this thesis is organized as follows:

Chapter 2: Includes a literature review designed to provide a summary of the base of knowledge already available involving the issues of interest. It presents the research works on fiber as well as particulate reinforced polymer composites by various investigators.

Chapter 3: Includes a description of the raw materials and the test procedures. It presents the details of fabrication and characterization of the composites under investigation and also an explanation of the Taguchi experimental design.

Chapter 4: Presents the physical and mechanical properties of the composites under study.

Chapter 5: Proposes a theoretical model for estimation of erosion wear rate.

Chapter 6: Includes the erosion characteristics of bamboo/glass-epoxy composites (with and without different particulate fillers). It establishes the validation of the proposed theoretical erosion model through experimentation and studies the effect of the fillers on the erosion behaviour of the composites.

Chapter 7: Provides summary of the findings of this research work, outlines specific conclusions drawn from both the experimental and analytical efforts and suggests ideas and directions for future research.

****

Chapter 2

LITERATURE REVIEW

The purpose of this literature review is to provide background information on the issues to be considered in this thesis and to emphasize the relevance of the present study. This treatise embraces various aspects of polymer composites with a special reference to their erosion wear characteristics. This chapter includes reviews of available research reports:

- On natural fibers and natural fiber reinforced composites
- On mechanical properties of natural fiber composites
- On bamboo and bamboo fiber reinforced composites
- On particulate filled polymer composites
- On utilization of industrial wastes like copper slag and red mud
- On erosion of polymer composites
- On erosion wear modelling

At the end of the chapter a summary of the literature survey and the knowledge gap in the earlier investigations are presented. Subsequently the objectives of the present research work are also outlined.

2.1 On Natural Fibers and Natural Fiber Reinforced Composites

In polymer composites, the reinforcing phase can either be fibrous or non-fibrous (particulates) in nature and if the fibers are derived from natural resources like plants or some other living species, they are called natural-fibers. Natural fibers as reinforcement in composite materials have recently attracted the attention of researchers because of their several advantages. These fibers can be divided into three groups based on their origin, i.e. vegetable/plant fibers (flax, hemp, sisal, etc.), animal/protein fibers (hair, wool, silk, chitin, etc.) and mineral fibres (asbestos, wollastonite etc.). Plant fibers are renewable with good mechanical properties, which justify their use as reinforcement for polymers.

These natural fibers are low-cost fibers with low density and high specific properties which are comparable to those of synthetic fibers used as reinforcements. Unlike other man-made fibers, these are readily available, biodegradable and nonabrasive in nature. It is also known that natural fibers are non-uniform with irregular cross sections, which make their structures quite unique and much different from man-made fibers such as glass fibers, carbon fibers etc. The properties of some of these fibers are presented in Table 2.1 [11].

Table 2.1 Properties of Natural Fibers [11]

Fiber	Tensile strength (MPa)	Young's modulus (GPa)	Elongation at break (%)	Density (g/cm^3)
Abaca	400	12	3-10	1.5
Alfa	350	22	5.8	0.89
Bagasse	290	17	-	1.25
Bamboo	140-230	11-17	-	0.6-1.1
Banana	500	12	5.9	1.35
Coir	175	4-6	30	1.2
Cotton	287-597	5.5-12.6	7-8	1.5-1.6
Curaua	500-1,150	11.8	3.7-4.3	1.4
Date palm	97-196	2.5-5.4	2-4.5	1-1.2
Flax	345-1,035	27.6	2.7-3.2	1.5
Hemp	690	70	1.6	1.48
Henequen	500 ± 70	13.2 ± 3.1	4.8 ± 1.1	1.2
Isora	500-600	-	5-6	1.2-1.3
Jute	393-773	26.5	1.5-1.8	1.3
Kenaf	930	53	1.6	-
Nettle	650	38	1.7	-
Oil palm	248	3.2	25	0.7-1.55
Piassava	134-143	1.07-4.59	21.9-7.8	1.4
Pineapple	400-627	1.44	14.5	0.8-1.6
Ramie	560	24.5	2.5	1.5
Sisal	511-635	9.4-22	2.0-2.5	1.5
E-Glass	3400	72	-	2.5

As can be seen from Table 2.1, the tensile strength of glass fiber is substantially higher than that of natural fibers even though the modulus is of the same order. However, when the specific modulus of natural fibers (modulus/specific gravity) is considered, the natural fibers show values that are comparable to or better than

those of glass fibers. These higher specific properties are the major advantages of using natural fiber composites for applications wherein the desired properties also include weight reduction. Table 2.2 shows the areas where the natural fibers have distinct advantages over the most commonly used synthetic fiber i.e. E-glass fiber [12].

Table 2.2 Comparison between natural and glass fibres [12]

	Natural fibres	Glass fibers
Density	Low	Twice that of natural fibers
Cost	Low	Low, but higher than natural fibers
Renewability	Yes	No
Recyclability	Yes	No
Energy consumption	Low	High
Distribution	Wide	Wide
CO_2 neutral	Yes	No
Abrasion to machines	No	Yes
Health risk when inhaled	No	Yes
Disposal	Biodegradable	Not biodegradable

In recent years, natural fiber reinforced polymer composites have attracted increasing research interests owing to their potential as an alternative for composites reinforced with synthetic fibers like glass or carbon [13-17]. The potential of natural fibres such as jute, sisal, pineapple, abaca and coir as reinforcement and filler in composites has already been studied in the past [18-27]. Saheb and Jog [12] have also presented a very elaborate and extensive review on natural fiber reinforced composites with special reference to the type of fibers, matrix polymers, treatment of fibers and fiber-matrix interface. The most commonly used natural fibers and matrices for composites are shown schematically in Figure 2.1[28].

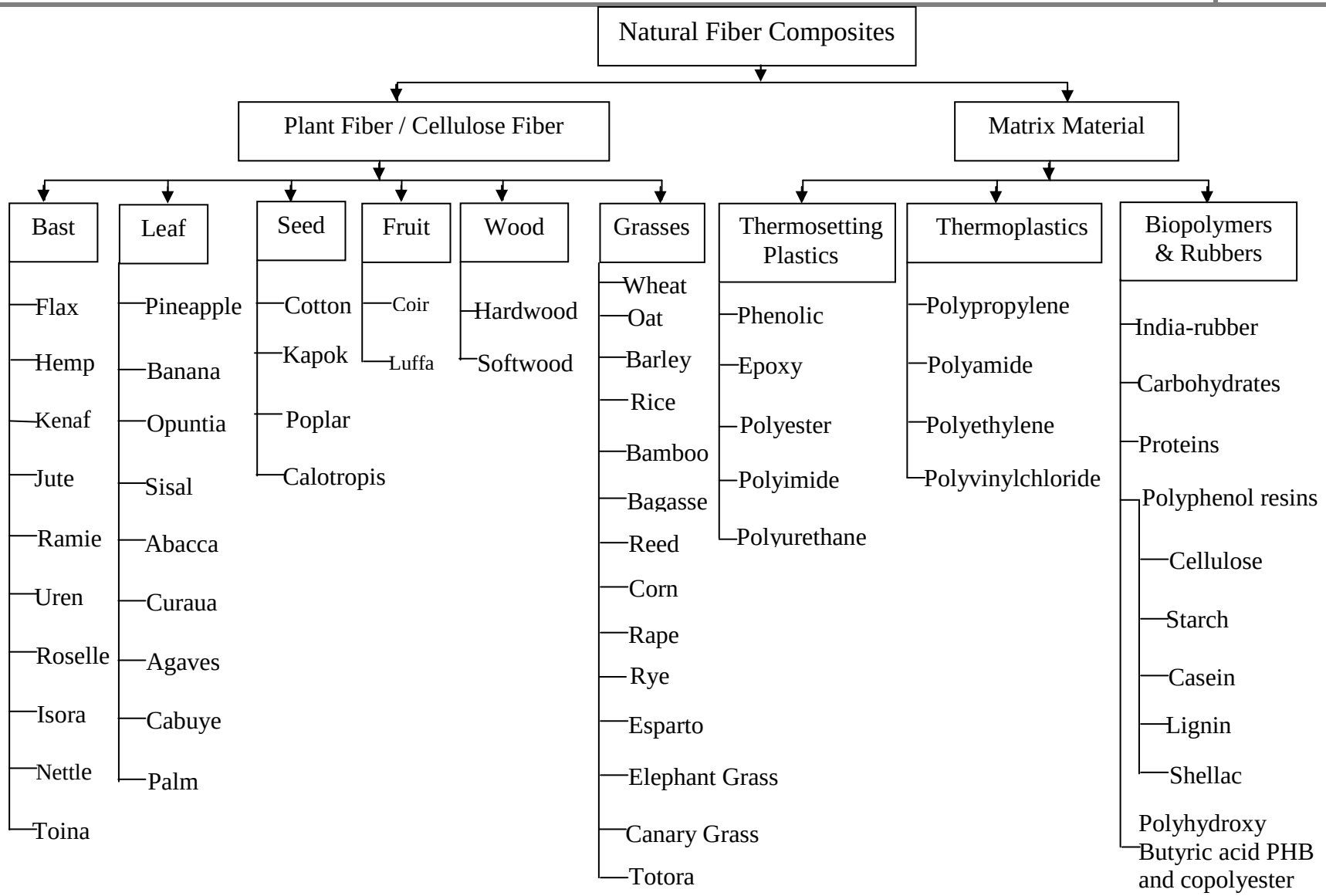

Figure 2.1 Commonly used natural fibers and matrices for polymer composites

2.2 On Mechanical Properties of Natural Fiber Composites

Most of the studies made on natural fiber composites reveal that their mechanical properties are strongly influenced by many factors such as volume fraction of the fibers, fiber aspect ratio, fiber-matrix adhesion, fiber orientation, stress transfer at the interface etc. [29]. A number of investigations have been made on various natural fibers such as kenaf, hemp, flax and jute to study the effect of these fibers on the mechanical properties of composite materials [30-32]. Gowda et al. [32] evaluated the mechanical properties of jute fabric-reinforced polyester composites and found that they have better strengths than those of wood based composites. Similarly, an investigation on pulp fiber reinforced thermoplastic composite exhibited that while the stiffness is increased by a factor of 5.2, the strength of the composite is increased by a factor of 2.3 relative to the virgin polymer [15]. A number of reports are available on investigations carried out on various aspects of polymer composites reinforced with banana fibers [13, 33-35]. Dynamic mechanical analysis of natural fibers like sisal, palf (pineapple leaf fiber), oil palm empty fruit bunch fiber etc. in various matrices has been made by Joseph et al. [36] and George et al. [37]. Amash and Zugenmaier [38] reported on the effectiveness of cellulose fiber in improving the stiffness and reducing the damping in polypropylene-cellulose composites. Luo and Netravali [39] studied the tensile and flexural properties of green composites with different pineapple fiber content and compared them with the virgin resin. Cazaurang et al. [40] carried out a systematic study on the properties of henequen fiber and pointed out that these fibers have mechanical properties suitable for reinforcement in thermoplastic resins. Schneider and Karmaker [41] developed composites using jute and kenaf fiber in polypropylene resin and reported that jute fiber provides better mechanical properties than kenaf fiber. Srivastav et al. [42] have studied the effect of different loading rate on mechanical behaviour of jute/glass reinforced epoxy hybrid composites. Shinichi et al. [43] have investigated the effects of the volume fraction and length of natural fibers like kenaf and bagasse on flexural properties of some biodegradable composites. Sapuan and Leenie [44] carried

out tensile and flexural tests on natural fiber reinforced musaceae/epoxy composites.

Several investigators have also reported on mechanical properties of natural fiber composites prepared by different manufacturing techniques. Chawla and Bastos [45] studied the effect of fiber volume fraction on Young's modulus, maximum tensile strength and impact strength of untreated jute fibers in unsaturated polyester resin, made by a leaky mould technique. Hepworth et al. [46] made unidirectional hemp fiber reinforced epoxy composites, with a fiber volume fraction of 0.2, a tensile strength of 90 MPa and Young's modulus of 8 GPa, by pinning-decortications and hand combing. Harriette et al. [47] studied the mechanical properties of flax/polypropylene compounds, manufactured both with a batch kneading and an extrusion process. The structural characteristics and mechanical properties of coir fiber/polyester composites were evaluated and the effect of the molding pressure on the flexural strength of the composites was studied [48].

A number of studies have also been devoted to the impact behaviour of natural fiber reinforced composites. Santulli [49] studied the post-impact behaviour of plain-woven jute/polyester composites subjected to low velocity impact and found that the impact performance of these composites was poor. Pavithran et al. [50] determined the fracture energies for sisal, pineapple, banana and coconut fiber reinforced polyester composites using Charpy impact tests. They found that, except for the coconut fiber, increasing fiber toughness was accompanied by increasing fracture energy of the composites. Tobias [51] examined the influence of fiber content and fiber length in banana fiber reinforced epoxy composites and noticed that the impact strength increased with higher fiber content and lower fiber length.

2.3 On bamboo and Bamboo Fiber Reinforced Composites

Bamboo is widely recognized as one of the most important non-timber forest resources because of the high socio-economic benefits from bamboo based

products. It is a natural composite, which consists of lignin matrix and cellulose fibers. Cellulose fibers provide high tensile, flexural strengths and rigidity in its longitudinal direction. Because the strength and modulus of bamboo fiber are at least one order of magnitude greater than those of lignin matrix, the bulk mechanical properties of the outer surface region in the reformed bamboo should be much higher than those of the inner surface. Bamboo has many advantages, such as ample availability, fast growth rate, lightweight, low cost and low energy consumption in the processing and biodegradability [52]. It is known to be one of the fastest growing plants in the world. There are about 1250 species of bamboo worldwide [53], covering a total area of about 22 million hectares with an annual yield of 2000 million tons [54]. Most of them grow in Asia, Africa and Latin America. Bamboo based products are widely used in housing, furniture, packing, transport and other fields. With the development of advanced processing technologies, the utilization of bamboo-based construction materials has significantly increased.

Liese [55] studied the anatomic structure along with the chemical, physical as well as the mechanical properties of bamboo and stated that the poly-lamellate wall structure of the bamboo fiber is responsible for its extremely high strength. Godbole and Lakkad [56] determined the effects of water absorption on mechanical properties of bamboo. The tensile strength, compressive strength, tensile modulus and inter-laminar shear strength of bamboo stem were found to be reduced after soaking or boiling in distilled water. However, they suggested that an epoxy coating covering the surface of bamboo can effectively prevent water absorption. Lakkad et al. [2] further compared the mechanical properties of bamboo specimens with those of mild steel and glass reinforced plastics and found that the specific modulus and strength of bamboo are higher than that of those materials. Thus, they have concluded that bamboo has considerable potential as reinforcement for composite materials. The literature available on bamboo fiber reinforced composites is extremely limited, some of which are briefly summarized below.

Shin et al. [57-59] investigated the mechanical properties and fracture mechanisms of bamboo-epoxy composites under different loading conditions. They also compared the mechanical properties of various types of composites of different combination of fibers and resins. In another investigation, Chen [60] studied the structure, morphology and properties of bamboo fiber reinforced polypropylene composites in details.

Research in the development of bamboo fiber reinforced composites has been increasing over the past decade [61-64], but the mechanical properties of bamboo fibers are not fully exploited in polymer composites. Research on the study of bamboo fiber reinforced composites using thermosetting plastics such as epoxy and polyester have been reported by few investigators. Rajulu et al. [65] investigated the effect of fiber length on the tensile properties of short bamboo fiber epoxy composites. Chen et al. [66] tested the mechanical properties of bamboo fiber reinforced polypropylene and compared them with those of commercial wood pulp. Thwe et al. [67] studied the effect of environmental aging on the mechanical properties of bamboo-glass fiber reinforced polymer hybrid composites. In another study, Okubo et al. [68] reported that the tensile strength and modulus of polypropylene based composites using steam-exploded bamboo fibers are higher than the composites using mechanically extracted fibers by about 15% and 30% respectively. The properties such as tensile strength, modulus, tear strength and elongation at the break of bamboo fiber reinforced natural rubber composites, with and without the presence of a bonding agent, were studied extensively by Ismail et al. [69]. They reported that the presence of bonding agent leads to shorter curing time and enhanced mechanical properties. Similar studies on the flexural behavior of bamboo fiber reinforced mortar laminates were also carried out by Yu and Li [70]. The fracture of bamboo/polymer composites is dominated by the cracking behavior of the matrix surrounding the fiber bundle. In order to improve the mechanical properties of bamboo fiber composites, many researchers have

sought to tailor the fiber/matrix interfacial properties [71-83], modify the fiber morphology [84, 85] and develop biodegradable polymer matrix materials [86].

2.4 On Particulate Filled Polymer Composites

Particulate filled composites have been used extensively in various fields due to their low production costs and the ease with which they can be formed into complex shapes. Besides, they behave isotropically and are not as sensitive as long fiber composites to the mismatch of thermal expansion between the matrix and the reinforcement [87, 88]. Generally fillers are used in polymers for a variety of reasons such as cost reduction, improved processing, density control, optical effects, thermal conductivity, control of thermal expansion, electrical properties, magnetic properties, flame retardancy, improved hardness and wear resistance.

Hard particulate fillers consisting of ceramic or metal particles and fiber-fillers made of glass are being used these days to improve the performance of polymer composites to a great extent [89]. Various kinds of polymers and polymer matrix composites reinforced with metal particles have a wide range of industrial applications such as heaters, electrodes [90], composites with thermal durability at high temperature etc. [91]. Similarly, ceramic filled polymer composites have also been the subject of extensive research in last two decades. When silica particles are added into a polymer matrix, they play an important role in improving electrical, mechanical and thermal properties of the composites [92, 93]. The mechanical properties of particulate filled polymer composites depend strongly on the particle size, particle-matrix interface adhesion and particle loading. Sumita et al. [94] underlined the interest of replacing micro-scale silica by its nano-scale counterpart, since nano-scale silica particles possess superior mechanical properties. Smaller particle size yields higher fracture toughness also for calcium carbonate filled high density polyethylene (HDPE) [95]. Similarly, epoxy filled with smaller alumina trihydrate particles shows higher fracture toughness [96]. Thus, particle size is being reduced rapidly and many recent

studies have focused on how single-particle size affects mechanical properties [97-103]. Yamamoto et al. [104] reported that the structure and shape of silica particle have significant effects on the mechanical properties such as fatigue resistance, tensile and fracture properties. Nakamura et al. [105-107] discussed the effects of size and shape of silica particle on the strength and fracture toughness based on particle-matrix adhesion and also found an increase in the flexural and tensile strength as specific surface area of particles increased. Usually the strength of a composite strongly depends on the stress transfer between the particles and the matrix [108]. For well-bonded particles, the applied stress can be effectively transferred to the particles from the matrix resulting in an improvement in the strength. However, for poorly bonded micro-particles, reduction in strength is found to have occurred. Nicolais and Nicodemo [109] studied the effect of particle shape on tensile properties of glassy thermoplastic composites. While most of these investigations have focused either on the particle shape or on particle size, the study made by Patnaik et al. [110] reported that the mechanical properties of polyester based hybrid composites are highly influenced also by the type and content of the filler materials.

2.5 On Utilization of Industrial Wastes like Copper Slag and Red Mud

Pollution is the major problem associated with rapid industrialization, urbanization and rise in the living standards of people. While industrialization is must for uplifting nation's economy in developing countries, it has also caused the generation of significant quantities of solid wastes that lead to serious problems relating to environmental pollution. Therefore, wastes seem to be a by-product of growth. But a country like India can ill afford to lose them as sheer waste. Moreover, with increasing demand for raw materials for industrial production, the non-renewable resources are dwindling day-by-day. Therefore, efforts are to be made for controlling pollution arising out of these unwanted wastes by their conversion into utilizable materials for various beneficial uses. Limited waste landfill space, increasing cost of waste disposal in combustion

facilities and landfills, depletion of the natural resources and the need for sustainable development have all amplified the need to reuse the materials that were once regarded as wastes. Over recent decades, intensive research works have been carried out to explore all possible reuse methods of a wide range of waste materials. Up to now, construction waste, blast furnace and steel slag, coal fly ash and bottom ash have been accepted in many places as alternative aggregates in embankment, road, pavement, foundation and building construction.

Production of industrial slag dates back to the beginning of extracting of metals from ores through metallurgical processes. Copper slag is such a by-product obtained during the matte smelting and refining of copper [111]. It has been estimated that production of one ton of copper generates approximately 2.2-3 tons of copper slag. In the United States, the amount of copper slag produced is about four million tons and in Japan, it is about two million tons per year [112, 113]. Approximately 360,000, 244,000 and 60,000 tons of copper slag are produced in Iran, Brazil and Oman respectively [114-117]. Current options for management of copper slag include recycling, recovering of metal, production of value added products and disposal in slag dumps or stockpiles. Some research papers have reviewed the use of copper slag in the production of value-added products such as abrasive tools, abrasive materials, cutting tools, tiles, glass and roofing granules [118, 119]. They also reported the potential use of copper slag as a partial substitute of cement and aggregates in concrete and asphalt mixtures. The use of copper slag in cement and concrete provides potential environmental as well as economic benefits for all related industries, particularly in areas where a considerable amount of copper slag is produced. Recently, Shi et al. [120] have reported a detailed review on utilization of copper slag in the manufacturing of cement and concrete.

Similarly, production of alumina from bauxite by the Bayer's process is associated with the generation of red mud as the major waste material in alumina

industries. Till today, almost all over the world, red mud is disposed off the plant site in two main ways depending on the facilities available and the surroundings. In countries such as France, England, Germany or Japan where availability of land for dumping is less and sea is nearby; the practice is to discharge the mud into the sea. Where free land is available nearby, as in India, the mud is pumped into pools and ponds constructed for this purpose. Probably the easiest use for the mud is some sort of useful landfill instead of just dumping. Some attempts in this direction are: filling material for mined or quarrying areas, land fill cover, road bed and levee material, alternative to natural marsh sediment, agricultural land soil neutralization, composting domestic waste, etc.

Attempts have been made over the years to study the usage of red mud as a partial substitute of clay in ceramic products like bricks, tiles etc. [121] and as an additive for mortar and concrete [122]. Use of red mud in agricultural applications such as in acidic soils or as a treatment for iron deficient soils has also been reported [123]. Red mud finds some applications in ceramic industries as well. Yalcin et al. [124] experimented with the red mud from Seydischir Aluminium Plant, Turkey and attempted to use it in the making of ceramic glazes such as porcelain, vitreous (sanitary ware glazes), tile and electro porcelain glazes in the ceramic industry. Recently Balasubramanian et al. [125] used specific mixtures of red mud, fly ash and spent pot liner to prepare glass-ceramic products, which showed excellent properties and aesthetic appearance for possible applications as decorative tiles in the building industry. A recent experimental study by Mahata et al. [126] confirmed formation of aluminium titanate-mullite composite from red mud rich in titanium. This material has potential uses as liquid metal flow regulators, risers, thermocouple sleeves, burner nozzles, ceramic filters etc.

A lot of efforts are being made globally to find out suitable uses of red mud so that alumina industry may end up with no residue at all [127]. For complete utilization of red mud, Kovalenko [128] proposed avenues such as building

material production as an additive to cement, production of colouring agent for paint works, of toned paper in the wood-pulp and paper industry, of iron ore sinter and pellets in the ferrous metallurgy and in agriculture for the purpose of improvement of the soil structure and as a neutralizer of pesticides. Satapathy et al. [129] have reported the coating potential of red mud for deposition on various metal substrates using plasma spray technology. Numerous other uses for red mud have been reported and well documented by Thakur and Das [130]. The uses range from making various building materials, adsorbents, colouring agents to even preparation of exotic ceramic glass materials.

2.6 On Erosion of Polymer Composites

The widest definition of wear, which has been recognized for at least 50 years, includes the loss of material from a surface, transfer of material from one surface to another or movement of material within a single surface [131]. Although a narrower definition of wear has been proposed as 'progressive loss of substance from the operating surface of a body occurring as a result of relative motion at the surface' [132], the wide range of engineering applications of concern to the tribologists is served better by a broader definition. A simple and useful statement is that wear is 'damage to a solid surface, generally involving progressive loss of material, due to relative motion between that surface and a contacting substance or substances' [133]. There are quite a few terms to describe various wear modes which can be clubbed into four principal categories viz. abrasion, adhesion, erosion and surface fatigue.

Solid particle erosion, a typical wear mode, is a dynamic process that occurs in different machine parts due to the impingement of solid particles leading to material removal and surface degradation. Similar to other tribological processes, solid particle erosion is also a combined process: the mechanical load may be associated with secondary thermal, chemical and physical reactions between the counterparts involved in the tribological system. Attempts to understand the basic mechanisms of the erosion started in the last half of the

20th century and have continued to the present. Finnie [134] after 40 years of involvement with erosion presented an article on the past and the future of erosion in 1995. In this article, the influencing parameters and dominating mechanisms during solid particle erosion of metals and ceramic materials were reviewed. In the same year, another article was published by Meng et al. [135] providing information about the existing wear models and prediction equations. This article was more general as it discussed all the frictional phenomena termed to wear including also the solid particle erosion. The main conclusion of this publication was that no universal predictive equation exists.

It has been reported in the literature that polymers and their related composites are extensively used in erosive wear situations. Consequently, many researchers have investigated the solid particle erosion behaviour of various polymers and their composites. Erosion characteristics of polymers that have been reported in the literature include polystyrene [136], polypropylene [137, 138], nylon [139], polyethylene [140], ultra high molecular weight polyethylene [141], poly-ether-ether-ketone [142], polycarbonate and poly-methyl-methacrylate [143], epoxy [144], bismileimide [145], elastomers [146, 147] and rubber [148]. Barkoula and Karger-Kocsis [149] have also presented a detailed review on important variables in erosion process and their effects on different classes of polymers and composites. Miyazaki and Hamao [150] studied the effect of matrix materials, reinforcement fibers, fiber-matrix interface strength, impact angle and particle velocity on the solid particle erosion behavior of fiber reinforced plastics. They observed that the erosion rate of a fiber reinforced polymer composite decreases with the increase of the interface strength between matrix material and fibers. Further, Miyazaki and Hamao [151] carried out another similar study on the erosion behavior of short fiber reinforced thermoplastic resins with special attention focussed on an incubation period of erosion. Harsha et al. [152] reported the influence of impingement angles and impact velocities on solid particle erosion of various poly-aryl-ether-ketones and their composites with short fiber reinforcement. In another investigation, Barkoula and Karger-Kocsis

[153] studied the effects of fiber content and relative fiber orientation on the solid particle erosion of glass fiber/polypropylene composites. A study by Tewari et al. [154], on the influence of impingement angle and fiber orientations concludes that unidirectional carbon and glass fibre reinforced epoxy composites show semi ductile erosion behaviour, with the maximum erosion rate occurring at 60° impingement angle. In another study, Arjula and Harsha [155] have discussed the usefulness of the erosion efficiency parameter to identify various mechanisms in solid particle erosion. This study presents extensively on the erosion response, erosion efficiency and wear mechanisms of various polymers and composites.

It is evident from the available literature that the presence of particulate fillers has significant influence on various properties of polymer composites. But as far as the erosion behaviour of composites reinforced with both particulates and fibers is concerned, in fact, very limited work has been reported in the literature. As a result, there is no clear understanding of the mechanism of erosion in such polymer composites. Thus, a possibility that the incorporation of both particles and fibers in polymer could provide an improved wear performance has not been adequately explored so far. However, few recent publications by Patnaik et al. [156-160] on erosion wear characteristics of glass-polyester composites filled with different particulate fillers suggest that in such hybrid composites, the rate of material loss due to solid particle erosion reduce significantly with the addition of hard particulate fillers into the matrix. This improvement in the wear resistance depends on both the type and the content of filler.

An overview of the recent studies carried out by various investigators on erosion characteristics of polymer composites along with the experimental conditions is presented in Table 2.3.

Table 2.3 Overview of erosion wear studies performed on polymer matrix composites after 2002.

Matrix	Fiber / Filler / V_f / W_f %	Erodent Material	Erodent Size (μm)	Angle (°)	Velocity (m/s)	Year of publ.	Ref
PEEK	65% CF, (V_f), unidirectional fibres	Steel balls	300-500	15, 30, 45, 60, 75, 90	45, 85	2002	161
PEEK, PEK, PEKK	0%, 20% GF, 30% GF,(10% CF +10% PTFE +10% Graphite) (W_f), short fibres	Silica sand	150-212	15,30, 60, 90	30, 68, 90	2003	162
EP	56% CF, 53% GF, (V_f), unidirectional fibres	Steel balls	300-500	15, 30, 45, 60, 75, 90	45	2003	154
EP, uncoated & two layer coated	Carbon-Kevlar	Al_2O_3	10	20, 90	229	2003	163
PUR	Al_2O_3 (0-64%), (W_f)	SiO_2	40-70	45	24.8	2005	164
Resin	Mat GF (9.4%, 17.1%, 24.5%), Cloth GF (12%, 27.9%, 32.4%), UD GF 27.8%, (V_f), chopped strand mats, plain weave, unidirectional (UD)	crashed glass powder	350	20-90	24.5	2006	165
EP	55.8% AF, 53.8% PBO, (V_f), cross ply	SiC	100-150	15-90	57.8	2006	166
EP, EP + Flyash (1:4)	GF, cross ply	Silica sand	150-250	30, 45, 60, 90	24, 35, 52	2006	167
PI, uncoated & coated	Coatings: PI + WC-Co powder, PI +WC-Co powder + zinc "binding" layer, Fibre: CF	Al_2O_3	50	20, 90	100	2006	168
PPS	40% GF + 25% $CaCO_3$, (W_f), short fibre	Silica sand	150-200	15, 30, 45, 60, 75, 90	20, 40, 60	2007	169
EP	55% GF, (V_f), [45/-45/0/45/-45/0]s	SiC	400-500	30, 60, 90	42.5	2007	170
PEI	40% CF, (V_f), plain weave	Silica sand	N/S	15, 30, 45, 60, 75, 90	26.88	2007	171
PEEK	CF, unidirectional fibres	Arizona Test Dust, Sieved Runway Sand	10, 100	15, 30, 45, 60, 90	61, 97.5, 152.4	2007	172

PEI	CF, unidirectional fibres	Silica sand	150-200	15, 30, 45, 60, 75, 90	1.96, 2.88	2007	173
PEI	0%, 20% GF, 30% GF, 40% GF, 25% CF, 25% GF +15% PTFE +15% (MoS_2 +graphite), (W_f), short fibres	Silica sand	150-300	15, 30, 60, 90	30, 52, 60, 88	2007	174
PPS	51% CF, (V_f), cross ply	Silica sand	150-200	15-90	20, 40, 60	2008	175
PEI	60% CF, (V_f), unidirectional fibres	Silica sand	150-250	15, 30, 60, 90	25-66	2008	176
EP	55% GF, (V_f), [45/-45/0/45/-45/0]s	SiC	400-500	30, 60, 90	42.5	2008	177
EP	66.4% GF, 59.4% GF, 64% CF, (V_f), unidirectional & bidirectional fibres	Silica sand	150-200	90	25, 37, 47, 60	2008	178
PET	30% GF, 40% GF, 50% GF, (W_f), cross ply	Silica sand	300, 500, 800	30, 60, 90	32, 45, 58	2008	156
PET	50% GF + 0%, 10%, 20% Alumina, (W_f), cross ply	Silica sand	300, 500, 800	45, 60, 90	32, 45, 58	2008	157
PET	50% GF + 0%, 10%, 20% SiC (W_f), cross ply	Silica sand	300, 500, 800	45, 60, 90	32, 45, 58	2008	158
PET	30% GF, 40% GF, 50% GF, (W_f), cross ply	Silica sand	300, 500, 800	30, 60, 90	32, 45, 58	2008	159
PET	50% GF + 0%, 10%, 20% Alumina, (W_f), cross ply	Silica sand	300, 500, 800	45, 60, 90	32, 45, 58	2008	160

2.7 On Erosion Wear Modelling

Several erosion models/correlations were developed by many researchers to provide a quick answer to design engineers in the absence of a comprehensive practical approach for erosion prediction. The theoretical model developed by Rabinowicz [179] was used to calculate the volume of material removed from the target surface due to impact of solid particles entrained in a liquid jet. The results indicated that the sand particle trajectories appeared to be governed by the secondary flows and that there was no simple liquid velocity profile that can be used to calculate the particle trajectories in order to make an accurate prediction of the location of the point of maximum wear. One of the early erosion prediction correlations is that developed by Finnie [180] expressing the

rate of erosion in terms of particle mass and impact velocity. In that correlation, the rate of erosion was proportional to the impact velocity squared. In a subsequent study, Nesic [181] found that Finnie's model over-predicts the erosion rate and presented another formula for the erosion rate in terms of a critical velocity rather than the impact velocity. The erosion model suggested by Bitter [182, 183] assumed that the erosion occurred in two main mechanisms; the first is caused by repeated deformation during collisions that eventually results in the breaking loose of a piece of material while the second is caused by the cutting action of the free-moving particles. Comparison between the obtained correlations and the test results showed a good agreement. It was concluded that cutting wear prevails in places where the impact angles are small (such as in risers and straight pipes) and it is sufficient to use hard material in such places to reduce erosion. Other erosion models were suggested by Laitone [184], Salama and Venkatesh [185], Bourgoyne [186], Chase et al. [187], Mc Laury [188], Svedeman and Arnold [189] and Jordan [190]. Recently, Shirazi and McLaury [191] presented a model for predicting multiphase erosion in elbows. The model was developed based on extensive empirical information gathered from many sources and it accounts for the physical variables affecting erosion, including fluid properties, sand production rate and the fluid-stream composition.

In most erosion processes, target material removal typically occurs as the result of a large number of impacts of irregular angular particles, usually carried in pressurized fluid streams. The fundamental mechanisms of material removal, however, are more easily understood by analysis of the impact of single particles of a known geometry. Such fundamental studies can then be used to guide development of erosion theories involving particle streams, in which a surface is impacted repeatedly. Single particle impact studies can also reveal the rebound kinematics of particles, which are very important for models which take into account the change in erosive potential due to collisions between incident and rebounding particles [192, 193]. A number of recent papers contain investigations on the rebound kinematics of spherical/angular particles [194-

199]. These works have demonstrated that the trajectory of the particle while impacting the material surface is of prime interest in predicting the material loss, since this determines the manner in which a crater is carved out. Further Sundararajan and co-workers [200-202] have also proposed a ductile erosion model and have studied the effect of material pile-up at the edge of the crater on the rebound kinematics of the spherical particles.

In order to develop a mathematical model for solid particle erosion of composite materials, it is important to understand the mechanisms responsible for the same. For a composite material, its surface damage by erosion depends on many factors, including the impact velocity, particle size and shape of the erodent, mechanical properties of both the target material and the erodent and the volume fraction, size and properties of the reinforcing phase as well as the bonding between the matrix and the reinforcing phase. The synergism of all these factors makes it difficult to experimentally investigate the erosion mechanism for composite materials. Fortunately, computer simulation provides an effective and economic approach for such investigation. Computer models proposed to simulate wear process may be broadly classified into two groups: macro-scale models and atomic-scale models. The macro-scale models were proposed based on various assumptions or theories such as the cutting mechanism [180] and the platelet mechanism [203]. The cutting mechanism is based on the assumption that individual erodent particle impinges a target surface, cutting out a swath of the material. However, this mechanism is only suitable for ductile materials. Regarding the platelet mechanism, plastic deformation and work hardening prior to fracture are taken into account and this makes it closer to reality. However, this mechanism is also suitable only for ductile materials. Few investigators have used the finite element analysis for erosion simulation [204, 205]. Another group of models based on fundamental physics laws are promising for wear modelling, such as the molecular dynamics simulation [206, 207] and the first-principle technique [208]. Besides, a micro-scale dynamic model was also proposed for wear simulation, which has been applied to investigate abrasive wear [209, 210].

This model was later applied to simulation of solid particle erosion of homogeneous materials [211].

The correlations between wear resistance and characteristic properties of polymers have been discussed in terms of various semi-empirical equations by some pioneers [212, 213]. Although these equations are quite helpful to estimate the wear behaviour of polymers in some special cases, wear normally is very complicated as it depends on many more mechanical and other parameters. This means that simple functions cannot always cover all the prevailing mechanisms under wear. For predictive purposes, an artificial neural network (ANN) approach has, therefore, been introduced recently into the field of wear of polymers and composites by Velten et al. [214] and Zhang et al. [215]. An ANN is a computational system that simulates the microstructure (neurons) of biological nervous system. The multi-layered neural network is the most widely applied neural network, which has been utilized in most of the research works related to polymer composites [216]. Recently, Patnaik et al. [159, 160] developed a theoretical model to estimate the erosion wear rate of polymer composites under multiple impact condition. This model is based on the assumption that the kinetic energy of the impinging particles is utilized to cause micro-indentation in the composite material and the material loss is a measure of the indentation. The erosion is the result of cumulative damage of such non-interacting, single particle impacts.

Statistical methods have commonly been used for analysis, prediction and/or optimization of a number of engineering processes. These methods enable the user to define and study the effect of every single condition possible in an experiment where numerous factors are involved. Wear processes in composites are such complex phenomena involving a number of operating variables and it is essential to understand how the wear characteristics of the composites are affected by different operating conditions. Selecting the proper operating conditions is always a major concern as traditional experimental design would

require many experimental runs to achieve satisfactory result. Thus, several mathematical models based on statistical regression techniques have been constructed to select the proper testing conditions [217-222] in order to obtain minimum wear rate. Taguchi and Konishi [223] advocated the use of orthogonal arrays and Taguchi [224] devised a new experimental design that applied signal-to-noise ratio with orthogonal arrays to the robust design of products and processes. In this procedure, the effect of a factor is measured by average results and therefore, the experimental results can be reproducible. Phadke [225], Wu and Moore [226] and others [227-230] have subsequently applied the Taguchi method to design the products and process parameters. This inexpensive and easy-to-operate experimental strategy based on Taguchi's parameter design has been applied successfully for parametric appraisal of erosion wear of polyester based composites [160].

2.8 The Knowledge Gap in Earlier Investigations

The literature survey presented above reveals the following knowledge gap in the research reported so far:

- Though much work has been done on a wide variety of natural fibers for polymer composites, very less has been reported on the reinforcing potential of bamboo fiber in spite of its several advantages over others. Many low-end application areas such as housing, furniture, packing, transport etc. are cited in the literature for bamboo based products, but there is hardly any mention of their potential use in tribological situations where synthetic fibers are widely used. Moreover, there is no report available in the literature on the erosion characteristics of bamboo based polymer composites.
- A number of research efforts have been devoted to the mechanical and wear characteristics of either fiber reinforced composites or particulate filled composites. However, a possibility that the incorporation of both particulates and fibers in polymer could provide a synergism in terms of

improved performance has not been adequately addressed so far. Besides, the potential of solid industrial wastes to be used as particulate fillers in polymer composites has rarely been reported.

- Though a number of avenues are being implemented for utilization and disposal of solid industrial wastes there is no report available in the existing literature on the use of wastes like red mud and copper slag in polymer composites.
- Though many investigators have proposed a number of models to predict erosion behaviour of polymer composites, none of them have considered the erodent temperature as a parameter influencing the erosion rate. As a result, no specific theoretical model based on the conservation of both the kinetic and thermal energy of the erodent has so far been developed.
- Studies carried out worldwide on erosion wear behaviour of composites have largely been experimental and the use of statistical techniques in analyzing wear characteristics has been rare. Taguchi method, being a simple, efficient and systematic approach to optimize designs for performance, quality and cost, is used in many engineering applications. However, its implementation in parametric appraisal of wear processes has hardly been reported.

2.9 Objectives of the Present Work

The knowledge gap in the existing literature summarized above has helped to set the objectives of this research work which are outlined as follows:

1. Fabrication of a new class of epoxy based hybrid composites reinforced with bamboo fibers and four different particulate fillers (red mud, copper slag, alumina and silicon carbide).
2. Development of a theoretical model to estimate erosion wear rate of polymer matrix composites under multiple impact conditions and its validation through experimentation.

3. Evaluation of mechanical properties and erosion wear characteristics of bamboo based hybrid composites and comparison with those of a similar set of composites reinforced with the most commonly used synthetic fiber (E-glass).
4. Statistical analysis based on Taguchi experimental design for parametric appraisal of the erosion process in the composites under study and development of predictive equations.

Chapter Summary

This chapter has provided

- An exhaustive review of research works on various aspects of polymer composites reported by previous investigators
- The knowledge gap in earlier investigations
- The objectives of the present work

The next chapter describes the materials and methods used for the processing of the composites, the experimental planning and the Taguchi method.

****

Chapter 3

MATERIALS AND METHODS

This chapter describes the materials and methods used for the processing of the composites under this investigation. It presents the details of the characterization and erosion tests which the composite samples are subjected to. The methodology based on Taguchi experimental design and the statistical interpretations by analysis of variance (ANOVA) are also presented in this part of the thesis.

3.1 Materials

3.1.1 Matrix Material

Matrix materials are of different types like metals, ceramics and polymers. Polymer matrices are most commonly used because of cost efficiency, ease of fabricating complex parts with less tooling cost and they also have excellent room temperature properties when compared to metal and ceramic matrices. Polymer matrices can be either thermoplastic or thermoset. Thermoset matrices are formed due to an irreversible chemical transformation of the resin into an amorphous cross-linked polymer matrix. Due to huge molecular structures, thermoset resins provide good electrical and thermal insulation. They have low viscosity, which allow proper fiber wet out, excellent thermal stability and better creep resistance. Normally, these resins can be formulated to give a wide range of properties upon the requirement [231].

The most commonly used thermoset resins are epoxy, polyester, vinyl ester and phenolics. Among them, the epoxy resins are being widely used for many advanced composites due to their excellent adhesion to wide variety of fibers, superior mechanical and electrical properties and good performance at elevated temperatures. In addition to that they have low shrinkage upon curing and good chemical resistance. Due to several advantages over other thermoset polymers as mentioned above, epoxy (LY 556) is chosen as the matrix material for the

present research work. Its common name is Bisphenol-A-Diglycidyl-Ether and it chemically belongs to the 'epoxide' family. The epoxy resin and the corresponding hardener HY-951 are procured from Ciba Geigy India Ltd.

3.1.2 Fiber Material

Generally, fiber is the reinforcing phase of a composite material. The present investigation employs bamboo as the natural fiber in the epoxy matrix to fabricate a series of hybrid composites. The scientific name of the type of bamboo used for this work is *Dendrocalamus strictus* [232]. This species occupies about 53 per cent of total bamboo area in India. This is one of the predominant species of bamboo in Uttar Pradesh, Madhya Pradesh, Orissa and Western Ghats in India. In general, bamboo is available everywhere around the world and is an abundant natural resource. It has been a conventional construction material since ancient times. The bamboo culm, in general, is a cylindrical shell, divided by transversal diaphragms at the nodes. Bamboo is an orthotropic material with high strength along and low strength transversal to its fibers. The structure of bamboo itself is a composite material, consisting of long and aligned cellulose fibers immersed in a ligneous matrix. In this work, roving bidirectional bamboo fiber mats are used as the reinforcing phase in the composites. The extracted fiber mats are dried in an oven at 105°C for 72 h prior to composite making to remove moisture. The average thickness of each bamboo fiber is about 1.5 mm.

Though the present research is focused mainly on the bamboo fiber reinforced composites, their relative evaluation can only be made on comparing them with a similar set of composites with some conventional synthetic fiber. Some commonly used synthetic fibers for composites are glass, carbon and aramid etc. Among them, glass fibers are the most commonly used fibers for engineering composites. Hence, glass fiber is chosen as the other reinforcing material in this work. Glass fiber is commercially available in abundance with good mechanical properties; thus is widely used in composite structures [231]. Based upon

different applications, glass fibers (silica-oxygen network) are classified into E glass, C glass and S glass fibers. E glass is used as an insulator and mostly used in electrical industry, hence got the name 'E' before the word 'glass'. E-glass also has good mechanical properties in addition to low cost and ease of usability. The letter 'S' in S-glass stands for structural applications. S-glass got different chemical formulation and it has higher strength to weight ratio and higher elongation strain percentage but it is quite expensive. C-glass fibers are advantageous in resisting chemical corrosion. Glass fibers are available in different forms like continuous, chopped and woven fabrics.

In the present work, woven roving E-glass fibers (supplied by Saint Gobain Ltd. India) have been used as the reinforcing material in the composites. The major constituents of E-glass are silicon oxide (54 wt.%), aluminum oxide (15 wt.%), calcium oxide (17 wt.%), boron oxide (8 wt.%) and magnesium oxide (4.5 wt.%). E-glass fiber has an elastic modulus of 72.5 GPa and possesses a density of 2.59 gm/cc.

The pictorial views of bi-directional roving bamboo and E-glass fiber mats used for composite fabrication for this study are given in Figure 3.1.

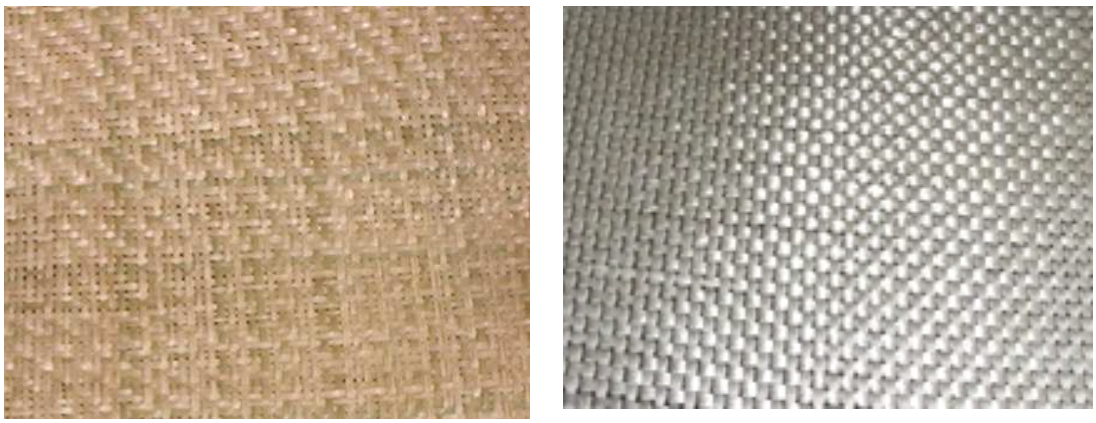

(a) bamboo fiber mat (b) E-glass fiber mat

Figure 3.1 Bidirectional roving bamboo and E-glass fiber mats

3.1.3 Particulate Filler Materials

A variety of natural or synthetic solid particulates, both organic and inorganic is already being commercially used as reinforcing fillers in polymeric composites. While ceramic powders such as alumina (Al_2O_3), silicon carbide (SiC) , silica (SiO_2), titania (TiO_2) etc. are widely used as conventional fillers, the use of industrial wastes for such purpose is hardly found. In view of this, in the present work two industrial wastes such as red mud and copper slag are chosen as particulate fillers to be used in the composites. To make an assessment of their reinforcing potential in terms of wear performance and mechanical properties, two other conventional ceramic fillers such as alumina and SiC are also considered for comparison. While alumina and SiC have conventionally been used in composites, the wastes red mud and copper slag are not known for being used as filler material in any polymeric matrix before.

Production of alumina from bauxite by the Bayer's process is associated with the generation of red mud as the major waste material in alumina industries worldwide. Depending upon the quality of bauxite, the quantity of red mud generated varies from 55-65% of the bauxite processed [233]. The enormous quantity of red mud discharged by these industries poses an environmental and economical problem. The treatment and disposal of this residue is a major operation in any alumina plant. Red mud, as the name suggests, is brick red in colour and slimy having average particle size of about 80-100 μm. It comprises of the iron, titanium and the silica part of the parent ore along with other minor constituents. It is alkaline, thixotropic and possesses high surface area in the range of 13-16 m^2/gm with a true density of 3.3 gm/cc. Depending on the source, these residues have a wide range of composition: Fe_2O_3 20-60%, Al_2O_3 10-30%, SiO_2 2-20%, Na_2O 2-10%, CaO 2-8%, TiO_2 traces 2-8%. The red mud used in this work has been collected from the site of NALCO alumina plant at Damanjodi in India. The other industrial waste used in this investigation is 'copper slag', which is produced during matte smelting and conversion steps in the pyro-metallurgical production of copper. During matte smelting, two

separate liquid phases, copper-rich matte (sulphides) and slag (oxides) are formed. It has been estimated that for every tonne of refined copper produced, about 2.2 tonne of slag is generated and every year, approximately 24.6 million tonne of slag is generated in copper production worldwide. The major slag producing regions are presented in Table 3.1 [234]. Slag containing < 0.8% copper are either discarded as waste or sold as products with properties similar to those of natural basalt (crystalline) or obsidian (amorphous). In the present study, copper slag collected from the plant site of Hindustan Copper Limited, at Ghatsila, India, is sieved to obtain average particle size of about 80 -100 μm. The composition of the copper slag used in this work is as follows: Fe_2O_3: 35.3%, SiO_2: 36.6%, CaO: 10%, Al_2O_3: 8.1%, CuO: 0.37%, MgO: 4.38%, Na_2O:0.47%, K_2O: 3.45%, PbO: 0.12%, Zn: 0.97% and Cu: 0.24%.

Table 3.1 Copper slag generation in various regions [234]

Regions	Copper slag generation/annum in million ton
Asia	7.26
North America	5.90
Europe	5.56
South America	4.18
Africa	1.23
Oceania	0.45

Alumina is an inorganic material that has the potential to be used as filler in various polymer matrices. Aluminium oxide (Al_2O_3) commonly referred to as alumina, can exist in several crystalline phases which all revert to the most stable hexagonal alpha phase at elevated temperatures. This is the phase of particular interest for structural applications. Alumina is the most cost effective and widely used material in the family of engineering ceramics. It is hard, wear-resistant, has excellent dielectric properties, resistance to strong acid and alkali attack at elevated temperatures, high strength and stiffness. With an excellent

combination of properties and a reasonable price, it is no surprise that fine grain technical grade alumina has a very wide range of applications.

Similarly, the other conventional filler chosen for this work is SiC, which has a great potential to be used in various polymeric matrices. It is the only chemical compound of carbon and silicon. It was originally produced by a high temperature electro-chemical reaction of sand and carbon. Today the material has been developed into a high quality technical grade ceramic with very good mechanical properties. It is used in abrasives, refractories, ceramics and in numerous high-performance structural and wear applications. This can also be made an electrical conductor and has applications in resistance heating, flame igniters and electronic components. SiC is composed of tetrahedra of carbon and silicon atoms with strong bonds in the crystal lattice. This produces a very hard and strong material. SiC is not attacked by any acids, alkalis or molten salts up to 800°C. It has low density of about 3.1 gm/cc, low thermal expansion, high elastic modulus, high strength, high thermal conductivity, high hardness, excellent thermal shock resistance and superior chemical inertness.

3.2 Composite Fabrication

Cross plied bamboo and E-glass fibers are reinforced separately in epoxy resin to prepare the fiber reinforced composites B_1 and Z_1 in which no particulate filler is used. The other composite samples B_2 – B_9 and Z_2 – Z_9 with four different particulate fillers of varied amount but with fixed fiber loading (50 wt %) are fabricated. The composition and designation of the composites prepared for this study are listed in Table 3.2. The fabrication of the composite slabs is done by conventional hand-lay-up technique followed by light compression moulding technique. The fillers are mixed thoroughly in the epoxy resin before the respective fiber mats are reinforced into the matrix body. The low temperature curing epoxy resin and corresponding hardener (HY951) are mixed in a ratio of 10:1 by weight as recommended. Each ply of fiber is of dimension 200 × 200 mm^2. A stainless steel mould having dimensions of 210 × 210 × 40 mm^3 is used.

A releasing agent (Silicon spray) is used to facilitate easy removal of the composite from the mould after curing. The cast of each composite is cured under a load of about 50kg for 24 h before it removed from the mould. Then this cast is post cured in the air for another 24 h after removing out of the mould. Specimens of suitable dimension are cut using a diamond cutter for physical/ mechanical characterization and erosion wear testing. Utmost care has been taken to maintain uniformity and homogeneity of the composites.

Table 3.2 Designations and detailed compositions of the composites

Designation	Composition
B_1	Epoxy (50 wt%) + Bamboo Fiber (50wt%)
B_2	Epoxy (40 wt%) + Bamboo Fiber (50wt%) + Red mud (10wt%)
B_3	Epoxy (30 wt%) + Bamboo Fiber (50wt%) + Red mud (20wt%)
B_4	Epoxy (40 wt%) + Bamboo Fiber (50wt%) + Copper slag (10wt%)
B_5	Epoxy (30 wt%) + Bamboo Fiber (50wt%) + Copper slag (20wt%)
B_6	Epoxy (40 wt%) + Bamboo Fiber (50wt%) + Alumina (10wt%)
B_7	Epoxy (30 wt%) + Bamboo Fiber (50wt%) + Alumina (20wt%)
B_8	Epoxy (40 wt%) + Bamboo Fiber (50wt%) + SiC (10wt%)
B_9	Epoxy (30 wt%) + Bamboo Fiber (50wt%) + SiC (20wt%)
Z_1	Epoxy (50 wt%) + Glass Fiber (50wt%)
Z_2	Epoxy (40 wt%) + Glass Fiber (50wt%) + Red mud (10wt%)
Z_3	Epoxy (30 wt%) + Glass Fiber (50wt%) + Red mud (20wt%)
Z_4	Epoxy (40 wt%) + Glass Fiber (50wt%) + Copper slag (10wt%)
Z_5	Epoxy (30 wt%) + Glass Fiber (50wt%) +Copper slag (20wt%)
Z_6	Epoxy (40 wt%) + Glass fiber (50wt%) + Alumina (10wt%)
Z_7	Epoxy (30 wt%) + Glass Fiber (50wt%) + Alumina (20wt%)
Z_8	Epoxy (40 wt%) + Glass Fiber (50wt%) + SiC (10wt%)
Z_9	Epoxy (30 wt%) + Glass Fiber (50wt%) + SiC (20wt%)

3.3 Mechanical Characterization

3.3.1 Density

The theoretical density (ρ_{ct}) of composite materials in terms of weight fractions of different constituents can easily be obtained as for the following equation given by Agarwal and Broutman [1].

$$\rho_{ct} = \frac{1}{(W_f/\rho_f)+(W_m/\rho_m)} \tag{3.1}$$

where, W and ρ represent the weight fraction and density respectively. The suffixes f and m stand for the fiber and matrix respectively. Since the composites under this investigation consist of three components namely matrix, fiber and particulate filler, the expression for the density has been modified as

$$\rho_{ct} = \frac{1}{(W_f/\rho_f)+(W_m/\rho_m)+(W_p/\rho_p)} \tag{3.2}$$

where, the suffix p stands for the particulate fillers. The actual density (ρ_{ce}) of the composite, however, can be determined experimentally by simple water immersion technique. The volume fraction of voids (V_v) in the composites is calculated using the following equation:

$$V_v = \frac{\rho_{ct} - \rho_{ce}}{\rho_{ct}} \tag{3.3}$$

3.3.2 Micro-hardness

Micro-hardness measurement is done using a Leitz micro-hardness tester. A diamond indenter, in the form of a right pyramid with a square base and an angle 136° between opposite faces, is forced into the material under a load F. The two diagonals X and Y of the indentation left on the surface of the material after removal of the load are measured and their arithmetic mean L is calculated. In the present study, the load considered F = 24.54N and Vickers hardness number is calculated using the following equation.

$$H_V = 0.1889\frac{F}{L^2} \tag{3.4}$$

and $L = \frac{X+Y}{2}$

where, F is the applied load (N), L is the diagonal of square impression (mm), X is the horizontal length (mm) and Y is the vertical length (mm).

3.3.3 Tensile Strength

The tensile test is generally performed on flat specimens. The dimension of the specimen is 150 mm ×10 mm × 4 mm and a uniaxial load is applied through both the ends. The ASTM standard test method for tensile properties of fiber-resin composites has the designation D 3039-76. In the present work, this test is performed in the universal testing machine Instron 1195 (Figure 3.2a) at a crosshead speed of 10 mm/min and the results are used to calculate the tensile strength of composite samples. The loading arrangement is shown in Figure 3.2b. Here, the test is repeated three times on each composite type and the mean value is reported as the tensile strength of that composite.

3.3.4 Flexural and Inter-Laminar Shear Strength (ILSS)

The flexural strength of a composite is the maximum tensile stress that it can withstand during bending before reaching the breaking point. The three point bend test is conducted on all the composite samples in the universal testing machine Instron 1195. The dimension of each specimen is 60 mm ×10 mm × 4 mm. Span length of 40 mm and the cross head speed of 10 mm/min are maintained. The loading arrangement is shown in Figure 3.2c. For both flexural strength and ILSS, the test is repeated three times for each composite type and the mean value is reported. The flexural strength of the composite specimen is determined using the following equation.

$$\text{Flexural Strength} = \frac{3PL}{2bt^2} \tag{3.5}$$

where, L is the span length of the sample (mm)

P is maximum load (N)

b the width of specimen (mm)

t the thickness of specimen (mm)

The data recorded during the 3-point bend test is used to evaluate the ILSS also. The ILSS values are calculated as follows:

$$\text{ILSS} = \frac{3P}{4bt} \tag{3.6}$$

(a) Universal testing machine Instron 1195

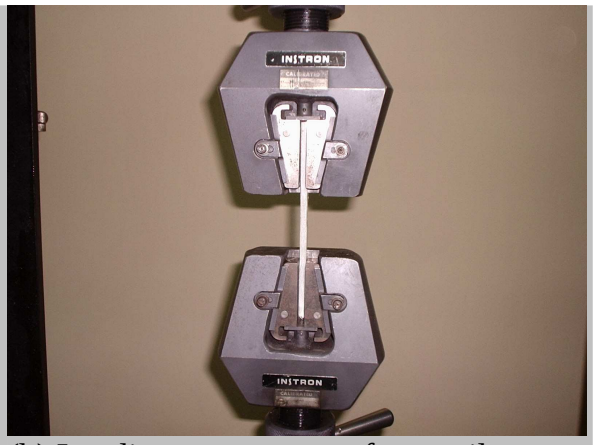

(b) Loading arrangement for tensile test

(c) Loading arrangement for flexural test

Figure 3.2 Universal testing machine (Instron 1195) and loading arrangement for tensile and flexural tests

3.3.4 Impact Strength

Low velocity instrumented impact tests are carried out on the composite specimens. The tests are done as per ASTM D 256 using an impact tester (Figure 3.3). The pendulum impact testing machine ascertains the notch impact strength of the material by shattering the V-notched specimen with a pendulum hammer, measuring the spent energy and relating it to the cross section of the specimen. The standard specimen size as per ASTM D 256 is 64 mm× 12.7 mm × 3.2 mm and the depth under the notch is 10 mm. The respective values of impact energy of different specimens are recorded directly from the dial indicator.

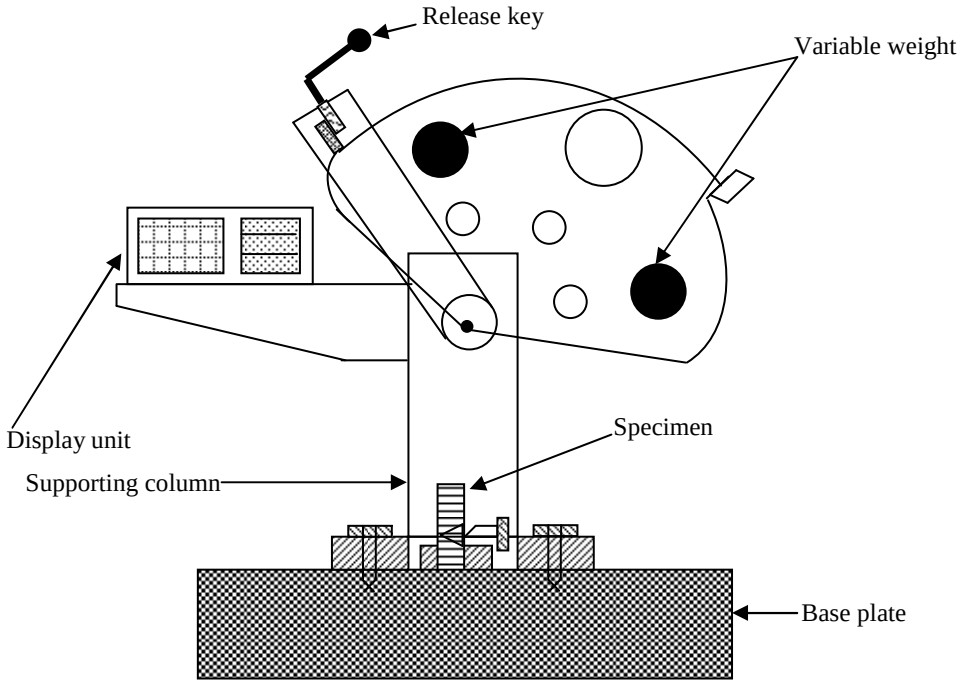

Figure 3.3 Schematic diagram of an impact tester

3.4 Scanning Electron Microscopy

The surfaces of the specimens are examined directly by scanning electron microscope JEOL JSM-6480LV (Figure 3.4). The composite samples are mounted on stubs with silver paste. To enhance the conductivity of the samples, a thin film of platinum is vacuum-evaporated onto them before the photomicrographs are taken.

3.5 Erosion Test Apparatus

The set up for the solid particle erosion wear test used in this study is capable of creating reproducible erosive situations for assessing erosion wear resistance of the prepared composite samples. The pictorial view and the schematic diagram of the erosion test rig are given in Figure 3.5 and Figure 3.6 respectively. The test rig consists of an air compressor, an air drying unit, a conveyor belt-type particle feeder and an air particle mixing and accelerating chamber. In the present study, dry silica sand (assumed to be square pyramidal shaped) of different particle sizes (300µm, 450µm and 600µm) are used as the erodent. The dried and compressed air is mixed with the erodent which is fed constantly by a conveyor belt feeder into the mixing chamber and then is accelerated by passing

the mixture through a convergent brass nozzle of 3 mm internal diameter. The erodent particles impact the specimen which can be held at different angles with respect to the direction of erodent flow using a swivel and an adjustable sample clip. The velocity of the eroding particles is determined using the standard double disc method [235]. The apparatus is equipped with a heater which can regulate and maintain the erodent temperature at any pre-determined fixed value during an erosion trial. The samples are cleaned in acetone, dried and weighed before and after the erosion trials using a precision electronic balance to an accuracy of ± 0.1 mg. The weight loss is recorded for subsequent calculation of erosion rate. The process is repeated till the erosion rate attains a constant value called steady state erosion rate. The erosion rate is defined as the ratio of this weight loss to the weight of the eroding particles causing the loss.

Figure 3.4 Scanning Electron Microscope (JEOL JSM-6480LV)

Figure 3.5 Solid particle erosion test set up

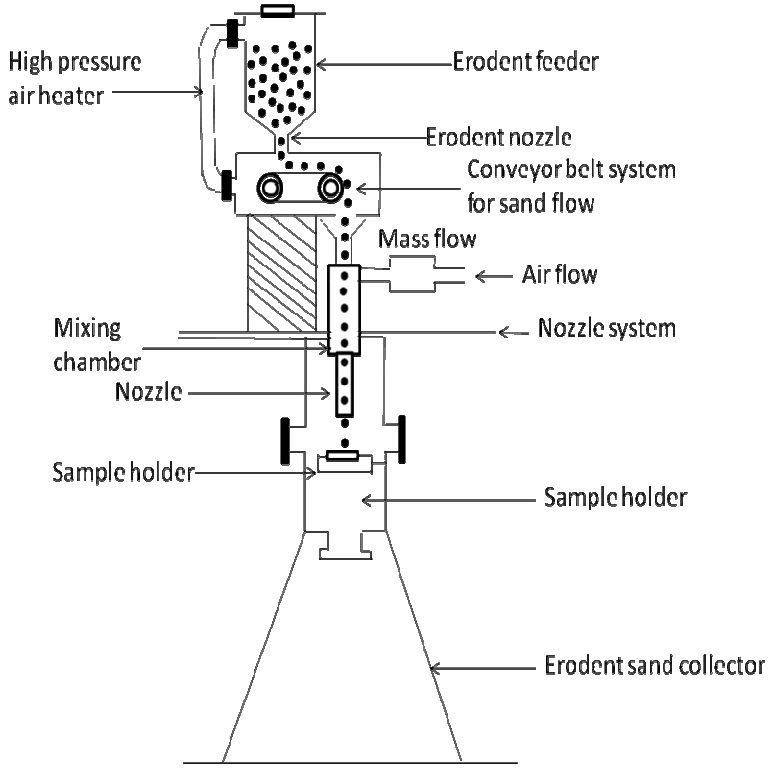

Figure 3.6 A schematic diagram of the erosion test rig

3.6 Taguchi Method

In any experimental research, since test procedures are generally expensive and time consuming, the need to satisfy the design objectives with the least number of tests is clearly an important requirement. In this context, Taguchi method provides the designer with a systematic and efficient approach for experimentation to determine near optimum settings of design parameters for performance and cost. This method involves laying out the experimental conditions using specially constructed tables known as 'orthogonal arrays'. Use of orthogonal arrays significantly reduces the number of experimental configurations to be studied. The conclusions drawn from small scale experiments are valid over the entire experimental region spanned by the control factors and their settings. The most important stage in the design of experiment lies in the selection of the control factors. Therefore, initially a large number of factors are included so that non-significant variables can be excluded at the earliest opportunity. Exhaustive literature review reveals that parameters viz., impact velocity, impingement angle, fiber loading, filler content, erodent size, stand-off distance etc. largely influence the erosion rate of polymer composites [159, 160]. However, the author has not come across any report on the influence of a factor like erodent temperature on wear performance of polymer composites. Therefore, in this work, to explore the possible effect of erodent temperature, it is also considered as a control factor in addition to impact velocity, impingement angle, filler content, erodent size and stand-off distance. Thus, the impact of six parameters are studied using L_{27} (3^{13}) orthogonal design. The control factors and the parameter settings for erosion test are given in Table 3.3. Table 3.4 presents the selected levels for various control factors. The tests are conducted as per the experimental design given in Table 3.5. The standard linear graph, as shown in Figure 3.7, is used to assign the factors and interactions to various columns of the orthogonal array [225].

Table 3.3 Parameter settings for erosion test.

Control Factors	Symbols	Fixed parameters	
Impact velocity	Factor A	Erodent	Silica sand
Filler content	Factor B	Erodent feed rate (g/min)	10.0 ± 1.0
Erodent Temperature	Factor C	Nozzle diameter (mm)	3
Impingement angle	Factor D	Length of nozzle (mm)	80
Stand-off distance	Factor E		
Erodent size	Factor F		

Table 3.4 Levels for various control factors

Control factor	Level			
	I	II	III	Units
A: Impact velocity	43	54	65	m/sec
B: Filler content	0	10	20	%
C: Erodent Temperature	40	50	60	°C
D: Impingement angle	30	60	90	degree
E: Stand-off distance	65	75	85	mm
F: Erodent size	300	450	600	µm

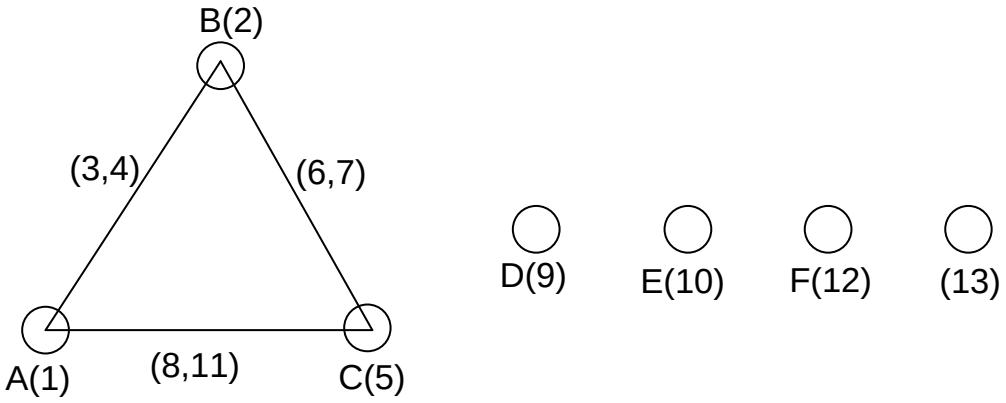

Figure 3.7 Linear graph for L_{27} orthogonal array

Table 3.5 Orthogonal array for L_{27} (3^{13}) Taguchi Design

$L_{27}(3^{13})$	1 A	2 B	3 $(AxB)_1$	4 $(AxB)_2$	5 C	6 $(BxC)_1$	7 $(BxC)_2$	8 $(AxC)_1$	9 D	10 E	11 $(AxC)_2$	12	13
1	1	1	1	1	1	1	1	1	1	1	1	1	1
2	1	1	1	1	2	2	2	2	2	2	2	2	2
3	1	1	1	1	3	3	3	3	3	3	3	3	3
4	1	2	2	2	1	1	1	2	2	2	3	3	3
5	1	2	2	2	2	2	2	3	3	3	1	1	1
6	1	2	2	2	3	3	3	1	1	1	2	2	2
7	1	3	3	3	1	1	1	3	3	3	2	2	2
8	1	3	3	3	2	2	2	1	1	1	3	3	3
9	1	3	3	3	3	3	3	2	2	2	1	1	1
10	2	1	2	3	1	2	3	1	2	3	1	2	3
11	2	1	2	3	2	3	1	2	3	1	2	3	1
12	2	1	2	3	3	1	2	3	1	2	3	1	2
13	2	2	3	1	1	2	3	2	3	1	3	1	2
14	2	2	3	1	2	3	1	3	1	2	1	2	3
15	2	2	3	1	3	1	2	1	2	3	2	3	1
16	2	3	1	2	1	2	3	3	1	2	2	3	1
17	2	3	1	2	2	3	1	1	2	3	3	1	2
18	2	3	1	2	3	1	2	2	3	1	1	2	3
19	3	1	3	2	1	3	2	1	3	2	1	3	2
20	3	1	3	2	2	1	3	2	1	3	2	1	3
21	3	1	3	2	3	2	1	3	2	1	3	2	1
22	3	2	1	3	1	3	2	2	1	3	3	2	1
23	3	2	1	3	2	1	3	3	2	1	1	3	2
24	3	2	1	3	3	2	1	1	3	2	2	1	3
25	3	3	2	1	1	3	2	3	2	1	2	1	3
26	3	3	2	1	2	1	3	1	3	2	3	2	1
27	3	3	2	1	3	2	1	2	1	3	1	3	2

The selected parameters viz., impact velocity, filler content, erodent temperature, stand-off distance, impingement angle and erodent size, each at three levels, are considered in this study. These six parameters each at three levels would require 3^6 = 729 runs in a full factorial experiment whereas Taguchi's experimental approach reduces it to 27 runs only offering a great advantage. The plan of the experiments as shown in Table 3.5 is as follows: the first, second, fifth, ninth, tenth and twelfth columns are assigned to impact velocity (A), filler content (B), erodent temperature (C), impingement angle (D), stand-off distance (E) and erodent size (F) respectively. The third and fourth column are assigned to $(A\times B)_1$ and $(A\times B)_2$ respectively to estimate interaction between impact velocity

(A) and filler content (B), the sixth and seventh column are assigned to $(B\times C)_1$ and $(B\times C)_2$ respectively to estimate interaction between filler content (B) and erodent temperature (C), the eighth and eleventh column are assigned to $(A\times C)_1$ and $(A\times C)_2$ respectively to estimate interaction between the impact velocity (A) and erodent temperature (C) and the remaining columns are used to estimate experimental errors.

The experimental observations are transformed into signal-to-noise (S/N) ratios. There are several S/N ratios available depending on the type of characteristics such as:

'Smaller-the-better' characteristic: $$\frac{S}{N}=-10\log\frac{1}{n}\left(\sum y^2\right) \quad (3.7)$$

'Nominal-the-better' characteristics: $$\frac{S}{N}=10\log\left(\sum\frac{\overline{Y}}{S^2}\right) \quad (3.8)$$

'Larger-the-better' characteristics : $$\frac{S}{N}=-10\log\frac{1}{n}\left(\sum\frac{1}{y^2}\right) \quad (3.9)$$

where n the number of observations, y the observed data, $\overline{Y}$ the mean and S the variance. The S/N ratio for minimum erosion rate comes under 'smaller is better' characteristic, which can be calculated as logarithmic transformation of the loss function by using Eq. (3.7).

Chapter Summary

This chapter has provided:

- The descriptions of materials used in the experiments
- The details of fabrication and characterization of the composites
- The description of erosion wear test
- An explanation of the Taguchi experimental design.

The next chapter presents the physical and mechanical properties of the polymer composites under this study.

****

Chapter 4

RESULTS AND DISCUSSION: MECHANICAL CHARACTERIZATION

This chapter presents the measured values of the physical and mechanical properties of the bamboo fiber reinforced epoxy composites filled with different particulate fillers. These results are compared with those of a similar set of glass fiber reinforced composites filled with same particulate fillers. The relative effects of different filler materials on various properties of the composites have also been discussed.

4.1 Density and Void Fraction

Density is a material property which is of prime importance in several weight sensitive applications. Thus, in many such applications polymer composites are found to replace conventional metals and materials primarily for their low densities. Density of a composite depends on the relative proportion of matrix and the reinforcing materials. There is always a difference between the measured and the theoretical density values of a composite due to the presence of voids and pores. These voids significantly affect some of the mechanical properties and even the performance of composites. Higher void contents usually mean lower fatigue resistance, greater susceptibility to water penetration and weathering [1]. The knowledge of void content is desirable for estimation of the quality of the composites. In the present research work, the theoretical and measured densities of bamboo-epoxy and glass-epoxy composites, along with the corresponding volume fraction of voids are presented in Table 4.1 and Table 4.2 respectively. It is found that the composite density values calculated theoretically from weight fractions using Eq. (3.2) are not equal to the experimentally measured values, as expected. It is evident from Table 4.1 that the density values for bamboo-epoxy composites increase with the particulate filler content. It is further observed that with the incorporation of particulate fillers, the void fractions in these composites also increase. Similar trends are noticed for the glass-epoxy composites as well irrespective of the filler type.

Table 4.1 Measured and theoretical densities along with the void fractions of the bamboo-epoxy composites with different particulate fillers

Composition		Measured density (gm/cc)	Theoretical density (gm/cc)	Volume fraction of voids (%)
B_1	Bamboo-Epoxy + 0 wt% filler	1.243	1.255	0.956
B_2	Bamboo-Epoxy + 10 wt% Red mud	1.296	1.358	4.565
B_3	Bamboo-Epoxy + 20 wt% Red mud	1.372	1.482	7.422
B_4	Bamboo-Epoxy + 10 wt% Copper slag	1.354	1.452	6.749
B_5	Bamboo-Epoxy + 20 wt% Copper slag	1.368	1.476	7.317
B_6	Bamboo-Epoxy + 10 wt% Alumina	1.348	1.421	5.137
B_7	Bamboo-Epoxy + 20 wt% Alumina	1.643	1.746	5.950
B_8	Bamboo-Epoxy + 10 wt% SiC	1.297	1.355	4.281
B_9	Bamboo-Epoxy + 20 wt% SiC	1.345	1.472	8.627

Table 4.2 Measured and theoretical densities along with the void fractions of the glass-epoxy composites with different particulate fillers

Composition		Measured density (gm/cc)	Theoretical density (gm/cc)	Volume fraction of voids (%)
Z_1	Glass-Epoxy + 0 wt% filler	1.530	1.544	0.906
Z_2	Glass-Epoxy + 10 wt% Red mud	1.650	1.705	3.225
Z_3	Glass-Epoxy + 20 wt% Red mud	1.752	1.900	7.894
Z_4	Glass-Epoxy + 10 wt% Copper slag	1.693	1.809	6.412
Z_5	Glass-Epoxy + 20 wt% Copper slag	1.701	1.846	7.854
Z_6	Glass-Epoxy + 10 wt% Alumina	1.627	1.717	5.241
Z_7	Glass-Epoxy + 20 wt% Alumina	1.800	1.933	6.880
Z_8	Glass-Epoxy + 10 wt% SiC	1.620	1.702	4.817
Z_9	Glass-Epoxy + 20 wt% SiC	1.742	1.894	8.025

4.2 Micro-hardness

Hardness is considered as one of the most important factors that govern the wear resistance of any material. In the present work, micro-hardness values of the

bamboo-epoxy composites with different particulate fillers have been obtained and are compared with those of a similar set of glass-epoxy composites. The test results (Figure 4.1) show that with the presence of particulate fillers, micro-hardness of the bamboo-epoxy composites is improved and this improvement is a function of the filler content. This trend of improvement of hardness with filler content is also observed in case of the glass-epoxy composites. As far as the comparison between the composites with bamboo and glass fiber reinforcement is concerned, the bamboo-epoxy composites exhibit superior micro-hardness values for all filler materials except SiC. Even the bamboo-epoxy composite without any particulate filler possesses greater hardness than the unfilled glass-epoxy composite. Among all the composites under this investigation, the maximum hardness value is recorded for bamboo-epoxy composite filled with 20 wt% alumina.

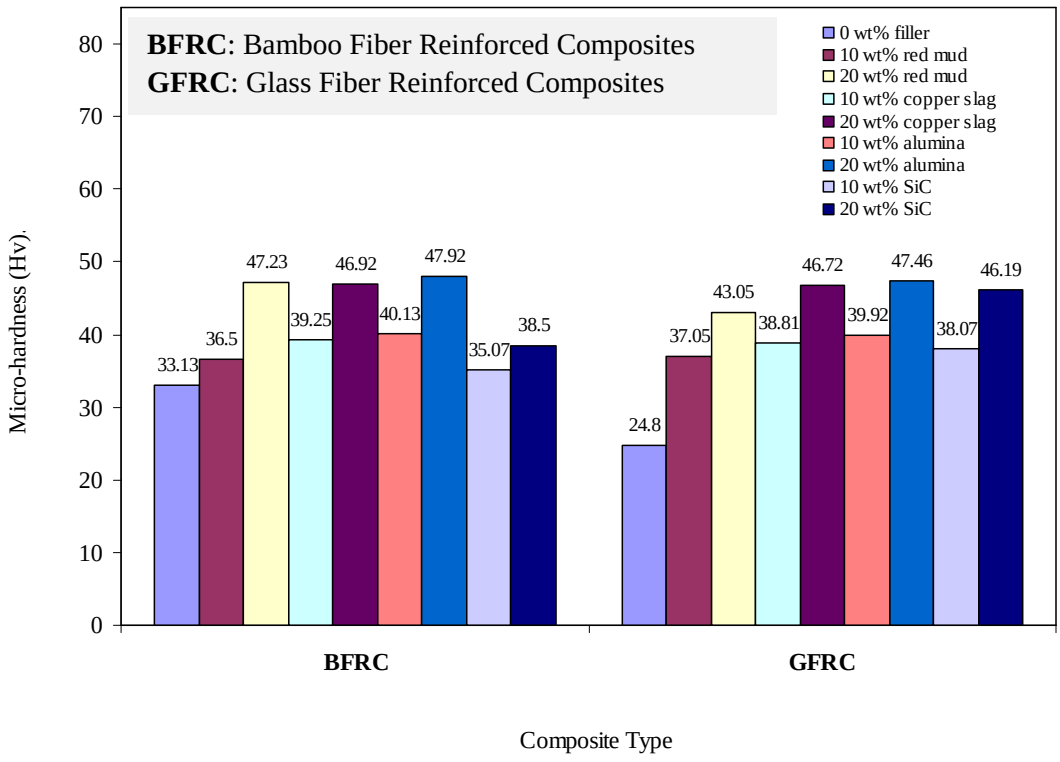

Figure 4.1 Micro-hardness of composites with different particulate fillers

4.3 Tensile Properties

The variation of tensile strength of both the bamboo-epoxy and glass-epoxy composites with different fillers is presented in Figure 4.2. Marginal

improvement in tensile strength for the bamboo-epoxy composites with the addition of 10 wt% of filler as compared to the unfilled ones is observed. However, with the incorporation of 20 wt% of the filler, the tensile strengths of these composites are found to be decreasing irrespective of the filler type. In case of glass-epoxy composites, the variation of tensile strength with filler content shows a different trend. As seen in Figure 4.2, the tensile strengths of these composites decrease invariably with increase in filler content irrespective of the type of filler. Similar observation has also been reported by previous investigators [110]**.**

This decline in strength may be attributed to two reasons: one possibility is that the due to the presence of pores at the interface between the filler particles and the matrix, the interfacial adhesion may be too weak to transfer the tensile stress; the other is that the corner points of the irregular shaped particulates result in stress concentration in the matrix body.

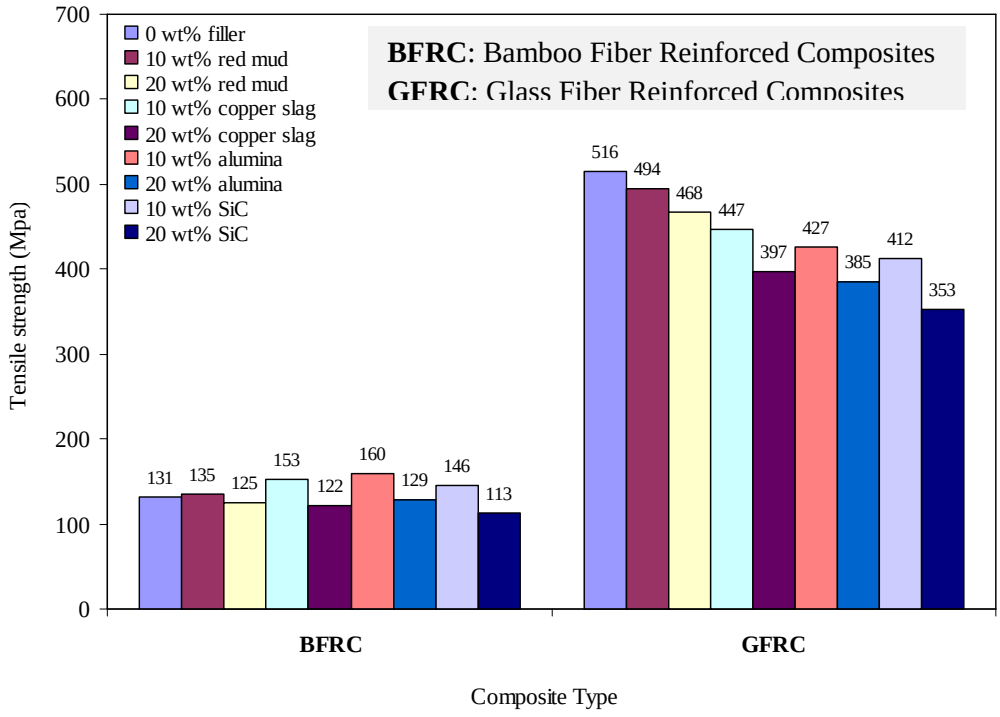

Figure 4.2 Tensile strength of composites with different particulate fillers

The variation of tensile modulus with filler content for both bamboo-epoxy as well as glass-epoxy composites with different fillers is shown in Figure 4.3. It is observed that the tensile moduli of bamboo-epoxy composites improve significantly with 10 wt% of filler content irrespective of filler type. But in case of glass-epoxy composites, similar trend is observed only for copper slag and SiC fillers. Previous reports demonstrate that normally the fibers in the composite restrain the deformation of the matrix polymer, reducing the tensile strain [236,237]. So even if the strength decreases with filler addition, the tensile modulus of the composite is expected to increase as has been observed in the present investigation. But further increase in filler content up to 20 wt%, the tensile moduli of the composites are found to be decreasing. It is further noted that as far as the tensile properties are concerned, bamboo-epoxy composites are found not as good as the glass-epoxy composites both with and without particulate fillers.

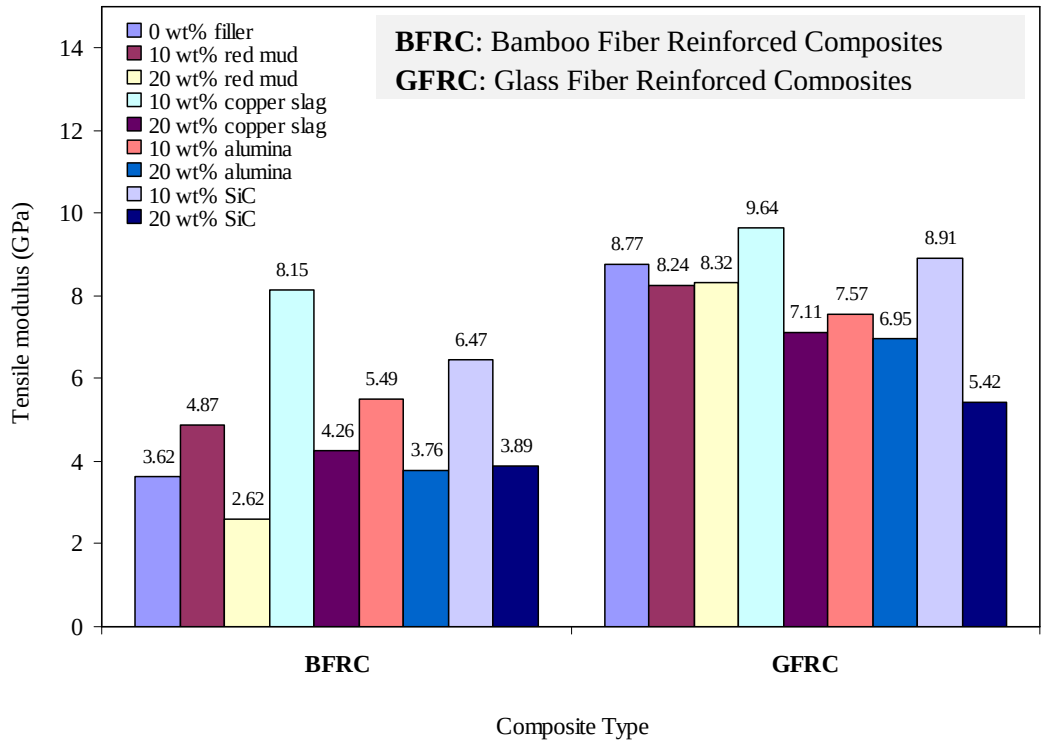

Figure 4.3 Tensile modulus of composites with different particulate fillers

4.4 Flexural Strength

Composite materials used in structures are prone to fail in bending and therefore the development of new composites with improved flexural characteristics is essential. In the present work, the variation of flexural strength of both the bamboo-epoxy and glass-epoxy composites with different particulate fillers is shown in Figure 4.4. A gradual improvement in flexural strength with filler content is recorded in case of red mud filled bamboo-epoxy composites. But for the composites with copper slag, there is a drop in flexural strength with 10 wt% of filler content followed by a marginal rise with 20 wt% of filler content. However, in case of the bamboo-epoxy composites filled with alumina and SiC, it is noticed that while the flexural strengths improve with 10wt% of filler content, further increase up to 20 wt%, the strengths are found to be decreasing.

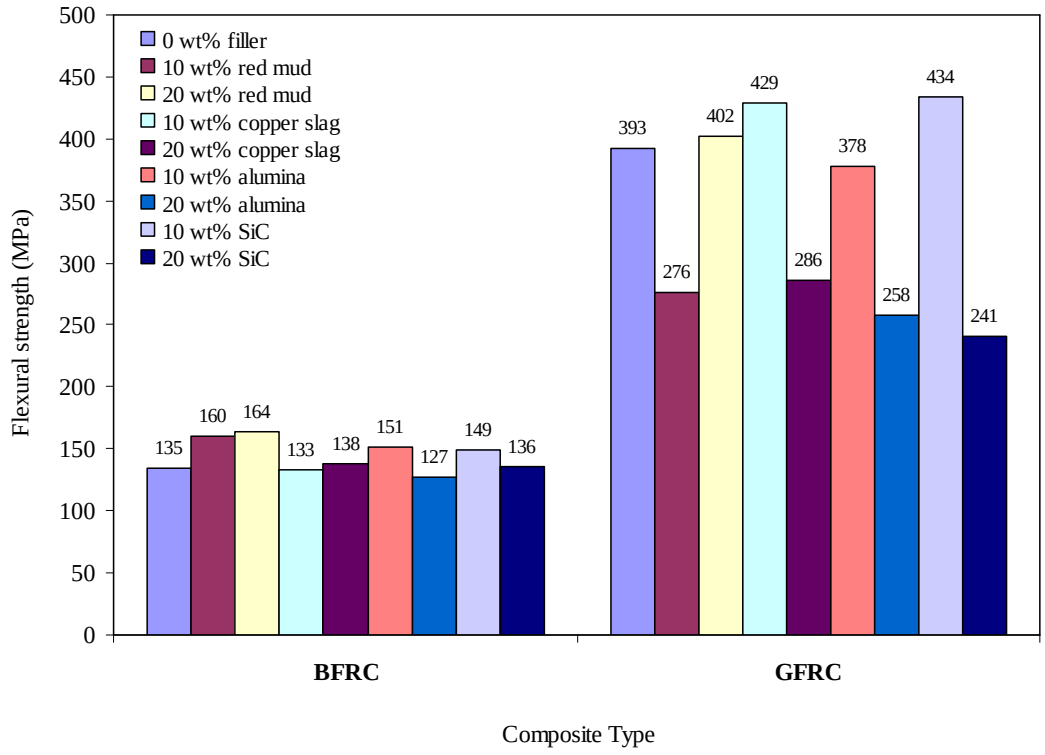

Figure 4.4 Flexural strength of composites with different particulate fillers

The reduction in the flexural strengths of the composites with filler content is probably caused by an incompatibility of the particulates and the epoxy matrix, leading to poor interfacial bonding. The lower values of flexural properties may also be attributed to fiber to fiber interaction, voids and dispersion problems.

However, it also depends on other factors such as the size, shape and type of the filler material. Influence of the particulate fillers on the flexural strength is noticed also for the glass-epoxy composites. Remarkable improvement in flexural strength is observed in copper slag (10 wt%) filled glass-epoxy and SiC (10 wt%) filled glass-epoxy composites as compared to the unfilled one. It is evident from this study that as far as the flexural strength is concerned, bamboo-epoxy composites are found not as good as the glass-epoxy composites either with or without particulate fillers.

4.5 Inter-Laminar Shear Strength (ILSS)

Short beam shear test is carried out on the composites with different particulate fillers to determine the inter-laminar shear strength (ILSS). The variation of ILSS of bamboo-epoxy and glass-epoxy composites with filler content is presented in Figure 4.5. It is observed that with the addition of 10 wt% red mud, the ILSS of bamboo-epoxy composite increases slightly but starts decreasing on further addition. In case of glass-epoxy composites, with the addition of red mud, no improvement of the ILSS value is noticed. For bamboo-epoxy composites filled with copper slag, the ILSS increases monotonically as the filler content increases from 0 wt% to 20 wt%. But the trend exhibited by the copper slag filled glass-epoxy composites is just opposite. There is a gradual reduction in ILSS with the copper slag weight percentage in the composites. With the addition of alumina, ILSS of the bamboo-epoxy composites decreases substantially. Similar trend is observed in case of alumina filled glass-epoxy composites as well. As far as the SiC filled composites are concerned, it is noted that the ILSS is increasing with the addition of filler up to 10 wt% and is decreasing with further increase in filler content up to 20 wt%. This trend is exhibited by both bamboo-epoxy as well as glass-epoxy composites filled with SiC particles. This reduction may be due to the formation of voids in the matrix which is generally located at the inter-laminar region of composites. It is interesting to note that the inter-laminar shear strengths of bamboo-epoxy composites with different particulate fillers are comparable to and often even

superior to those of glass-epoxy composites. In the present investigation, the maximum value of ILSS has been recorded for the bamboo-epoxy composite with 20 wt% of copper slag.

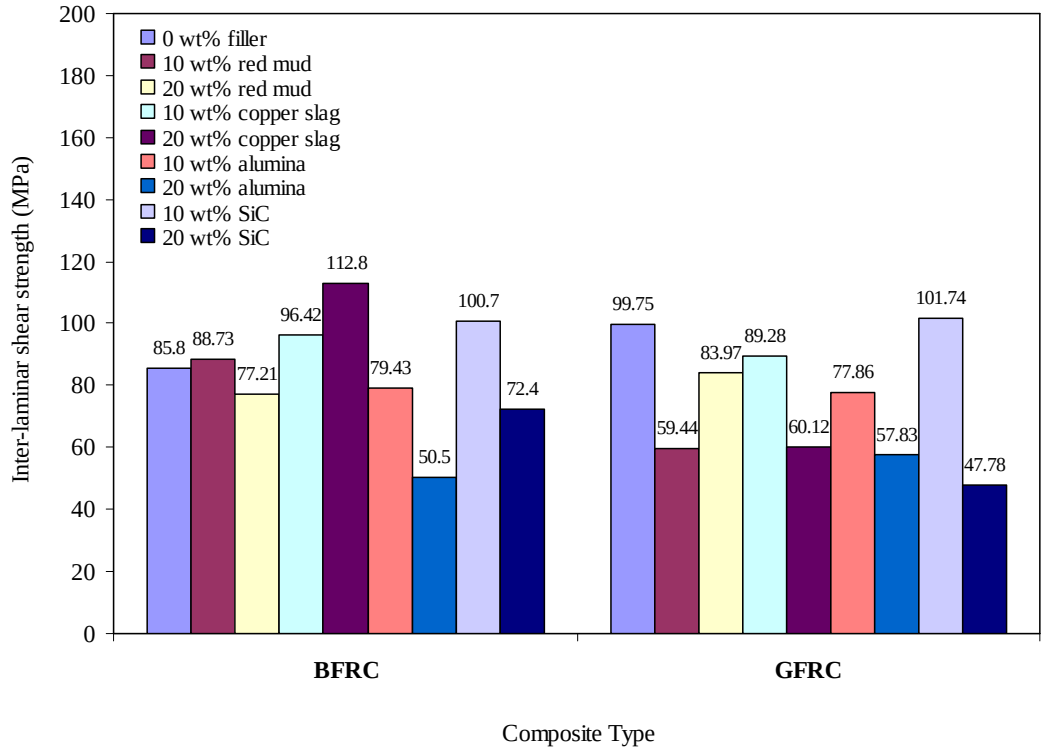

Figure 4.5 Inter-laminar shear strength of composites with different fillers

4.6 Impact Strength

The impact strength of a material is its capacity to absorb and dissipate energies under impact or shock loading. Figure 4.6 presents the measured impact energy values of the various particulate filled composites under this investigation. It is seen from this figure that the impact energies of the bamboo-epoxy composites increase gradually with the filler content increasing from 0 wt% to 20 wt% for all the fillers except SiC. In the SiC filled composites, the impact energy is found to be increasing initially with filler content of 10 wt%, but with further addition (20 wt%), there is reduction in the impact energy value. The variation of impact energy with filler content is not uniform in case of glass-epoxy composites as well. For copper slag filled glass-epoxy and alumina filled glass-epoxy composites, gradual improvements in the impact energy value with filler content

are recorded. However, for red mud filled glass-epoxy and SiC filled glass-epoxy composites, the impact energy is found to be increasing with 10 wt% of filler and then with further filler addition (20 wt%), it is seen to decrease.

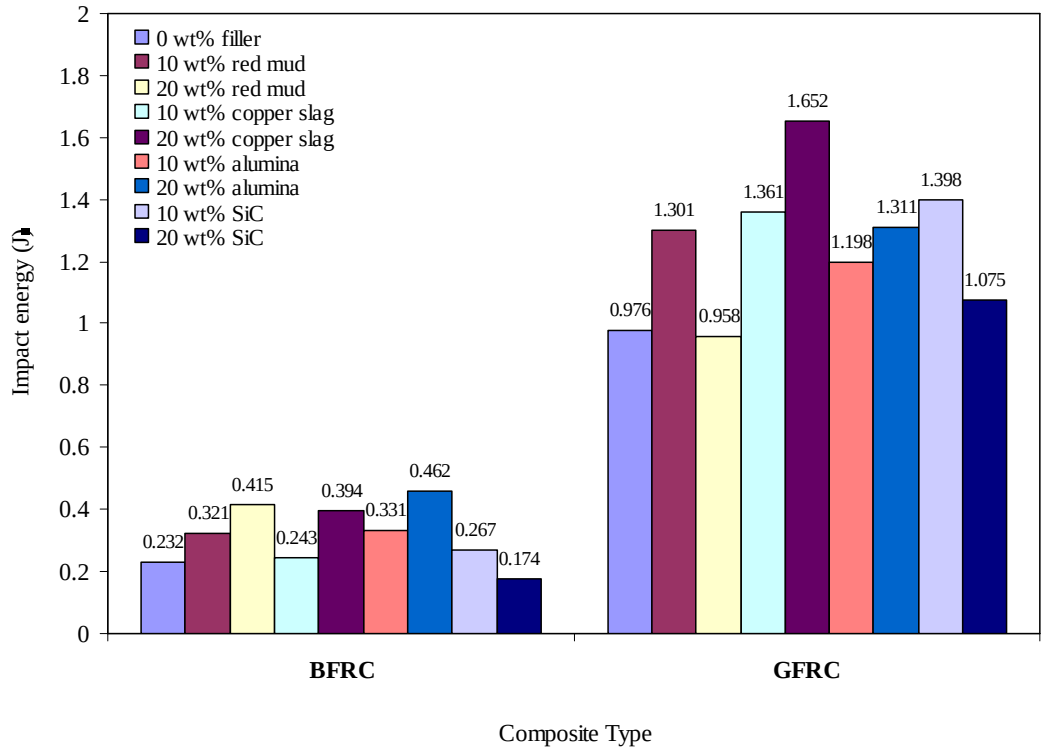

Figure 4.6 Impact strength of composites with different particulate fillers

It is clear from this investigation that the bamboo-epoxy composites have lower impact strength than their glass fiber counterparts irrespective of the filler type. However, bamboo fiber composites demonstrate better impact properties than composites reinforced with other natural fibers such as jute and kenaf [238]. Hence, for high performance applications, it is important to find ways to improve various strength properties of composites with bamboo fiber reinforcement.

Chapter Summary

This chapter has provided:

- The mechanical characterization of the bamboo-epoxy composites with different particulate fillers and a comparison with a similar set of glass-epoxy composites

- The relative effects of type and content of different particulate fillers on various properties of these composites

The next chapter presents the development of a theoretical model for estimation of erosion wear rate of polymer composites

****

Chapter 5

DEVELOPMENT OF A THEORETICAL MODEL FOR EROSION WEAR RATE ESTIMATION

This chapter focuses on the issues related to mechanism of material removal from the surface of a composite due to erosion wear and presents the development of a theoretical model for estimating the erosion wear rate caused by solid particle impact.

5.1 Nomenclature

The following symbols are used:

a	Characteristic dimension of the square pyramidal shaped erodent (m).
δ	indentation depth (m)
e_v	volumetric wear loss per impact (m^3)
E_V	total volumetric erosion rate (m^3/sec)
α	angle of impingement (degree)
U	impact velocity (m/sec)
P	force on the indenter (N)
H	hardness (N/m^2)
m	mass of single erodent particle (kg)
M	mass flow rate of the erodent (kg/sec)
N	number of impact per unit time (sec^{-1})
θ	erodent temperature (°C)
θ_o	room temperature (°C)
ρ_c	density of composite (kg/m^3)
ρ	density of erodent (kg/m^3)
η_{normal}	erosion efficiency with normal impact
η	erosion efficiency
S	specific heat of silica sand (J/Kg K)
E_r	erosion rate (kg/kg)
E_{rth}	theoretical erosion wear rate (kg/kg)

Solid particle erosion is a wear process in which the material is removed from a surface by the action of a high velocity stream of erodent particles. The particles strike against the surface and promote material loss. During flight, a particle carries momentum and kinetic energy which can be dissipated during the impact due to its interaction with a target surface. As far as erosion study of polymer matrix composites is concerned, no specific model has been developed and thus the study of their erosion behaviour has been mostly experimental. However, Mishra [239] proposed a mathematical model for material removal rate in abrasive jet machining process in which the material is removed from the work piece in a similar fashion. This model assumes that the volume of material removed is same as the volume of indentation caused by the impact. This has a serious limitation as in a real erosion process the volume of material removed is actually different from the indentation volume. Further, this model considers only the normal impact i.e $\alpha = 90°$ whereas in actual practice, particles may impinge on the surface at any angle ($0° \leq \alpha \leq 90°$). The proposed model addresses these shortcomings in an effective manner. It considers the real situation in which the volume of material removed by erosion is not same as the volume of material displaced and therefore, an additional term 'erosion efficiency' (η) is incorporated in the erosion wear rate formulation. In the case of a stream of particles impacting a surface normally (i.e. at $\alpha = 90°$), erosion efficiency (η_{normal}) defined by Sundararajan et al. [240] is given as

$$\eta_{normal} = \frac{2\,ErH}{\rho\,U^2} \tag{5.1}$$

But considering impact of erodent at any angle α to the surface, the actual erosion efficiency can be obtained by modifying Eq. (5.1) as

$$\eta = \frac{2\,ErH}{\rho\,U^2 \sin^2\alpha} \tag{5.2}$$

Another model proposed recently by Patnaik et al. [159] assumes that the kinetic energy of the impinging particles is utilized to cause indentation on the composite surface and the material loss is a measure of this indentation. It also

assumes that both the erodent material and the target material are at same temperature and therefore there is no exchange of any thermal energy between them during the impact. This may be true for a room temperature erosion situation, but when the erodent is at an elevated temperature, as in the case of hot air carrying pulverised coal powders in a pipe, there will be dissipation of the kinetic energy as well as the thermal energy from the erodent body to the target. Research on erosion of composite materials by high temperature erodent particles is rare and there is no specific model that includes the possibility of this thermal energy contributing to the magnitude of wear. Besides, while all previous models have been developed assuming the shape of erodent to be spherical, in the real situation, the erodent particles are actually irregular shaped bodies having sharp edges (Figure 5.1).

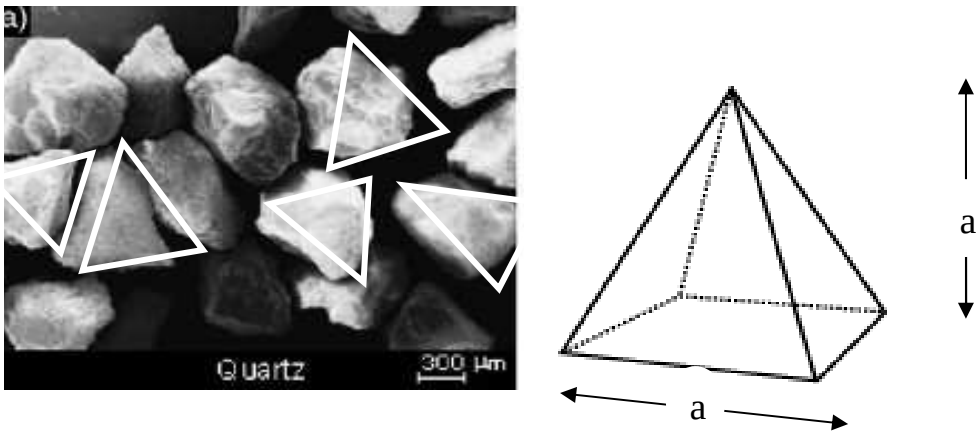

Figure 5.1 Shape of the erodent used

Considering the erodent particles to be square-pyramidal shaped bodies is a more realistic assumption as compared to assuming them simply spherical. The model proposed in the present work addresses to all these shortcomings. It assumes the erodent particles to be rigid, square-pyramidal shaped bodies of height and base length equal to the average grit size. It is further based on the assumption that the loss in both kinetic as well as thermal energy of the impinging particles is utilized to cause micro-indentation in the composite material and the material loss is a measure of the indentation. The erosion is the result of cumulative damage of such non-interacting, single particle impacts. The

model is developed with the simplified approach of energy conservation which equals the loss in erodent kinetic energy and thermal energy during impact to the work done in creating the indentation. It proceeds as follows.

At time t after initial contact, the particle of mass m will have indented the surface to a depth x; the cross-sectional area of the indentation at the surface will be A(x), where A(x) is normally determined by the shape of the erodent. The material removal mechanism is schematically shown in Figure 5.2.

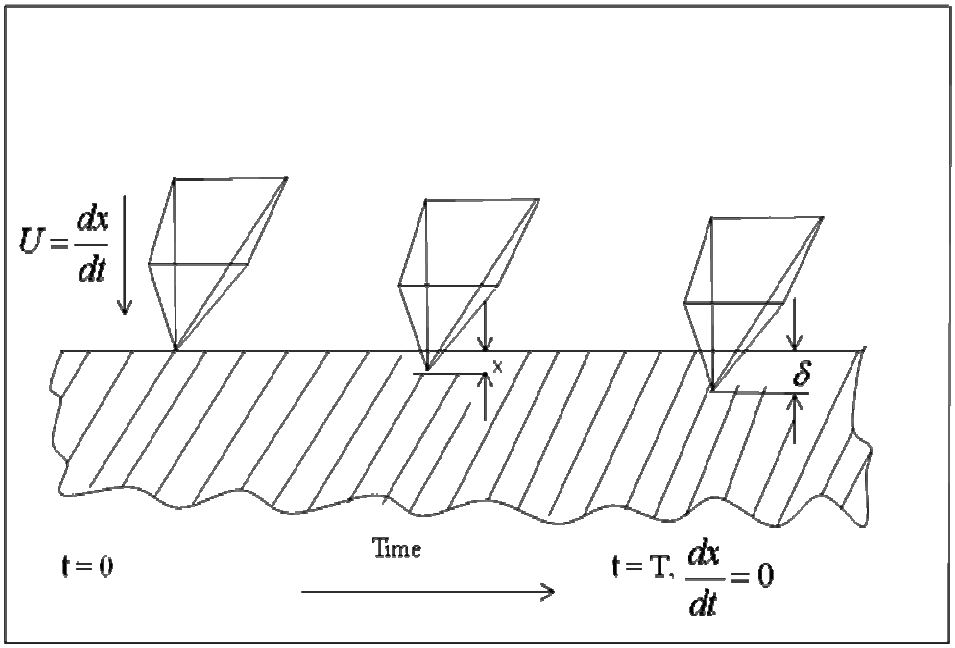

Figure 5.2 Scheme of material removal mechanism

The upward force decelerating the particle will be that due to the plastic flow pressure acting over A(x); and the equation of motion of the particle can therefore be written as: $m \frac{d^2 x}{dt^2} = - HA(x)$ (5.3)

For simple particle shapes, this equation can readily be solved analytically. But to know the final volume of indentation when the particle comes to rest at a depth δ at time t =T, as shown in Figure 5.2, the work done by the retarding force will be equal to the sum of the kinetic energy and the loss of thermal

energy of the particle. The conservation of energy can be represented by the equation

$$\int_0^{\delta} H\ A(x)\ dx = \frac{1}{2} m\ .\ U^2 + m\ .\ S(\theta - \theta_0) \qquad (5.4)$$

The impact velocity will have two components; one normal to the composite surface and another parallel to it. At an impingement angle $\alpha = 0°$, it is assumed that there is negligible wear because eroding particles do not practically impact the target surface [241]. Consequently, there will be no erosion due to the parallel component and the indentation is assumed to be caused entirely by the component normal to the composite surface as shown in Figure 5.3.

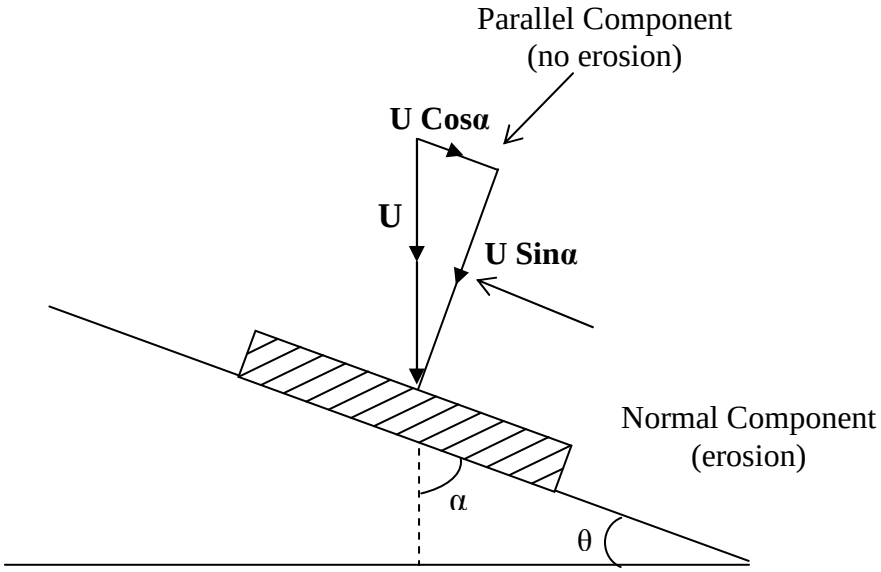

Figure 5.3 Resolution of impact velocity in normal and parallel directions

Thus, in case of oblique impact, the kinetic energy corresponding to the normal component of velocity is considered and Eq. (5.4) becomes:

$$\int_0^{\delta} HA(x)dx = \frac{1}{2} m.U^2 \sin^2\alpha + m.S(\theta - \theta_0) \qquad (5.5)$$

$$\text{Now, } \int_0^{\delta} A(x)dx = \int_0^{\delta} x^2\, dx = \frac{\delta^3}{3} \qquad (5.6)$$

So, the volumetric wear loss per particle impact is given by

e_v = Volume of indentation$\times\eta$ = $\eta.\frac{\delta^3}{3}$

Considering N number of particle impacts per unit time, the volumetric erosion wear loss will be

$$Ev = N\frac{\delta^3}{3}\eta \tag{5.7}$$

Now applying conservation of energy to the single impact erosion process, the sum of the kinetic energy associated with the normal velocity component and the loss of thermal energy of a single erodent particle is equal to the work done in the indentation of composite. The energy of impact introduces a force P on the indenter to cause the indentation in the composite. Thus,

$$\frac{1}{2}.P\times\delta = \frac{1}{2}m.U^2.\sin^2\alpha + m.S(\theta-\theta_0) \tag{5.8}$$

$$\frac{1}{2}\delta^3\times H = \frac{m.U^2.\sin^2\alpha + 2.m.S(\theta-\theta_0)}{2} \tag{5.9}$$

$$e_v = \eta\left[\frac{m.U^2.\sin^2\alpha + 2.m.S(\theta-\theta_0)}{3H}\right] \tag{5.10}$$

For multiple impact $E_V = \eta.m.N\left[\frac{U^2.\sin^2\alpha + 2.S.(\theta-\theta_0)}{3H}\right]$ (5.11)

$$\text{Or, } E_V = \eta.M\left[\frac{U^2.\sin^2\alpha + 2.S.(\theta-\theta_0)}{3H}\right] \tag{5.12}$$

The non-dimensional erosion rate, defined as the composite mass loss per unit time due to erosion divided by the mass of the erodent causing the loss, is now expressed as

$$E_r = \frac{\eta.\rho_C}{3H}\left[U^2\sin^2\alpha + 2.S(\theta-\theta_0)\right] \tag{5.13}$$

The mathematical expression in Eq. (5.13) can be used for predictive purpose to make an approximate assessment of the erosion damage from the composite

surface. When the erodent temperature is same as room temperature, Eq. (5.13) reduces to:

$$E_r = \frac{\eta \cdot \rho_c}{3H} \left[U^2 \mathrm{Sin}^2 \alpha \right] \quad (5.14)$$

Chapter Summary

This chapter has presented the development of a theoretical model for estimating the erosion wear rate caused by solid particle impact. But since, material removal by impact erosion wear involves complex mechanisms; a simplified theoretical model for such a process may appear inadequate unless its assessment against experimental results is made. So, for the validation of the proposed model, erosion tests on the composites are to be conducted at various operating conditions.

The next chapter presents the erosion test results for the composites and their statistical interpretation.

****

Chapter 6

RESULTS AND DISCUSSION: EROSION WEAR CHARACTERISTICS

This chapter reports on the effects of different particulate fillers on the erosion wear characteristics of bamboo-epoxy composites and presents a comparison with those of a similar set of glass-epoxy composites under identical test conditions. The experimental results of erosion trials carried out on these hybrid composites are presented and compared with the calculated values obtained from the theoretical model proposed in Chapter 5. Besides, the critical analysis of the test results using Taguchi method and analysis of variance (ANOVA) are also given. The relative wear performance of composites with industrial waste fillers (red mud and copper slag) against the conventional fillers (alumina and silicon carbide) is discussed. Consequently this chapter is divided into four parts, each part describing the erosion study of composites filled with a different filler material.

6.1 PART 1: RED MUD FILLED COMPOSITES

This part presents the analysis and comparison of erosion response of bamboo-epoxy and glass-epoxy composites filled with red mud. The experiments have been carried out using Taguchi experimental design (L_{27} orthogonal array) given in Table 3.5 and the subsequent analysis of the test results is made using the popular software specifically used for design of experiment applications known as MINITAB 14. Finally, the micro-structural features of the composite samples eroded under different operating conditions are described based on SEM micrographs.

6.1.1 Taguchi Experimental Analysis

The results of erosion experiments carried out according to the predetermined design on red mud filled bamboo-epoxy and glass-epoxy composites are presented in Table 6.1. This table provides the experimental erosion rate along

with the signal-to-noise ratio for each individual test run. Each value of the erosion rate is the average of three replications. Here the ninth and eleventh columns represent S/N ratio of the erosion rates for bamboo-epoxy and glass-epoxy composites respectively.

Table 6.1 Comparison of erosion rates of bamboo-epoxy composites with those of glass-epoxy composites under different test conditions as per L_{27} orthogonal array

Expt. No.	A (m/sec)	B (%)	C (°C)	D (Degree)	E (mm)	F (µm)	E_r (b) (mg/kg)	S/N ratio (b) (db)	E_r (g) (mg/kg)	S/N ratio (g) (db)
1	43	0	40	30	65	300	150.000	-43.5218	204.348	-46.2074
2	43	0	50	60	75	450	133.330	-42.4986	342.029	-50.6813
3	43	0	60	90	85	600	250.000	-47.9588	413.720	-52.3341
4	43	10	40	60	75	600	150.000	-43.5218	256.522	-48.1825
5	43	10	50	90	85	300	201.000	-46.0639	376.124	-51.5066
6	43	10	60	30	65	450	137.220	-42.7483	266.667	-48.5194
7	43	20	40	90	85	450	200.000	-46.0206	222.663	-46.953
8	43	20	50	30	65	600	350.000	-50.8814	121.739	-41.7086
9	43	20	60	60	75	300	140.000	-42.9226	175.362	-44.8787
10	54	0	40	60	85	450	277.770	-48.8737	226.087	-47.0855
11	54	0	50	90	65	600	225.000	-47.0437	353.623	-50.9708
12	54	0	60	30	75	300	290.000	-49.2480	382.147	-51.6446
13	54	10	40	90	65	300	165.000	-44.3497	139.130	-42.8684
14	54	10	50	30	75	450	152.220	-43.6494	157.342	-43.9369
15	54	10	60	60	85	600	182.500	-45.2253	191.304	-45.6345
16	54	20	40	30	75	600	125.000	-41.9382	140.192	-42.9345
17	54	20	50	60	85	300	320.000	-50.1030	274.638	-48.7752
18	54	20	60	90	65	450	211.111	-46.4902	226.087	-47.0855
19	65	0	40	90	75	600	175.000	-44.8608	163.768	-44.2846
20	65	0	50	30	85	300	390.000	-51.8213	359.420	-51.112
21	65	0	60	60	65	450	322.220	-50.1630	443.712	-52.942
22	65	10	40	30	85	450	244.440	-47.7634	173.913	-44.8066
23	65	10	50	60	65	600	215.000	-46.6488	198.193	-45.9418
24	65	10	60	90	75	300	250.000	-47.9588	168.116	-44.5122
25	65	20	40	60	65	300	330.000	-50.3703	318.152	-50.0527
26	65	20	50	90	75	450	155.550	-43.8374	214.493	-46.6283
27	65	20	60	30	85	600	275.000	-48.7867	295.652	-49.4156

Note: Er (b): Erosion rate of bamboo-epoxy composites
Er (g): Erosion rate of glass-epoxy composites

The overall mean of the S/N ratios is found to be -46.49 db for bamboo based composites and -47.47db for the glass based ones. It can be seen from Table 6.1 that for similar test conditions, bamboo-epoxy composites exhibit much lower

wear rates than those by glass-epoxy composites. Figures 6.1 and 6.2 illustrate the effect of control factors on erosion rate of bamboo-epoxy and glass-epoxy composites respectively. Analysis of the results leads to the conclusion that factor combination of A_1(Impact velocity: 43m/sec), B_2 (Filler content: 10wt%), C_1(Erodent temperature: 40°C), D_3 (Impingement angle: 90°), E_2 (Stand-off distance: 75mm) and F_2 (Erodent size: 450μm) gives minimum erosion rate (Figure 6.1) for bamboo-epoxy composites and the factor combination of A_2 (Impact velocity:54m/sec), B_2 (Filler content: 10wt%), C_1(Erodent temperature: 40°C), D_1 (Impingement angle: 30°), E_2 (Stand-off distance: 75mm) and F_3 (Erodent size: 600μm) gives minimum erosion rate (Figure 6.2) for glass epoxy composites. The respective interaction graphs are shown in the Figures 6.3 and 6.4 for bamboo epoxy and glass-epoxy composites respectively.

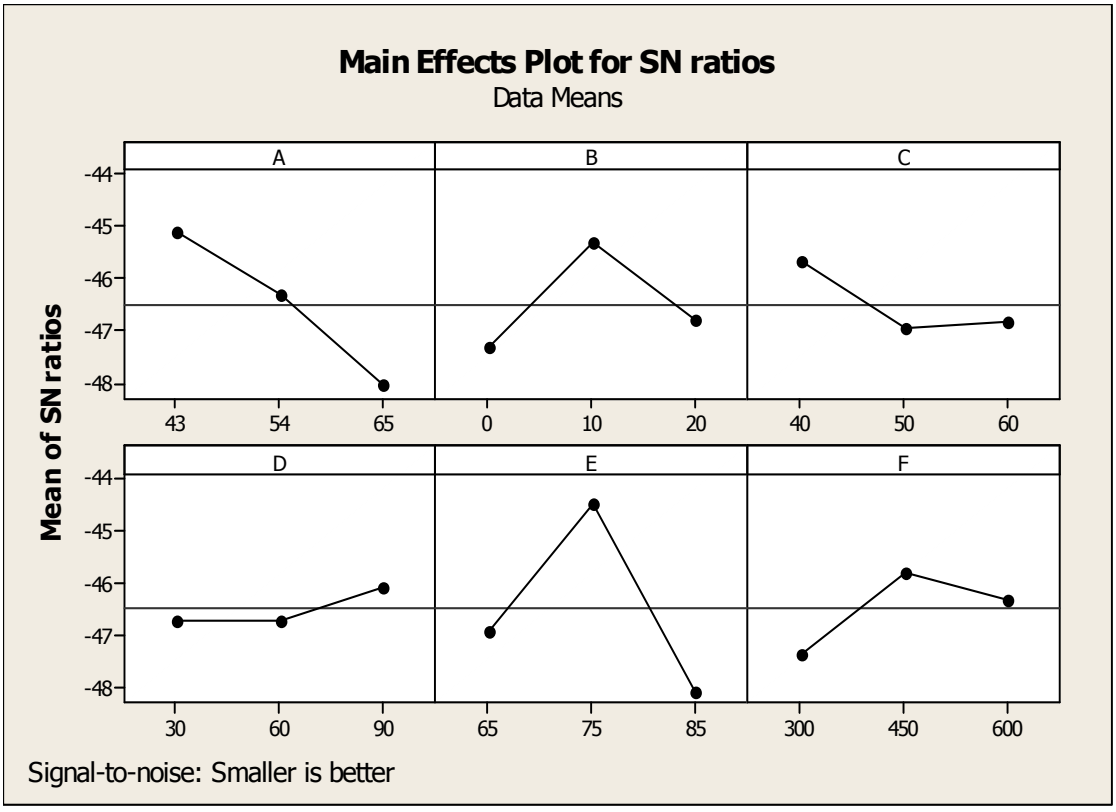

Figure 6.1 Effect of control factors on erosion rate (For red mud filled bamboo-epoxy composites)

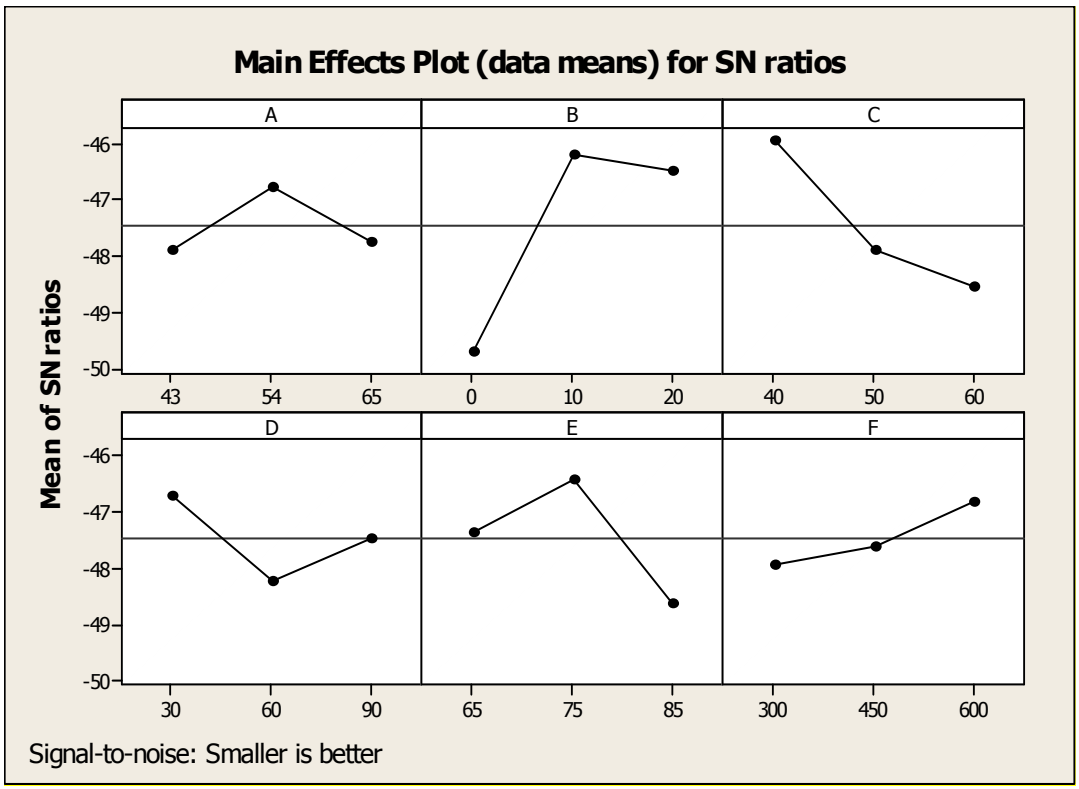

Figure 6.2 Effect of control factors on erosion rate (For red mud filled glass-epoxy composites)

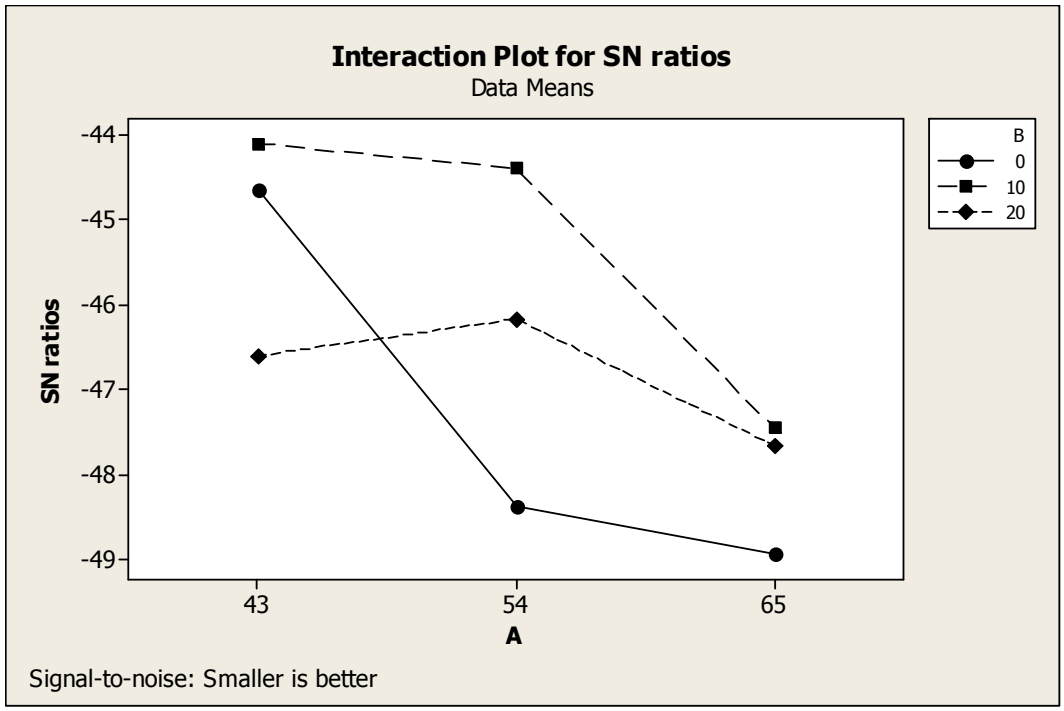

Figure 6.3 Interaction graph between impact velocity and filler content (A×B) for erosion rate (For red mud filled bamboo-epoxy composites)

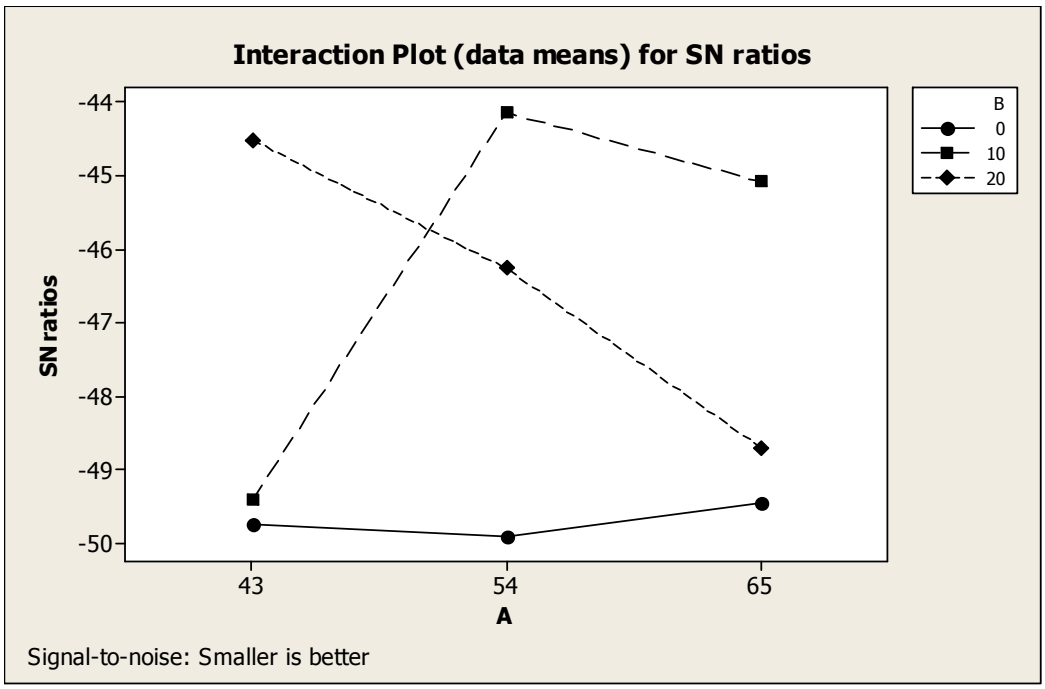

Figure 6.4 Interaction graph between impact velocity and filler content (A×B) for erosion rate (For red mud filled glass- epoxy composites)

6.1.2 ANOVA and the Effects of Factors

In order to find out statistical significance of various factors like impact velocity (A), red mud content (B), erodent temperature (C), impingement angle (D), stand-off distance (E) and erodent size (F) on erosion rate, analysis of variance (ANOVA) is performed on experimental data. Table 6.2 and Table 6.3 show the results of the ANOVA for the erosion rate of bamboo-epoxy composites and glass -epoxy composites respectively. The last column of the table indicates percentage contribution of the control factors and their interactions on the performance output i.e erosion rate [242].

From Table 6.2, it can be observed for the red mud filled bamboo-epoxy composites that stand-off distance (p=0.342), impact velocity (p = 0.450), filler content (p = 0.615), erodent size (p= 0.726) and erodent temperature (p=0.782) have considerable influence on erosion rate. The interaction of impact velocity and red mud content (p=0.861) as well as red mud content and erodent temperature (p=0.864) show significant contribution on the erosion rate but the

remaining factors and interactions have relatively less significant contribution on erosion rate.

Table 6.2 ANOVA table for erosion rate
(For red mud filled bamboo-epoxy composites)

Source	DF	Seq SS	Adj SS	Adj MS	F	P
A	2	38.14	38.14	19.07	1.22	0.450
B	2	19.55	19.55	9.77	0.63	0.615
C	2	8.71	8.71	4.35	0.28	0.782
D	2	2.46	2.46	1.23	0.08	0.927
E	2	59.93	59.93	29.97	1.92	0.342
F	2	11.79	11.79	5.89	0.38	0.726
A×B	4	18.56	18.56	4.64	0.30	0.861
A×C	4	10.98	10.98	2.75	0.18	0.932
B×C	4	18.19	18.19	4.55	0.29	0.864
Error	2	31.17	31.17	15.59		
Total	26	219.48				

[**]DF: degree of freedom, [##]Seq SS: sequential sum of squares, [$]Adj. SS: extra sum of squares[$$] Seq MS: sequential mean squares, [***]F: F-test, [###]P: percent contribution

Table 6.3 ANOVA table for erosion rate
(For red mud filled glass-epoxy composites)

Source	DF	Seq SS	Adj SS	Adj MS	F	P
A	2	6.633	6.633	3.316	10.97	0.084
B	2	67.430	67.430	33.715	111.52	0.009
C	2	33.668	33.668	16.834	55.68	0.018
D	2	10.717	10.717	5.358	17.72	0.053
E	2	22.225	22.225	11.112	36.76	0.026
F	2	6.069	6.069	3.034	10.04	0.091
A×B	4	67.335	67.335	16.834	55.68	0.018
A×C	4	7.254	7.254	1.813	6.00	0.148
B×C	4	43.687	43.687	10.922	36.13	0.027
Error	2	0.605	0.605	0.302		
Total	26	265.621				

[**]DF: degree of freedom, [##]Seq SS: sequential sum of squares, [$]Adj. SS: extra sum of squares[$$] Seq MS: sequential mean squares, [***]F: F-test, [###]P: percent contribution

Similarly, from Table 6.3, it can be observed for the red mud filled epoxy composites with glass reinforcement that red mud content (p=0.009), erodent temperature (p = 0.018), stand-off distance (p = 0.026), impingement angle (p= 0.053) and impact velocity (p=0.084) have great influence on erosion rate. The interaction of impact velocity and red mud content (p=0.018) as well as red mud content and erodent temperature (p=0.027) show significant contribution on the erosion rate but the remaining factors and interactions have relatively less significant contribution on erosion rate.

6.1.3 Confirmation Experiment

The optimal combination of control factors has been determined in the previous analysis. However, the final step in any design of experiment approach is to predict and verify improvements in observed values through the use of the optimal combination level of control factors. The confirmation experiment is performed by taking an arbitrary set of factor combination $A_2B_3C_2E_1F_3$. Here, factor D has been omitted for being the least significant. Similarly, for glass-epoxy composites the arbitrary set of factor combination $A_3B_3C_2D_3E_1$ is taken.

The estimated S/N ratio for erosion rate can be calculated with the help of following prediction equation:

$$\bar{\eta}_{\text{BF-red mud}} = \bar{T} + (\bar{A}_2 - \bar{T}) + (\bar{B}_3 - \bar{T}) + [(\bar{A}_2\bar{B}_3 - \bar{T}) - (\bar{A}_2 - \bar{T}) - (\bar{B}_3 - \bar{T})] + (\bar{C}_2 - \bar{T}) + [(\bar{B}_3\bar{C}_2 - T) - (\bar{B}_3 - \bar{T}) - (\bar{C}_2 - \bar{T})] + (\bar{E}_1 - \bar{T}) + (\bar{F}_3 - \bar{T}) \quad (6.1)$$

$$\bar{\eta}_{\text{GF-red mud}} = \bar{T} + (\bar{A}_3 - \bar{T}) + (\bar{B}_3 - \bar{T}) + [(\bar{A}_3\bar{B}_3 - \bar{T}) - (\bar{A}_3 - \bar{T}) - (\bar{B}_3 - \bar{T})] + (\bar{C}_2 - \bar{T}) + [(\bar{B}_3\bar{C}_2 - T) - (\bar{B}_3 - \bar{T}) - (\bar{C}_2 - \bar{T})] + (\bar{D}_3 - \bar{T}) + (\bar{E}_1 - \bar{T}) \quad (6.2)$$

$\bar{\eta}_{\text{BF-red mud}}, \bar{\eta}_{\text{GF-red mud}}$: Predicted average for red mud filled bamboo-epoxy composites and glass-epoxy composites respectively.

$\bar{T}$: Overall experimental average

$\bar{A}_2, \bar{A}_3\ \bar{B}_3, \bar{C}_2, \bar{D}_3, \bar{E}_1$ and $\bar{F}_3$: Mean response for factors and interactions at designated levels.

By combining like terms, the equation reduces to

$$\bar{\eta}_{\text{BF-red mud}} = \bar{A}_2\bar{B}_3 + \bar{B}_3\bar{C}_2 - \bar{B}_3 + \bar{E}_1 + \bar{F}_3 - 2\bar{T} \quad (6.3)$$

$$\bar{\eta}_{\text{GF-red mud}} = \bar{A}_3\bar{B}_3 + \bar{B}_3\bar{C}_2 - \bar{B}_3 + \bar{D}_3 + \bar{E}_1 - 2\bar{T} \quad (6.4)$$

A new combination of factor levels A_2, A_3, B_3, C_2, D_3, E_1 and F_3 is used to predict erosion rate through prediction equation and it is found to be $\bar{\eta}_{\text{BF-red mud}} = -47.8828\,\text{dB}$ and $\bar{\eta}_{\text{GF-red mud}} = -47.8035\,\text{dB}$ respectively.

For each performance measure, an experiment is conducted for the same set of factor combinations and the obtained S/N ratio value is compared with that obtained from the predictive equation as shown in Table 6.4.

The resulting model seems to be capable of predicting erosion rate to a reasonable accuracy. An error of 4.63 % and 3.61 % for the S/N ratio of erosion rate is observed for bamboo-epoxy composites and glass-epoxy composites respectively. If the observed S/N ratios under the recommended settings are close to their respective prediction, then we conclude that the chosen design is functionally adequate. Otherwise, a new design cycle will be initiated since this will indicate that some of the assumptions made during the analysis may not be valid, for example, the effects of ignoring interaction between different design factors. However, the error can be further reduced if the number of measurements is increased. This validates the mathematical model for predicting the measures of performance based on knowledge of the input parameters.

Table 6.4 Results of the confirmation experiments for erosion rate

	Optimal control parameters (For bamboo-epoxy composites)		Optimal control parameters (For glass-epoxy composites)	
	Prediction	Experimental	Prediction	Experimental
Level	$A_2B_3C_2E_1F_3$	$A_2B_3C_2E_1F_3$	$A_3B_3C_2D_3E_1$	$A_3B_3C_2D_3E_1$
S/N ratio for Erosion rate (db)	-47.8828	-45.6658	-47.8035	-46.0775

6.1.4 Effect of Impingement Angle and Erodent Temperature on Erosion

Generally, the erosion behavior of materials is broadly classified as either ductile or brittle depending on the variation of erosion rate with impingement angle. Ductile behavior is characterized by maximum erosion occurring at low impingement angles in the range of 10-30°. On the other hand, if maximum erosion occurs at 90°, then the behavior is said to be brittle. However, most of the reinforced polymer composites have been found to exhibit semi-ductile behavior with maximum erosion rate at intermediate angles typically in the range of 45-60° [225]. In the present study, the variation of erosion rate of the red mud filled bamboo-epoxy and glass-epoxy composites with impingement angle is obtained by conducting experiments under specified operating conditions (Figure 6.5). It shows the peak erosion taking place at an impingement angle of 60° for the unfilled as well as for the red mud filled bamboo-epoxy and glass-epoxy composites. This clearly indicates that these composites respond to solid particle impact neither in a purely ductile nor in a purely brittle manner. This behaviour can be termed as semi-ductile in nature which is in agreement with the trend observed in previous investigations [243].

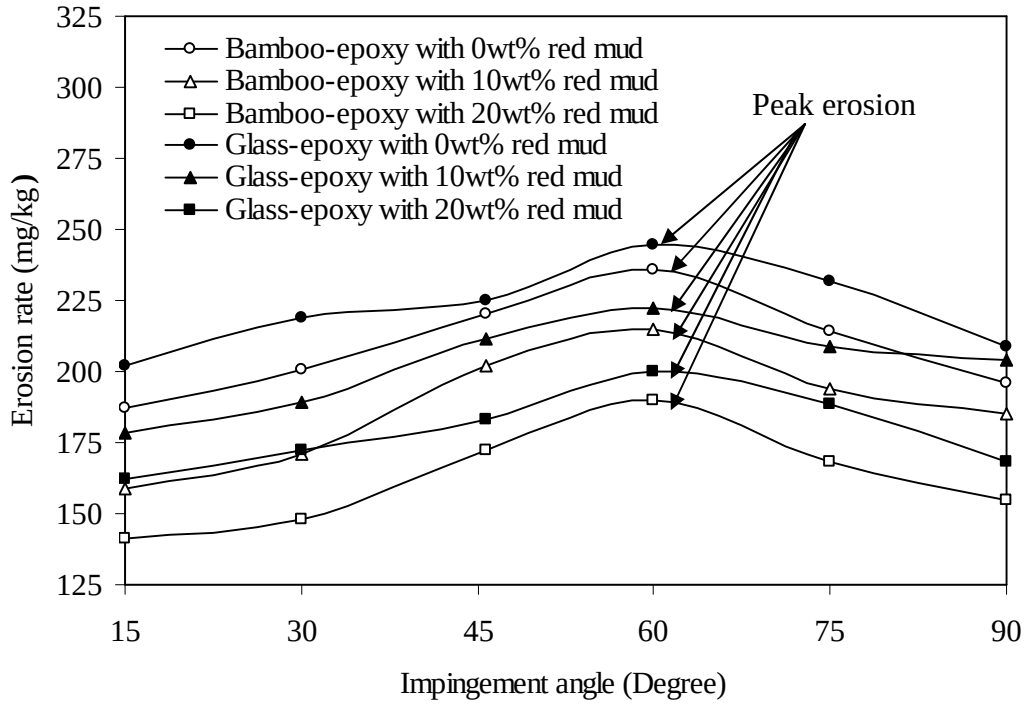

Figure 6.5 Effect of impingement angle on the erosion rate of the composites

Similarly, erosion trials are conducted at seven different erodent temperatures under normal impact condition and the variation of erosion rate of unfilled and red mud filled composites with erodent temperature is shown in Figure 6.6. It is evident from the figure that for all the composite samples, the erosion rates remain almost unaffected by the change in erodent temperature from ambient to 40°C. However, the effect of erodent temperature on erosion rate is significant above 40°C and the rate of increase in erosion rate is greater at higher erodent temperatures. The increase in erosion rate with erodent temperature can be attributed to increased penetration of particles on impact as a result of dissipation of greater amount of particle thermal energy to the target surface. This leads to surface damage, enhanced crack growth and consequently to the reduction in erosion resistance.

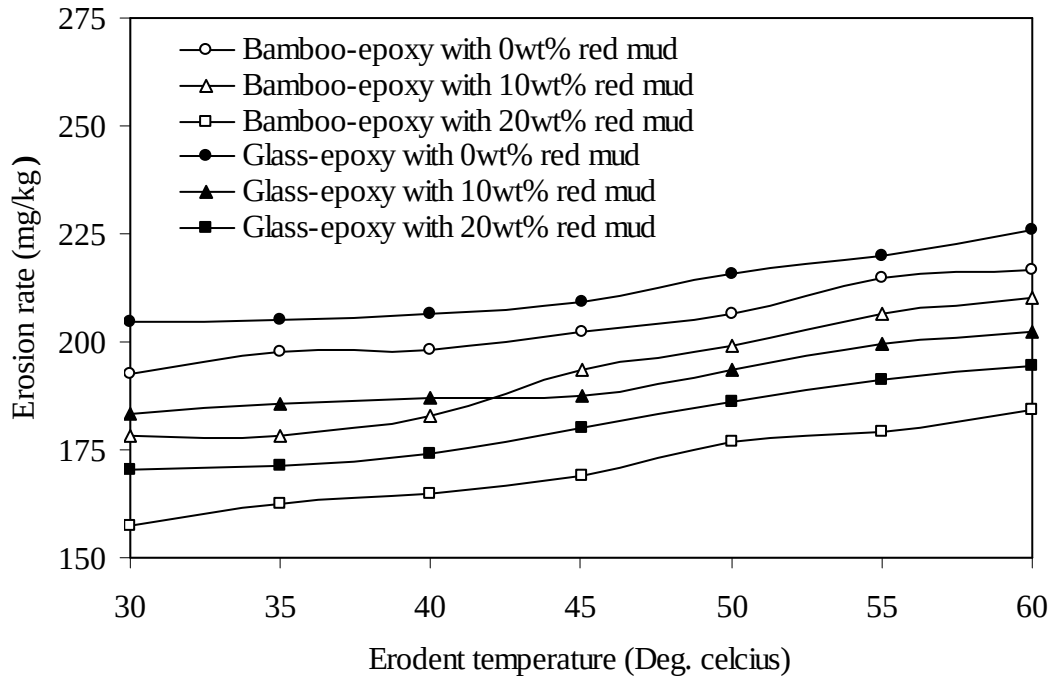

Figure 6.6 Effect of erodent temperature on the erosion rate of the composites

6.1.5 Erosion Efficiency

The hardness alone is unable to provide sufficient correlation with erosion rate, largely because it determines only the volume displaced by each impact and not really the volume eroded. Thus a parameter which will reflect the efficiency with which the volume that is displaced is removed should be combined with

hardness to obtain a better correlation and the erosion efficiency is obviously one such parameter. This thought has already been reflected during the development of the theoretical model proposed in Chapter 5, but the evaluation of erosion efficiency can only be made on the basis of experimental data. Hence, the values of erosion efficiencies of these composites calculated using Eq. (5.2) is summarized in Table 6.5 for bamboo-epoxy composites and Table 6.6 for glass-epoxy composites along with their density and operating conditions.

Table 6.5 Erosion efficiency of red mud filled bamboo-epoxy composites

Expt. No.	Impact Velocity (U) m/sec	Density of eroding material (ρ) kg/m^3	Hardness of eroding material (H_v)	Erosion rate (Er) mg/kg	Erosion efficiency (η)%
1	43	1255	33.13	150.000	16.801
2	43	1255	33.13	133.330	4.978
3	43	1255	33.13	250.000	7.000
4	43	1358	27.50	150.000	4.296
5	43	1358	27.50	201.000	4.317
6	43	1358	27.50	137.220	11.790
7	43	1482	47.23	200.000	6.761
8	43	1482	47.23	350.000	47.328
9	43	1482	47.23	140.000	6.310
10	54	1255	33.13	277.770	6.576
11	54	1255	33.13	225.000	3.995
12	54	1255	33.13	290.000	20.597
13	54	1358	27.50	165.000	2.247
14	54	1358	27.50	152.220	8.293
15	54	1358	27.50	182.500	3.314
16	54	1482	47.23	125.000	10.718
17	54	1482	47.23	320.000	9.146
18	54	1482	47.23	211.111	4.525
19	65	1255	33.13	175.000	2.144
20	65	1255	33.13	390.000	19.117
21	65	1255	33.13	322.220	5.265
22	65	1358	27.50	244.440	6.383
23	65	1358	27.50	215.000	2.695
24	65	1358	27.50	250.000	2.350
25	65	1482	47.23	330.000	6.510
26	65	1482	47.23	155.550	2.301
27	65	1482	47.23	275.000	16.274

It clearly shows that erosion efficiency is not exclusively a material property; but also depends on other operational variables such as impingement angle and impact velocity. The erosion efficiencies of these composites under normal

impact (η_{normal}) vary from 3-6%, 6-9% and 9-12% for impact velocities 65m/sec, 54m/sec and 43m/sec respectively. The value of η for a particular impact velocity under oblique impact can be obtained simply by multiplying a factor $1/Sin^2\alpha$ with η_{normal}. Similar observation on velocity dependence of erosion efficiency has previously been reported by few investigators [159, 160].

Table 6.6 Erosion efficiency of red mud filled glass-epoxy composites

Expt. no.	Impact Velocity (U) m/sec	Density of eroding material (ρ) kg/m^3	Hardness of eroding material (H_v)	Erosion rate (Er) mg/kg	Erosion efficiency (η)
1	43	1530	24.80	204.348	14.054
2	43	1530	24.80	342.029	7.841
3	43	1530	24.80	413.720	7.113
4	43	1650	37.05	256.522	8.147
5	43	1650	37.05	376.124	8.959
6	43	1650	37.05	266.667	25.407
7	43	1752	43.05	222.663	5.803
8	43	1752	43.05	121.739	12.692
9	43	1752	43.05	175.362	6.094
10	54	1530	24.80	226.087	3.286
11	54	1530	24.80	353.623	3.855
12	54	1530	24.80	382.147	16.665
13	54	1650	37.05	139.130	2.101
14	54	1650	37.05	157.342	9.505
15	54	1650	37.05	191.304	3.852
16	54	1752	43.05	140.192	9.268
17	54	1752	43.05	274.638	6.052
18	54	1752	43.05	226.087	3.736
19	65	1530	24.80	163.768	1.232
20	65	1530	24.80	359.420	10.818
21	65	1530	24.80	443.712	4.452
22	65	1650	37.05	173.913	5.035
23	65	1650	37.05	198.193	2.754
24	65	1650	37.05	168.116	1.752
25	65	1752	43.05	318.152	4.839
26	65	1752	43.05	214.493	2.446
27	65	1752	43.05	295.652	13.490

The theoretical erosion wear rate (E_{rth}) of the red mud filled bamboo-epoxy composites are calculated using Eq. (5.13). These values are compared with those obtained from experiments (E_{rexpt}) conducted under similar operating

conditions. Table 6.7 presents a comparison among the theoretical and experimental results and the associated percentage errors for both red mud filled bamboo-epoxy as well as glass-epoxy composites. The errors in experimental results with respect to the theoretical ones lie in the range 0-14%.

Table 6.7 Comparison of theoretical and experimental erosion rates along with the percentage errors for red mud filled bamboo-epoxy and glass-epoxy composites

Expt. No.	E_{rbth} (b) (mg/kg)	$E_{rbexpt.}$(b) (mg/kg)	Error (b) (%)	E_{rth} (g) (mg/kg)	$E_{rexpt.}$(g) (mg/kg)	Error (g) (%)
1	170.086	150.000	11.809	231.712	204.348	11.809
2	151.192	133.330	11.814	387.851	342.029	11.814
3	289.180	250.000	13.548	479.506	413.720	13.719
4	163.365	150.000	8.181	248.364	256.522	03.284
5	194.286	201.000	3.455	346.136	376.124	08.663
6	141.383	137.220	2.945	244.771	266.667	08.945
7	186.695	200.000	7.126	254.253	222.663	12.424
8	343.939	350.000	1.762	137.891	121.739	11.713
9	158.371	140.000	11.600	203.632	175.362	13.883
10	281.179	277.770	1.2126	236.075	226.087	4.230
11	209.197	225.000	7.553	329.054	353.623	07.466
12	271.586	290.000	6.780	358.521	382.147	06.589
13	158.914	165.000	3.829	132.813	139.130	04.755
14	139.181	152.220	9.367	169.921	157.342	07.403
15	208.016	182.500	12.266	218.533	191.304	12.460
16	122.924	125.000	1.688	134.217	140.192	04.451
17	337.898	320.000	5.296	264.174	274.638	03.960
18	192.654	211.111	9.580	206.321	226.087	09.580
19	162.100	175.000	7.957	159.040	163.768	02.972
20	372.461	390.000	4.708	417.574	359.420	13.926
21	289.323	322.220	11.370	475.002	443.712	6.587
22	235.579	244.440	3.761	168.002	173.913	03.518
23	204.757	215.000	5.002	205.786	198.193	03.689
24	232.623	250.000	7.469	169.358	168.116	00.733
25	293.379	330.000	12.482	307.745	318.152	03.381
26	164.858	155.550	5.646	189.435	214.493	13.227
27	260.542	275.000	5.549	310.147	295.652	04.673

Note: (b): bamboo-epoxy composites

(g): glass-epoxy composites

The magnitude of η can be used to characterize the nature and mechanism of erosion. For example, ideal micro-ploughing involving just the displacement of

the material from the crater without any fracture (and hence no erosion) will result in η=0. In contrast, if the material removal is by ideal micro-cutting, η = 1.0 or 100%. If erosion occurs by lip or platelet formation and their fracture by repeated impact, as is usually in the case of ductile materials, the magnitude of η will be very low, i.e η ≤ 10%. In the case of brittle materials, erosion occurs usually by spalling and removal of large chunks of materials resulting from the interlinking of lateral or radial cracks and thus η can be expected to be even greater than 100% [155]. The erosion efficiencies of the composites under the present study indicate that at low impact velocity the erosion response is semi-ductile (η=10-100%). On the other hand at relatively higher impact velocity the composites exhibit ductile (η < 10%) erosion behaviour [225].

6.1.6 Surface Morphology

To ascertain the wear mechanism in composites, scanning electron microscopy (SEM) has been done and the micrographs of the surfaces of unfilled and red mud filled composites eroded at different impingement angles are shown in Figures 6.7 and 6.8 respectively. Figure 6.7 presents the SEM of the unfilled bamboo-epoxy composite surfaces eroded under various test conditions. In Figure 6.7a, no cracks or craters are seen on the composite surface after erosion due to impact of dry silica sand particles (temperature 40°C) of smallest erodent size (300 µm) with a lower impact velocity (43 m/sec) at an impingement angle of 90°. But as the erosion tests are carried out at higher erodent temperature (60°C) and erodent size (450 µm), the morphology of the eroded surface becomes different as in Figure 6.7b. Generally, in ductile erosion response, repeated impacts lead to plastic indentation and heavily strained regions on the surface while in the case of brittle response, the propagation of cracks towards the surface and their intersection to form a wear particle separated from the surface lead to material loss. As seen in Figure 6.7a, both processes appear to be operative. Initially the surface is strained and displaced in the plane by repeated impacts of the erodent particles. Regions are formed due to simultaneous generation of cracks exhibiting a brittle response. The extent of plastic

indentation, however, decreased as the angle of impingement is lowered as seen in other micrographs (Figures 6.7b-f).

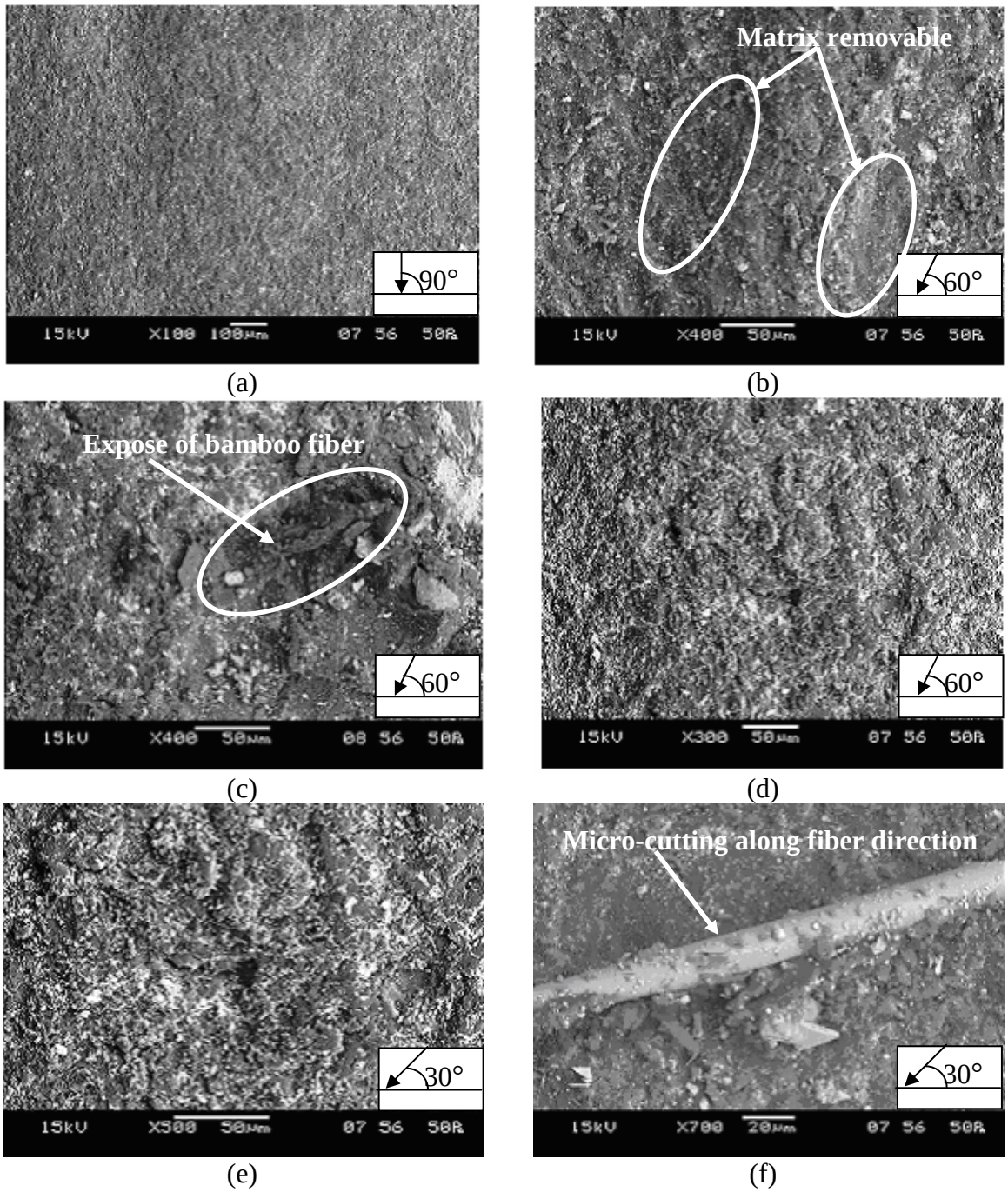

Figure 6.7 SEM graph of bamboo fiber reinforced epoxy composites

When the impingement angle is changed to 60°, the features seen are quite different (Figure 6.7b). The normal component of the impact force was still effective in producing plastic indentation creating patches similar to Figure 6.7a.

The tangential component, on other hand is now operative in cutting action. Most parts of the micrograph show evidence of material flow in the direction of impingement. As seen in Figures 6.7c, d and e with impact velocity of 65 m/sec and at an erodent temperature of 60°C, the dominance of plastic indentation reduce with impingement angle, though micro-cracking persists. Figure 6.7f shows unique features as the entire surface indicates the dominance of the micro-cutting process, a characteristic failure feature for ductile materials at very low angle. This mechanism is responsible for the highest material removal at an erodent temperature of 50°C and impact velocity of 54m/sec. It is also evident from these microstructures that for higher erodent temperature and impact velocity, the damage to the surface is also relatively greater.

Morphologies of the worn surfaces of red mud filled bamboo-epoxy composites are shown in Figure 6.8. The removal of matrix material from the impact surface of the composite with 10wt % of red mud eroded at lower impingement angle (30°), lower impact velocity (43m/sec) resulting in exposure of small amount of fibers to erosive environment can be clearly seen (Figure 6.8a). The fibers are still held firmly in place as yet by the matrix surrounding them (Figure 6.8b). The fiber-matrix debonding, brittle fracture of matrix and pulverization of fibers are also reflected in the micrograph (Figure 6.8b). When impact velocity increases to 54m/sec, impingement angle changes to 60°, erodent temperature at 60°C and filler content 20wt%, the fibers are completely broken by means of shearing action and protruding of fibers from matrix are seen in Figures 6.8c and 6.8d. Figures 6.8e and 6.8f show worn surfaces of bamboo-epoxy composite with 20 wt% red mud at higher impact velocity (65m/sec), higher impingement angle (90°) and higher erodent temperature (60°C). Here, the erosion mechanism is characterized by clean removal of the matrix and exposure of bamboo fibers. Further damage is characterized by separation and detachment of broken fibers from the resin matrix. There is an evidence of fiber removal leaving behind cavities along the length of fibers (Figure 6.8e). At higher impact velocity (65m/sec) due to continuous exposure of fibers to erosion environment results in

fiber thinning, detachment of fibers from the matrix and cavities left after fiber being dislodged may also be seen (Figure 6.8f). Micro-cracking, micro-cutting and pulverization of matrix and fibers appear to be the main features in the micrograph. The damage at higher impact velocity is more severe, because of excessive wear and the fibers seem to be washed away from the surface (Figures 6.8c-f).

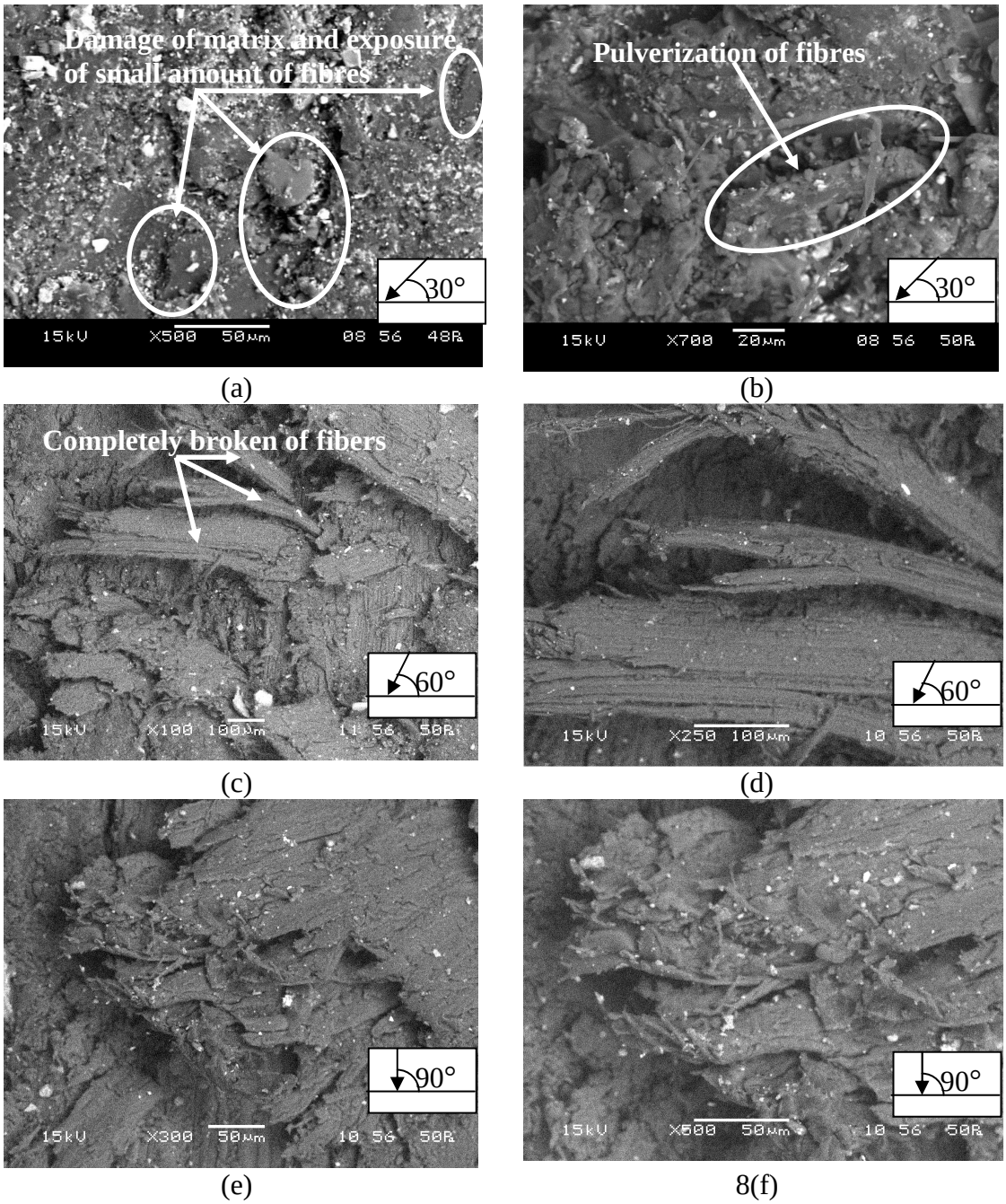

Figure 6.8 SEM micrographs of the eroded bamboo-epoxy composites filled with red mud

The magnitude of erosion rates caused by sand particle impact in bamboo-epoxy composites is found to be different from that in case of glass-epoxy composites although the same filler material i.e. red mud is present in both. So, in an attempt to get an insight to the material removal mechanism in these composites, SEM study of some of the eroded samples of glass-epoxy composites is also done.

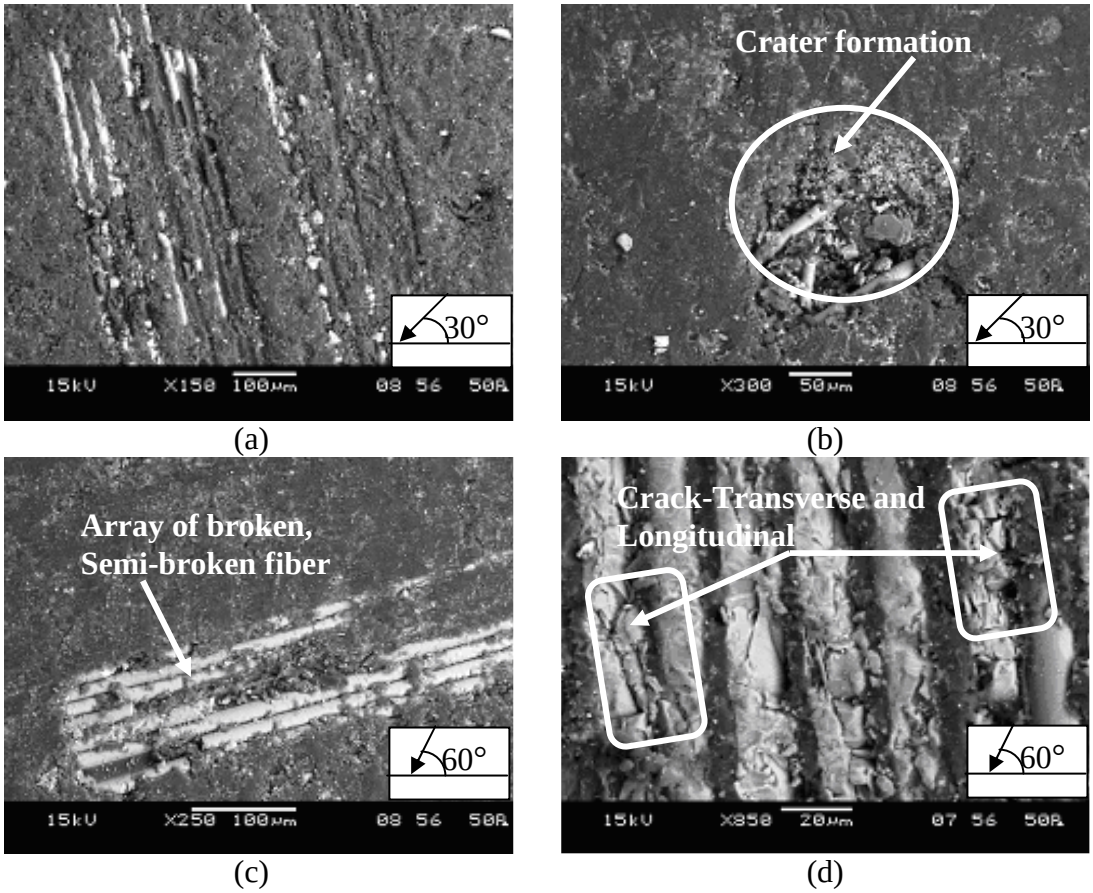

Figure 6.9 SEM images of eroded surfaces of the unfilled glass-epoxy composites

Figure 6.9 presents the SEM of surfaces of the unfilled glass-epoxy composite eroded under various test conditions. In Figure 6.9a the matrix is chipped off and the glass fibers are clearly visible beneath the matrix layer after the impact of dry silica sand particles (temperature 40°C) of size (300 µm) with a lower impact velocity (43 m/sec) at a low impingement angle of 30°. The micrograph with a higher magnification presented in Figure 6.9b distinctly illustrates a crater formed due to material loss and the arrays of broken and semi-broken glass fibers within. Due to repeated impact of hard and high temperature sand particles

there is initiation of cracks on the fibers and as erosion progresses, these cracks subsequently propagate on the fiber bodies both in transverse as well as in longitudinal manner. But when the erosion tests are carried out with higher erodent temperature (60°C), impingement angle of 60° and erodent size (450 µm), the morphology of the eroded surface is different as shown in Figures 6.9c and 6.9d. From the SEM observations of the eroded surfaces of the glass-epoxy composites filled with different red mud content, shown in Figure 6.10, it appears that composites under consideration exhibit several stages of erosion and material removal process. Very small craters and short cracks are seen on the eroded surface of the composite with 10 wt% red mud indicating the initiation of matrix material loss from the surface (Figure 6.10a). Figures 6.10a and 6.10b also show signs of plastic deformation of the matrix material and when impacting at a low angle (30°), the hard erodent particles penetrate the surface and cause material removal mostly by micro-ploughing. Figure 6.10c shows the micrograph of the same composite surface eroded at an impingement angle of 60° and an impact velocity of 54 m/sec. The matrix covering the fiber seems to be chipped off and the crater thus formed shows the fiber body which is almost intact. Repeated impact of the erodent has caused roughening of the surface. Fragmentation of the fibers as a result of cracks and multiple fractures are also distinctly shown in Figure 6.10d. Figures 6.10e-h are the SEM images for the glass-epoxy composites filled with 20 wt% red mud. At low impact velocity (43m/sec) and impingement angle (30°), the damage to the surface is minimal as seen in Figures 6.10e and 6.10f. After the local removal of matrix, the arrays of fibers are normally exposed to erosive environment and subsequently the material removal becomes faster. The wear trace is distinctly visible and there is protrusion of fibers beneath the matrix layer as seen in Figure 6.10g. The broken fiber and fragmented red mud particles, seen in Figure 6.10h, are mixed with the matrix micro-flake debris and the damage of the composite is characterized by the separation and detachment of this debris.

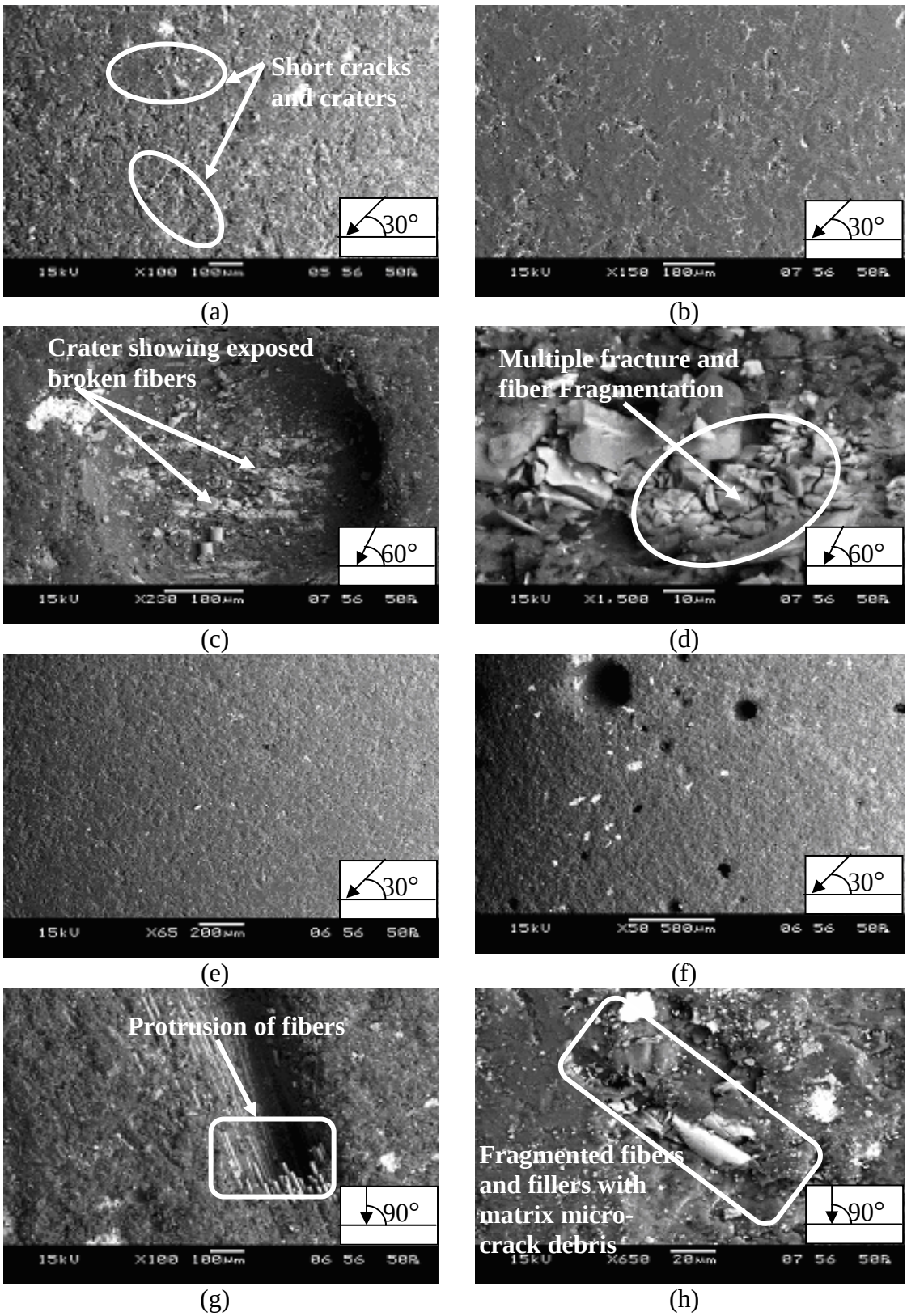

Figure 6.10 SEM micrographs of eroded glass-epoxy composites filled with red mud

6.2 PART 2: COPPER SLAG FILLED COMPOSITES

This part presents the analysis and comparison of erosion response of bamboo-epoxy and glass-epoxy composites filled with copper slag.

6.2.1 Taguchi Experimental Analysis

The results of erosion experiments carried out according to Taguchi experimental design on copper slag filled bamboo-epoxy and glass-epoxy composites are presented in Table 6.8. The overall mean for the S/N ratio of the erosion rate is found to be -47.08 db for bamboo based composites and -47.62 db for glass based ones (Table 6.8).

Table 6.8 Comparison of erosion rates of bamboo-epoxy composites with those of glass-epoxy composites under different test conditions as per L_{27} orthogonal array

Expt. No.	A (m/sec)	B (%)	C (^{0}C)	D (Degree)	E (mm)	F (µm)	E_r (b) (mg/kg)	S/N ratio (b) (db)	E_r (g) mg/kg)	S/N ratio (g) (db)
1	43	0	40	30	65	300	150.00	-43.521	204.348	-46.207
2	43	0	50	60	75	450	133.33	-42.498	342.029	-50.681
3	43	0	60	90	85	600	250.00	-47.958	413.720	-52.334
4	43	10	40	60	75	600	237.50	-47.513	273.913	-48.752
5	43	10	50	90	85	300	139.00	-42.860	284.058	-49.068
6	43	10	60	30	65	450	233.33	-47.359	389.247	-51.804
7	43	20	40	90	85	450	211.11	-46.490	163.768	-44.284
8	43	20	50	30	65	600	287.50	-49.172	234.319	-47.396
9	43	20	60	60	75	300	170.00	-44.609	239.192	-47.574
10	54	0	40	60	85	450	277.77	-48.873	226.087	-47.085
11	54	0	50	90	65	600	225.00	-47.043	353.623	-50.970
12	54	0	60	30	75	300	290.00	-49.248	382.147	-51.644
13	54	10	40	90	65	300	172.00	-44.710	307.246	-49.749
14	54	10	50	30	75	450	244.44	-47.763	156.522	-43.891
15	54	10	60	60	85	600	187.50	-45.460	200.197	-46.029
16	54	20	40	30	75	600	262.50	-48.382	204.348	-46.207
17	54	20	50	60	85	300	240.00	-47.604	214.493	-46.628
18	54	20	60	90	65	450	133.33	-42.498	276.371	-48.829
19	65	0	40	90	75	600	175.00	-44.860	163.768	-44.284
20	65	0	50	30	85	300	390.00	-51.821	359.420	-51.112
21	65	0	60	60	65	450	322.22	-50.163	443.712	-52.942
22	65	10	40	30	85	450	255.55	-48.149	121.739	-41.708
23	65	10	50	60	65	600	262.50	-48.382	197.101	-45.893
24	65	10	60	90	75	300	247.00	-47.853	221.890	-46.922
25	65	20	40	60	65	300	360.00	-51.126	144.928	-43.223
26	65	20	50	90	75	450	200.00	-46.020	202.899	-46.145
27	65	20	60	30	85	600	287.50	-49.172	167.892	-44.500

Note: Er (b): Erosion rate of bamboo-epoxy composites
Er (g): Erosion rate of glass-epoxy composites

The effect of control factors on erosion rate of copper slag filled bamboo-epoxy composites is shown in Figure 6.11. Analysis of the results leads to the conclusion that factor combination: A_1 (impact velocity = 43 m/sec), B_2 (filler content = 10 wt%), C_2 (erodent temperature = 50°C), D_3 (impingement angle = 90°), E_2 (stand-off distance = 75 mm) and F_2 (erodent size = 450 μm) gives minimum erosion rate. But in case of copper slag filled glass-epoxy composite the factor combination: A_3 (impact velocity = 65 m/sec), B_3 (filler content = 20 wt %), C_1 (erodent temperature = 40°C), D_1 (impingement angle = 30°), E_3 (stand-off distance = 85mm) and F_3 (erodent size = 600 μm)) gives minimum erosion rate as shown in Figure 6.12. The respective interaction graphs are shown in the Figures 6.13 and 6.14 for bamboo-epoxy and glass-epoxy composites respectively. It is observed that for similar test conditions copper slag filled bamboo-epoxy composites exhibit much lower wear rates than those by glass-epoxy composites.

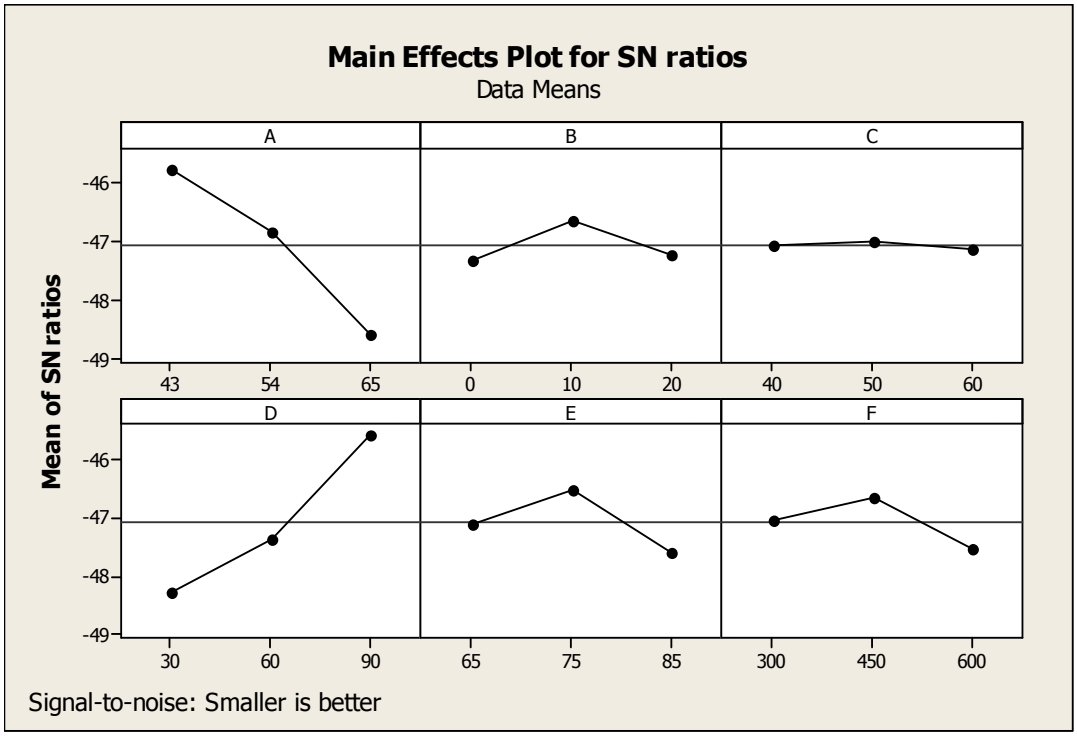

Figure 6.11 Effect of control factors on erosion rate (For copper slag filled bamboo-epoxy composites)

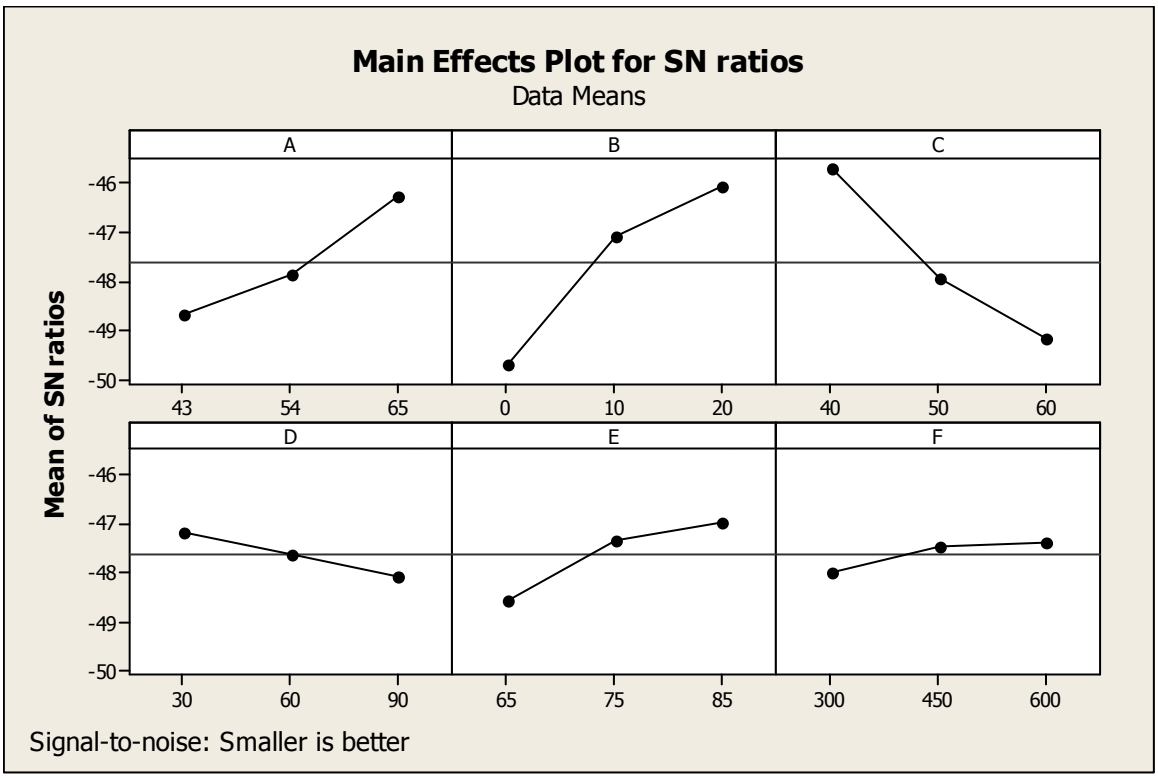

Figure 6.12 Effect of control factors on erosion rate (For copper slag filled glass-epoxy composites)

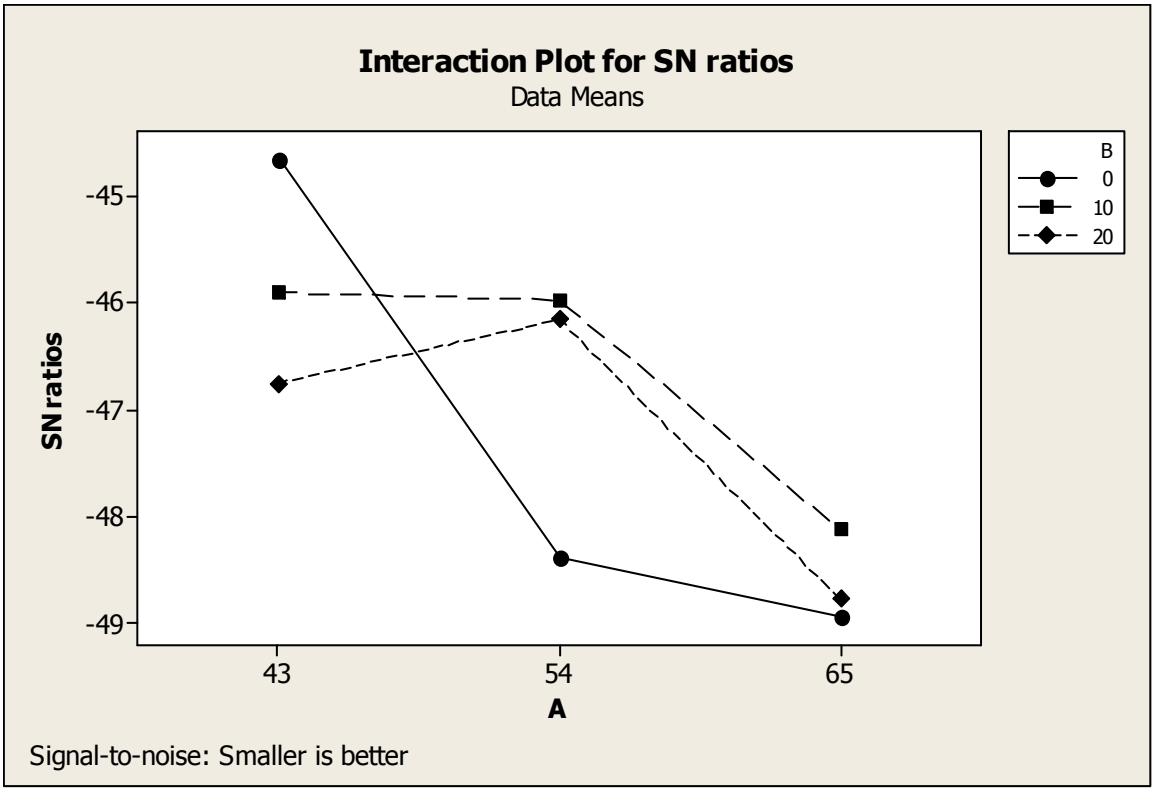

Figure 6.13 Interaction graph between impact velocity and filler content (A×B) for erosion rate (For copper slag filled bamboo-epoxy composites)

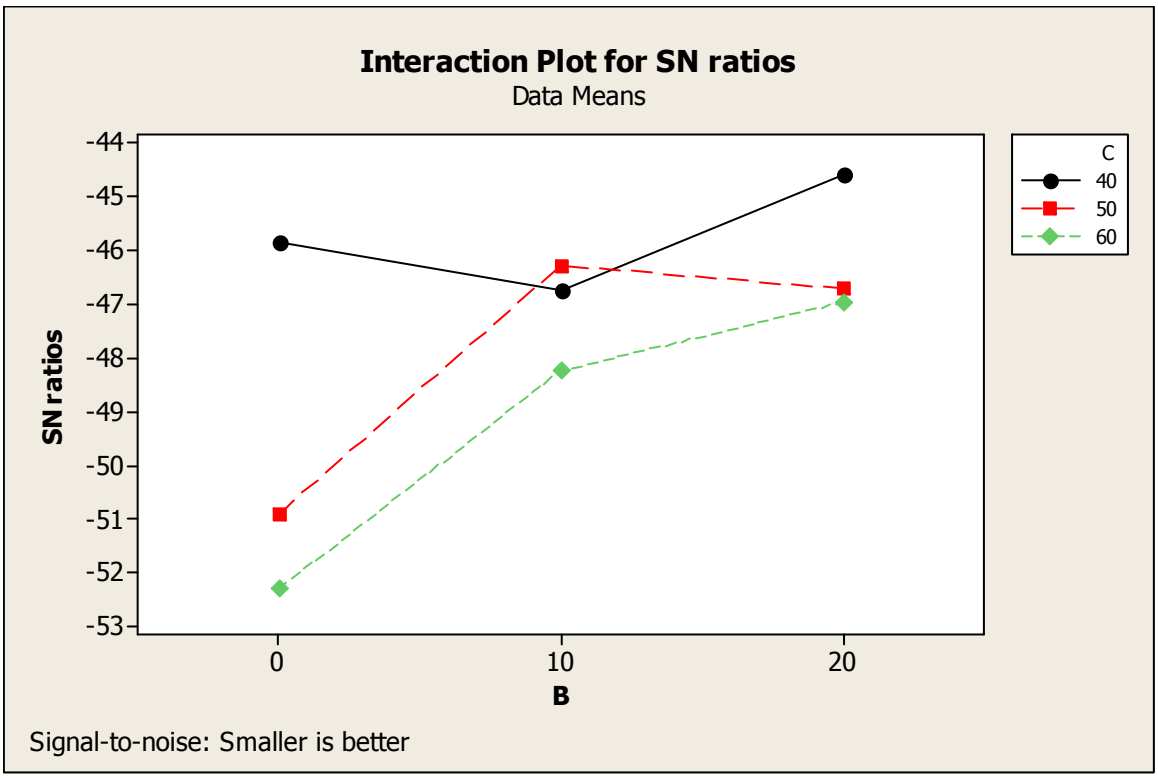

Figure 6.14 Interaction graph between filler content and erodent temperature (B×C) for erosion rate (For copper slag filled glass-epoxy composites)

6.2.2 ANOVA and the Effects of Factors

Table 6.9 and Table 6.10 show the results of the ANOVA for the erosion rate of bamboo-epoxy composites and glass-epoxy composites respectively. The last column of the table indicates percentage contribution of the control factors and their interactions on the performance output i.e erosion rate [224]. From Table 6.9, it can be observed for the copper slag filled bamboo-epoxy composites that impact velocity (p=0.358), impingement angle (p= 0.379), stand-off distance (p = 0.800), erodent size (p = 0.848) and copper slag content (p = 0.901) have considerable influence on erosion rate. The interaction of impact velocity and copper slag content (p = 0.613) as well as copper slag content and erodent temperature (p = 0.805) show significant contribution on the erosion rate but the remaining factors and interactions have relatively less significant effect.

Similarly, from Table 6.10, one can observe that copper slag content (p=0.008), erodent temperature (p = 0.009), impact velocity (p=0.019), stand-off distance (p

= 0.041) and impingement angle (p= 0.125) have great influence on erosion rate. The interaction of copper slag content and erodent temperature (p = 0.033) as well as impact velocity and copper slag content (p = 0.042) show significant contribution on the erosion rate but the remaining factor and interactions have relatively less significant contribution.

Table 6.9 ANOVA table for erosion rate
(For copper slag filled bamboo-epoxy composites)

Source	DF	Seq SS	Adj SS	Adj MS	F	P
A	2	37.06	37.06	18.53	1.79	0.358
B	2	2.27	2.27	1.14	0.11	0.901
C	2	0.08	0.08	0.04	0.00	0.996
D	2	33.85	33.85	16.93	1.64	0.379
E	2	5.18	5.18	2.59	0.25	0.800
F	2	3.69	3.69	1.85	0.18	0.848
A×B	4	16.33	16.33	4.08	0.40	0.613
A×C	4	11.97	11.97	2.99	0.29	0.865
B×C	4	34.05	34.05	8.51	0.82	0.805
Error	2	20.65	20.65	10.33		
Total	26	165.14				

[**]DF: degree of freedom, [##]Seq SS: sequential sum of squares, [$]Adj. SS: extra sum of squares[$$] Seq MS: sequential mean squares, [***]F: F-test, [###]P: percent contribution.

Table 6.10 ANOVA table for erosion rate
(For copper slag filled glass-epoxy composites)

Source	DF	Seq SS	Adj SS	Adj MS	F	P
A	2	26.3417	26.3417	13.1709	50.40	0.019
B	2	62.4257	62.4257	31.2129	119.44	0.008
C	2	55.3305	55.3305	27.6652	105.86	0.009
D	2	3.6664	3.6664	1.8332	7.01	0.125
E	2	12.3650	12.3650	6.1825	23.66	0.041
F	2	2.1053	2.1053	1.0527	4.03	0.199
A×B	4	23.8847	23.8847	5.9712	22.85	0.042
A×C	4	22.8317	22.8317	5.7079	21.84	0.044
B×C	4	30.5954	30.5954	7.6489	29.27	0.033
Error	2	0.5227	0.5227	0.2613		
Total	26	240.0692				

[**]DF: degree of freedom, [##]Seq SS: sequential sum of squares, [$]Adj. SS: extra sum of squares[$$] Seq MS: sequential mean squares, [***]F: F-test, [###]P: percent contribution

6.2.3 Confirmation Experiment

The confirmation experiment is performed for bamboo-epoxy composites by taking an arbitrary set of factor combination $A_2B_3C_3D_2E_1F_3$. Although factor C has the least effect on performance characteristics, it is not omitted from this series since its interaction with factor B has significant effect as evident from Table 6.9. Similarly, for glass-epoxy composites, an arbitrary set of factor combination $A_2B_2C_2D_2E_3$ is considered. Factor F has been omitted since it has least effect on performance characteristics. The estimated S/N ratio for erosion rate can be calculated with the help of following prediction equation:

$$\bar{\eta}_{\text{BF-copper slag}} = \bar{T} + (\bar{A}_2 - \bar{T}) + (\bar{B}_3 - \bar{T}) + [(\bar{A}_2\bar{B}_3 - \bar{T}) - (\bar{A}_2 - \bar{T}) - (\bar{B}_3 - \bar{T})] + (\bar{C}_3 - \bar{T}) + [(\bar{B}_3\bar{C}_3 - T) - (\bar{B}_3 - \bar{T}) - (\bar{C}_3 - \bar{T})] + (\bar{D}_2 - \bar{T}) + (\bar{E}_1 - \bar{T}) + (\bar{F}_3 - \bar{T}) \quad (6.5)$$

$$\bar{\eta}_{\text{GF-copper slag}} = \bar{T} + (\bar{A}_2 - \bar{T}) + (\bar{B}_2 - \bar{T}) + [(\bar{A}_2\bar{B}_2 - \bar{T}) - (\bar{A}_2 - \bar{T}) - (\bar{B}_2 - \bar{T})] + (\bar{C}_2 - \bar{T}) + [(\bar{B}_2\bar{C}_2 - T) - (\bar{B}_2 - \bar{T}) - (\bar{C}_2 - \bar{T})] + (\bar{D}_2 - \bar{T}) + (\bar{E}_3 - \bar{T}) \quad (6.6)$$

$\bar{\eta}_{\text{BF-copper slag}}$ and $\bar{\eta}_{\text{BF-copper slag}}$: Predicted average for copper slag filled bamboo fiber based and glass fiber based composites respectively.

$\bar{T}$: Overall experimental average

$\bar{A}_2, \bar{B}_2, \bar{B}_3, \bar{C}_2, \bar{C}_3, \bar{D}_3, \bar{E}_1, \bar{E}_3$ and $\bar{F}_3$ Mean response for factors and interactions at designated levels.

By combining like terms, the equation reduces to

$$\bar{\eta}_{\text{BF-copper slag}} = \bar{A}_2\bar{B}_3 + \bar{B}_3\bar{C}_3 - \bar{B}_3 + \bar{D}_2 + \bar{E}_1 + \bar{F}_3 - 3\bar{T} \quad (6.7)$$

$$\bar{\eta}_{\text{GF-copper slag}} = \bar{A}_2\bar{B}_2 + \bar{B}_2\bar{C}_2 - \bar{B}_2 + \bar{D}_2 + \bar{E}_3 - 2\bar{T} \quad (6.8)$$

A new combination of factor levels A_2, B_3, B_2, C_2,C_3, D_3, E_1, E_3 and F_3 is used to predict erosion rate through prediction equation and it is found to be $\bar{\eta}_{\text{BF-copper slag}} = -45.1397$ db and $\bar{\eta}_{\text{GF-copper slag}} = -45.1182$ db respectively.

For each performance measure, an experiment is conducted for the same set of factor combinations and the obtained S/N ratio value is compared with that obtained from the predictive equation as shown in Table 6.11. The resulting model seems to be capable of predicting erosion rate to a reasonable accuracy. An error of 4.96 % and 6.63 % for the S/N ratio of erosion rate is observed for

bamboo-epoxy composite and glass-epoxy composites respectively. However, the error can be further reduced if the number of measurements is increased. This validates the mathematical model for predicting the measures of performance based on knowledge of the input parameters.

Table 6.11 Results of the confirmation experiments for erosion rate

	Optimal control parameters (For bamboo-epoxy composites)		Optimal control parameters (For glass-epoxy Composites)	
	Prediction	Experimental	Prediction	Experimental
Level	$A_2 B_3 C_3 D_2 E_1 F_3$	$A_2 B_3 C_3 D_2 E_1 F_3$	$A_2 B_2 C_2 D_2 E_3$	$A_2 B_2 C_2 D_2 E_3$
S/N ratio for Erosion rate (db)	-45.1397	-42.9007	-45.1182	-42.1268

6.2.4 Effect of Impingement Angle and Erodent Temperature on Erosion

The variation of erosion rate of the copper slag filled bamboo-epoxy and glass-epoxy composites with impingement angle is obtained by conducting experiments under specified operating conditions (Figure 6.15). The results show that the peak erosion takes place at an impingement angle of 60° for the unfilled composites whereas for the copper slag filled composites it occurs at 45° impingement angle for both glass and bamboo fiber reinforcement. This clearly indicates that these composites respond to solid particle impact neither in a purely ductile nor in a purely brittle manner, rather the erosion behaviour is semi-ductile. This behaviour may be attributed to the incorporation of fibers and copper slag particles within the epoxy body. Similarly, the variation of erosion rate of unfilled and copper slag filled composites with erodent temperature is shown in Figure 6.16. This figure also presents a comparison between the erosion rate of bamboo-epoxy composites and glass-epoxy composites for different erodent temperatures. It is seen, in this figure, that for all the composite samples, the erosion rates remain almost unaffected by the change in erodent temperature from ambient to 40°C. The effect of erodent temperature on erosion is significant above 40°C and the rate of increase in erosion rate is greater at higher temperatures. The increase in erosion rate with erodent temperature can be attributed to increased penetration of particles on impact as a result of

dissipation of greater amount of particle thermal energy to the target surface. This leads to more surface damage, enhanced sub-critical crack growth etc. and consequently to the reduction in erosion resistance as observed in case of red mud filled bamboo-epoxy and glass-epoxy composites.

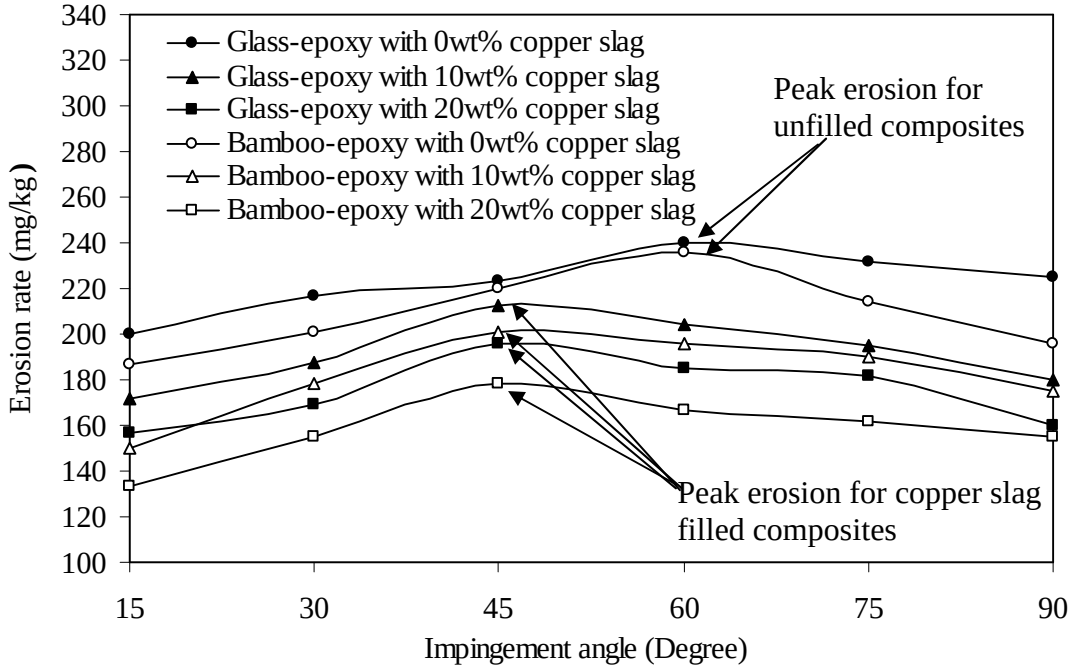

Figure 6.15 Effect of impingement angle on the erosion wear rate of copper slag filled bamboo-epoxy and glass-epoxy composites

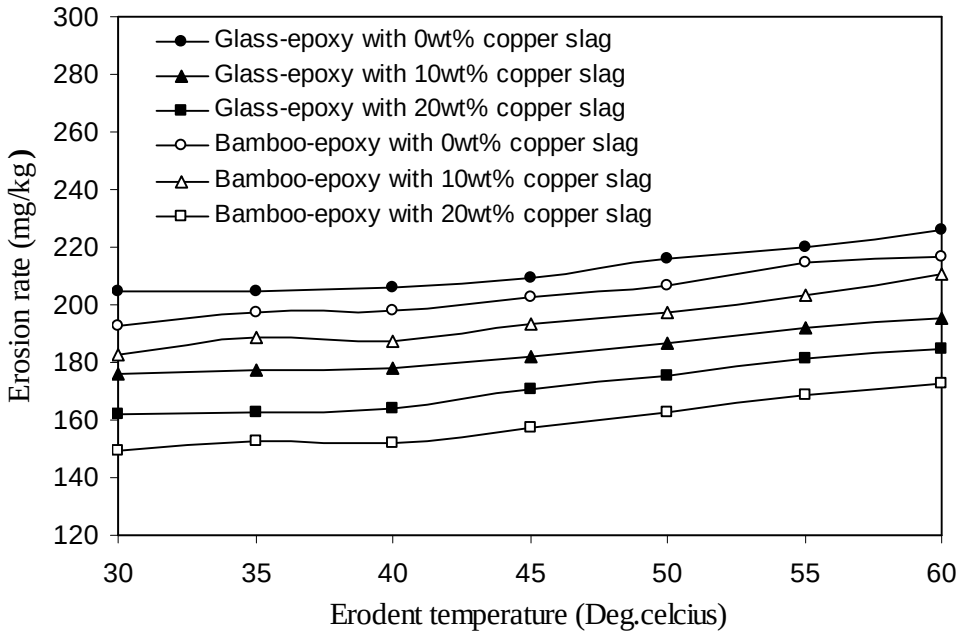

Figure 6.16 Effect of erodent temperature on the erosion wear rate of copper slag filled bamboo-epoxy and glass-epoxy composites

6.2.5 Erosion Efficiency

The values of erosion efficiencies of copper slag filled bamboo-epoxy and glass-epoxy composites calculated using Eq. (5.2) is given in Table 6.12 and Table 6.13 respectively. The erosion efficiencies of these composites under normal impact (η_{normal}) vary from 3-6%, 6-9% and 9-12% for impact velocities 65m/sec, 54m/sec and 43m/sec respectively.

Table 6.12 Erosion efficiency of copper slag filled bamboo-epoxy composites

Expt. No.	Impact velocity (U) m/sec	Density of eroding material (ρ_c) kg/m^3	Hardness of Eroding material (H_v)	Erosion rate (Er)mg/kg	Erosion efficiency (η)%
1	43	1243	33.13	150.00	16.964
2	43	1243	33.13	133.33	5.026
3	43	1243	33.13	250.00	7.068
4	43	1354	36.25	237.50	8.993
5	43	1354	36.25	139.00	3.947
6	43	1354	36.25	233.33	26.506
7	43	1368	39.00	211.11	6.384
8	43	1368	39.00	287.50	34.778
9	43	1368	39.00	170.00	6.855
10	54	1243	33.13	277.77	6.640
11	54	1243	33.13	225.00	4.033
12	54	1243	33.13	290.00	20.796
13	54	1354	36.25	172.00	3.097
14	54	1354	36.25	244.44	17.607
15	54	1354	36.25	187.50	4.502
16	54	1368	39.00	262.50	20.134
17	54	1368	39.00	240.00	6.136
18	54	1368	39.00	133.33	2.556
19	65	1243	33.13	175.00	2.165
20	65	1243	33.13	390.00	19.302
21	65	1243	33.13	322.22	5.316
22	65	1354	36.25	255.55	8.822
23	65	1354	36.25	262.50	4.350
24	65	1354	36.25	247.00	3.069
25	65	1368	39.00	360.00	6.353
26	65	1368	39.00	200.00	2.646
27	65	1368	39.00	287.50	15.220

The theoretical erosion wear rate (E_{rth}) of the copper slag filled bamboo-epoxy composites are calculated using Eq. 5.13. These values are compared with those

obtained from experiments (E_{rexpt}) conducted under similar operating conditions. Table 6.14 presents a comparison among the theoretical and experimental results and the associated percentage errors for both copper slag filled bamboo-epoxy as well as glass-epoxy composites. The errors in experimental results with respect to the theoretical ones lie in the range 0-14%. The erosion efficiencies of the composites under the present study indicate that at low impact velocity the erosion response is semi-ductile (η=10-100%). On the other hand at relatively higher impact velocity the composites exhibit ductile (η < 10%) erosion behaviour [225].

Table 6.13 Erosion efficiency of copper slag filled glass-epoxy composites

Expt. No.	Impact Velocity (U) m/sec	Density of eroding material (ρ) kg/m^3	Hardness of eroding material (H_v)	Erosion rate (Er)mg/kg	Erosion efficiency (η)%
1	43	1530	24.80	204.348	14.054
2	43	1530	24.80	342.029	7.841
3	43	1530	24.80	413.720	7.113
4	43	1650	37.05	256.522	8.147
5	43	1650	37.05	376.124	8.959
6	43	1650	37.05	266.667	25.407
7	43	1752	43.05	222.663	5.803
8	43	1752	43.05	121.739	12.692
9	43	1752	43.05	175.362	6.094
10	54	1530	24.80	226.087	3.286
11	54	1530	24.80	353.623	3.855
12	54	1530	24.80	382.147	16.665
13	54	1650	37.05	139.130	2.101
14	54	1650	37.05	157.342	9.505
15	54	1650	37.05	191.304	3.852
16	54	1752	43.05	140.192	9.268
17	54	1752	43.05	274.638	6.052
18	54	1752	43.05	226.087	3.736
19	65	1530	24.80	163.768	1.232
20	65	1530	24.80	359.420	10.818
21	65	1530	24.80	443.712	4.452
22	65	1650	37.05	173.913	5.035
23	65	1650	37.05	198.193	2.754
24	65	1650	37.05	168.116	1.752
25	65	1752	43.05	318.152	4.839
26	65	1752	43.05	214.493	2.446
27	65	1752	43.05	295.652	13.490

Table 6.14 Comparison of theoretical and experimental erosion rates along with the percentage errors for copper slag filled bamboo-epoxy and glass-epoxy composites

Expt. No.	E_{rbth} (b) (mg/kg)	$E_{rbexpt.}$(b) (mg/kg)	Error (b) (%)	E_{rth} (g) (mg/kg)	$E_{rexpt.}$(g) (mg/kg)	Error (g) (%)
1	170.086	150	11.809	231.712	204.348	11.809
2	151.192	133.33	11.814	387.851	342.029	11.814
3	350.180	250.00	28.608	469.506	413.720	11.881
4	210.328	237.50	12.918	265.710	273.913	3.087
5	125.526	139.00	10.733	266.306	284.058	6.665
6	226.655	233.33	2.945	353.057	389.247	10.250
7	227.400	211.11	7.163	154.613	163.768	5.921
8	269.664	287.50	6.614	245.847	234.319	4.689
9	193.736	170.00	12.252	241.431	239.192	0.927
10	281.179	277.77	1.212	246.075	226.087	8.122
11	229.197	225.00	1.831	343.054	353.623	3.080
12	300.586	290.00	3.521	368.521	382.147	3.697
13	158.565	172.00	8.472	312.463	307.246	1.669
14	222.552	244.44	9.834	148.202	156.522	5.613
15	173.989	187.50	7.765	219.157	200.197	8.651
16	295.140	262.50	11.059	191.910	204.348	6.480
17	278.423	240.00	13.800	229.461	214.493	6.523
18	121.673	133.33	9.580	252.209	276.371	9.580
19	162.100	175.00	7.957	160.040	163.768	2.329
20	372.461	390.00	4.708	327.574	359.420	9.721
21	292.323	322.22	10.227	395.002	443.712	12.331
22	299.923	255.55	14.795	137.601	121.739	11.528
23	240.110	262.50	9.324	175.203	197.101	12.498
24	260.671	247.00	5.244	244.337	221.890	9.187
25	380.050	360.00	5.275	132.226	144.928	9.605
26	183.392	200.00	9.055	204.601	202.899	0.831
27	290.567	287.50	1.055	153.271	167.892	9.538

6.2.6 Surface Morphology

Microstructures of the un-eroded surfaces of a copper slag filled bamboo-epoxy composite are presented in Figures 6.17a and 6.17b. Copper slag particles are seen to be scattered on the upper surface and their distribution is reasonably uniform although at places the particles are seen to have formed small and big clusters. In the case of the worn surface of the composite eroded at low impact velocity (Figures 6.17c and 6.17d), however, fracture and often plastic deformation are visible. Fiber fracture and failure inside the matrix is not clearly observed at an impingement angle of 30° although only matrix cracks and deformation are evident.

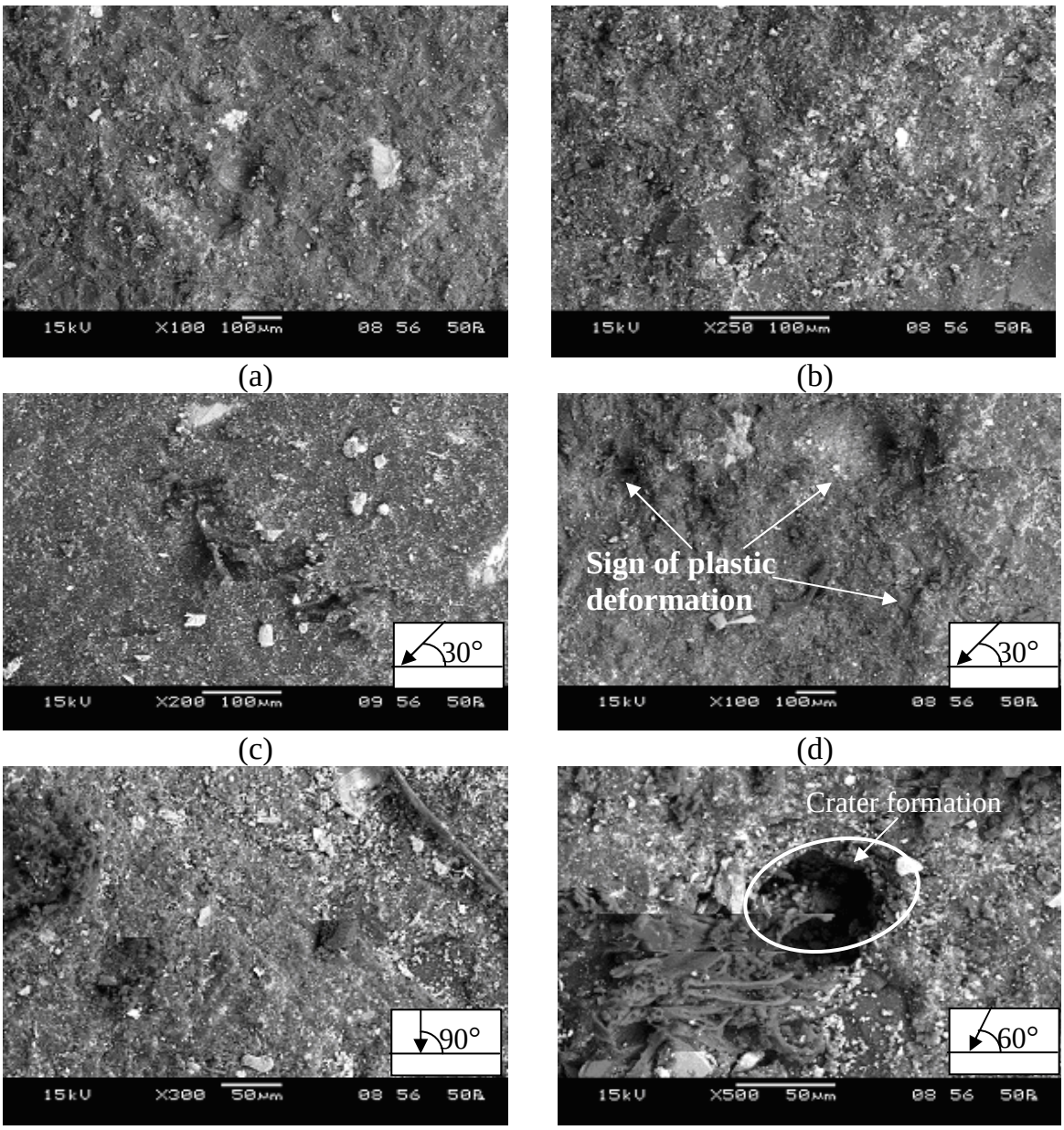

Figure 6.17 SEM images of the eroded copper slag filled bamboo-epoxy composites

Figure 6.17e for the composite eroded at 90° shows mainly matrix fracture. At this impingement angle, there is no parallel component of impact velocity of the particle and hence, no wear is expected. Figure 6.17f presents the SEM image of the eroded surface of the same composite where fibers are seen to have cracked into small fragments and they are removed from their places partly with the surrounding matrix like spalled fragments. The worn surface exhibits crater formation and sign of plastic deformation in the matrix regime. Repeated impacts gradually form larger craters and fibre-matrix debonding.

Figure 6.18a shows the micro-structural features of copper slag filled (10 wt%) glass-epoxy composite eroded at an impingement angle of 90° and a velocity of 43 m/sec at room temperature. In this case the erodent particles and the composite specimen are at same ambient conditions. When the composite is subjected to erosion trial by a stream of sand particles having an elevated temperature of 50°C, the micro-structure of the eroded surface appears quite different. These differences are illustrated in Figures 6.18a and 6.18b.

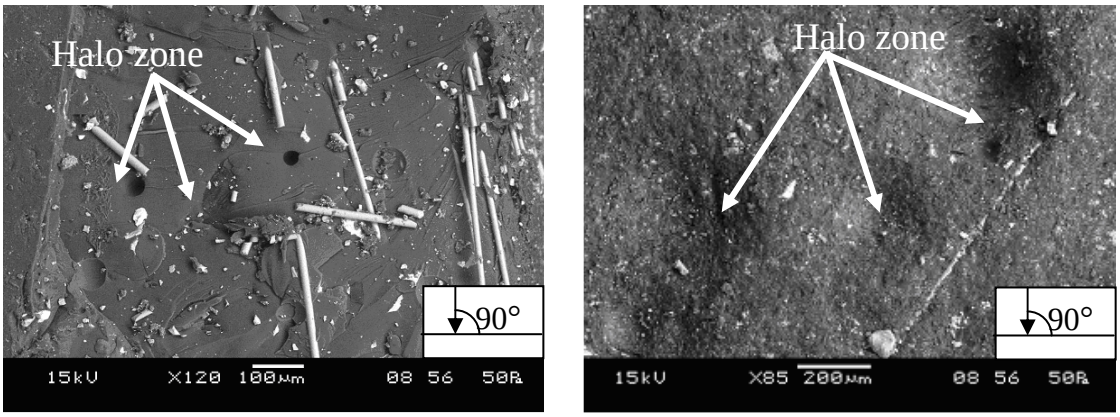

(a) (b)

Figure 6.18 Scanning electron micrograph of the glass-epoxy composite (with 10 wt% copper slag) at 43 m/sec impact velocity and erodent size 450 µm (a) erodent at room temperature and (b) erodent temperature 50°C

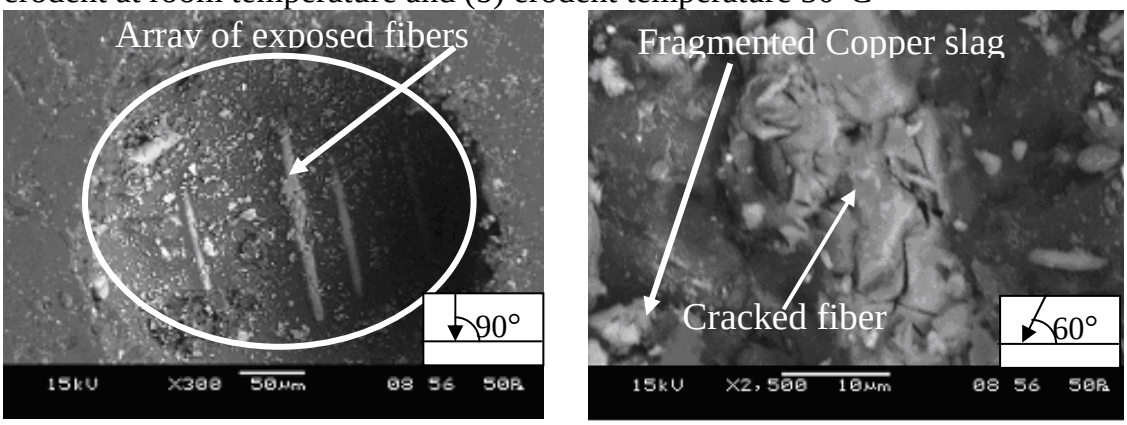

(a) (b)

Figure 6.19 Scanning electron micrograph of the glass-epoxy composite (with 10 wt% copper slag) eroded at 43 m/sec impact velocity, (a) C = 50°C, D = 90°, E = 85 mm, F =300µm and (b) C = 60°C, D = 60°, E = 75 mm, F = 600µm

The deformation of the surface eroded by the erodent particles at room temperature appears to be mostly due to plastic deformation and occasional micro-cracking. It is evident from Figure 6.18a and 6.18b that the matrix is chipped away and the material left in its location seems to be in the glassy phase

in plastically deformed condition. Some morphological differences can also be seen in the halo zone of the erosion crater formed, as shown in Figure 6.18b. The damaged surface gives an appearance of localized rounded features and there is some evidence of ploughing. Figure 6.19a shows that an erodent particle penetrated deeply into the surface forming a crater of substantial size showing an array of almost intact fibers. There are no cracks seen on the fiber body and the surrounding material has undergone severe plastic deformation. The copper slag filled epoxy matrix covering the glass fibers has been chipped off due to repeated impact of hard silica sand particles. After the local removal of matrix this array of fibers is exposed to erosive environment. This is the case of maximum material loss due to erosion at normal impact. Similarly, Figure 6.19b shows fragments of copper slag particles and the cracks on the fiber body which are results of continued sand impact. The broken fiber and filler fragments are mixed with the matrix micro-flake debris and the damage of the composite is characterized by separation and detachment of this debris.

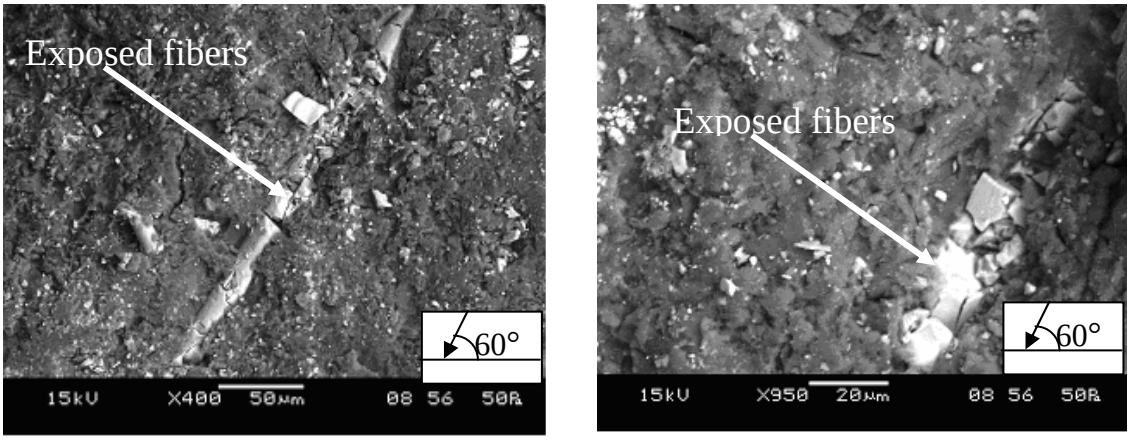

(a) (b)

Figure 6.20 Scanning electron micrograph of the glass-epoxy composite (with 10wt% copper slag) eroded at 60° impingement angle and erodent size 600 µm, (a) A = 54 m/sec, C = 60°C, E = 85mm and (b) A= 65 m/sec, C = 50°C, E = 65mm.

Figures 6.20 and 6.21 show worn surfaces of glass-epoxy composites filled with copper slag (10 wt %). The erosion trials are carried out at room temperature while the erodent temperatures are kept at 60°C and 50°C respectively. It is evident that the erosion proceeds by clean removal of the matrix and exposure of

glass fibers. Further damage is characterized by separation and detachment of broken fibers from the matrix and cavities left behind along the length of fibers (Figure 6.20a). The fibers are often half embedded in the matrix as can be seen in Figure 6.20b. At higher impingement angle, fiber thinning and detachment of fibers occur and cavities form in the matrix as seen in Figures 6.21a and 6.21b

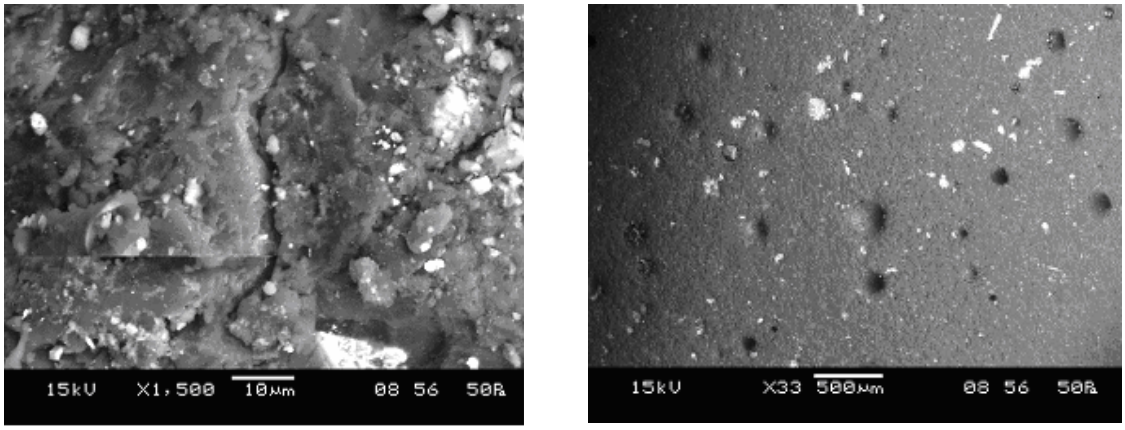

(a) (b)

Figure 6.21 Scanning electron micrograph of the glass-epoxy composite (with 10wt% copper slag) eroded at (a) A = 54 m/sec, C = 40°C, D = 90°, E = 65mm, F = 300 µm and (b) A = 65 m/sec, C = 50°C, D = 90°, E = 85mm, F = 450 µm.

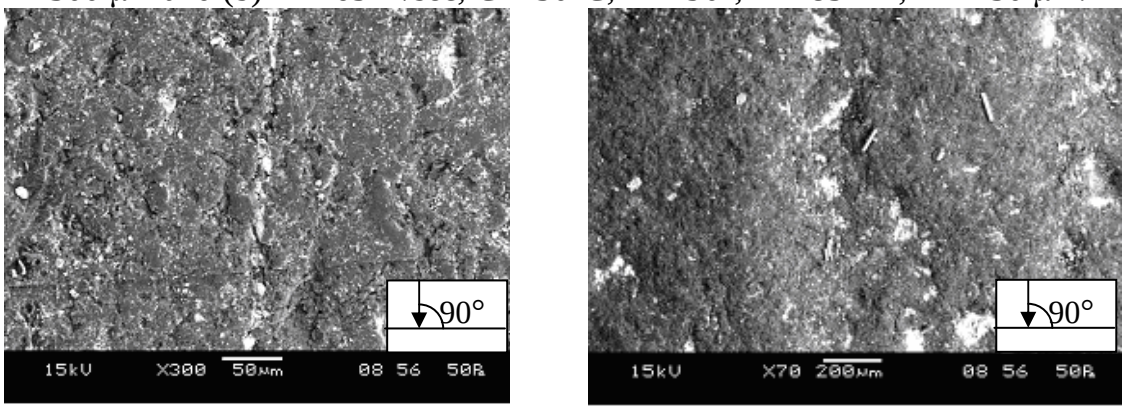

(a) (b)

Figure 6.22 Scanning electron micrograph of the glass-epoxy composite (with 20 wt% copper slag) eroded at 90° impingement angle and erodent size 450µm, (a) A = 65 m/sec, C = 50°C, E = 75mm and (b) A = 54 m/sec, C = 60°C, E = 65mm.

Figure 6.22 illustrates the surface morphology of the glass-epoxy composite sample using 20 wt% copper slag. At normal impact, the damage to the surface is not so high even with a high impact velocity (65 m/sec). No large craters or cracks are visible although there are signs of plastic deformation on the surface. This may be attributed to the higher weight percentage (20 wt%) of hard copper

slag fillers (Figure 6.22a). Similarly, Figure 6.22b shows a relatively small fraction of the material being removed from the surface although formation of large amount of grooves is visible. However, crack formation and propagation is not seen.

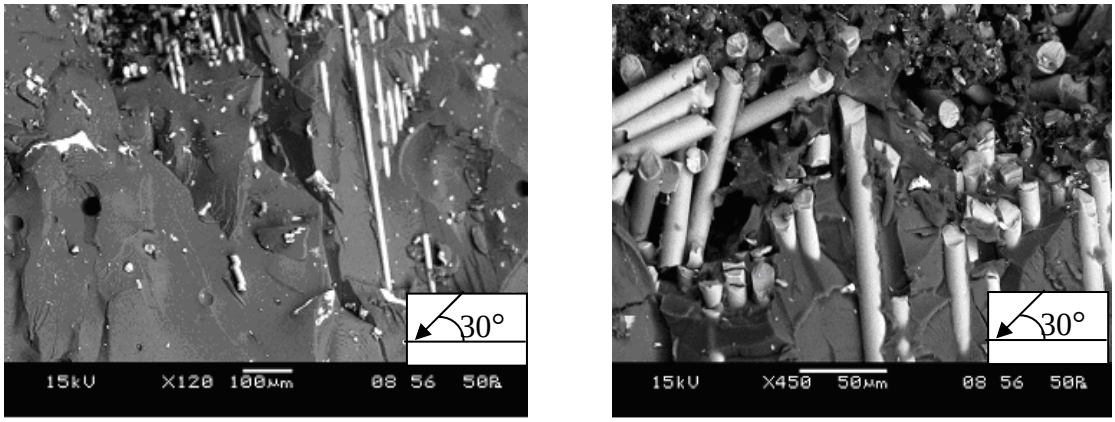

(a) (b)

Figure 6.23 Scanning electron micrograph of the glass-epoxy composite (with 20 wt% copper slag) eroded at 30° impingement angle, 65 m/sec impact velocity and erodent temperature 60°C, SOD 85 mm and erodent size 600µm.

Surface morphologies of the same composite eroded under a different test condition (impingement angle 30°, erodent temperature 60°C) are found to be distinctly different (Figure 6.23). There are plastic deformations as well as cracks in the matrix resin leading to exposure and protrusion of fibers. In Figure 6.23a, the fibers are still held firmly in place by the matrix surrounding them. Some of the occurrences during erosion like fiber-matrix debonding, brittle fracture of matrix and pulverization of fibers etc. are reflected in the micrograph shown in Figure 6.23b. On impact, the kinetic energy and a part of thermal energy of the erodent particles are transferred to the composite body that leads to crater formation and subsequently material loss. As already mentioned, the presence of hard copper slag particles in the matrix helps in absorbing a good fraction of this energy and therefore energy available for the plastic deformation of matrix becomes less. This also delays the initiation of fiber exposure as compared to the composite without any filler. All these factors combined together result in exhibition of fairly good erosion response by the copper slag filled composites both for bamboo and glass fiber reinforcements.

6.3 PART 3: ALUMINA FILLED COMPOSITES

This part of the chapter presents the analysis and comparison of erosion response of bamboo-epoxy and glass-epoxy composites filled with alumina (Al_2O_3).

6.3.1 Taguchi Experimental Analysis

Table 6.15 shows the experimental results for erosion of alumina filled bamboo-epoxy and glass-epoxy composites. The overall mean for the S/N ratio of the erosion rate is found to be -47.73db for the bamboo based composites and -47.47db for the glass based ones.

Table 6.15 Comparison of erosion rates of bamboo-epoxy composites with those of glass-epoxy composites under different test conditions as per L_{27} orthogonal array

Expt. No.	A (m/sec)	B (%)	C (^{0}C)	D (Degree)	E (mm)	F (µm)	E_r (b) (mg/kg)	S/N ratio (b) (db)	E_r (g) (mg/kg)	S/N ratio (g) (db)
1	43	0	40	30	65	300	150.00	-43.521	204.348	-46.207
2	43	0	50	60	75	450	133.33	-42.498	342.029	-50.681
3	43	0	60	90	85	600	250.00	-47.958	413.720	-52.334
4	43	10	40	60	75	600	275.00	-48.786	220.290	-46.86
5	43	10	50	90	85	300	360.00	-51.126	183.333	-45.265
6	43	10	60	30	65	450	244.44	-47.763	197.134	-45.895
7	43	20	40	90	85	450	144.44	-43.193	289.855	-49.244
8	43	20	50	30	65	600	200.00	-46.020	173.913	-44.807
9	43	20	60	60	75	300	300.00	-49.542	207.891	-46.357
10	54	0	40	60	85	450	277.77	-48.873	226.087	-47.086
11	54	0	50	90	65	600	225.00	-47.043	353.623	-50.971
12	54	0	60	30	75	300	290.00	-49.248	382.147	-51.645
13	54	10	40	90	65	300	160.00	-44.082	150.725	-43.564
14	54	10	50	30	75	450	264.44	-48.446	289.855	-49.244
15	54	10	60	60	85	600	175.00	-44.860	301.159	-49.576
16	54	20	40	30	75	600	300.00	-49.542	226.087	-47.086
17	54	20	50	60	85	300	230.00	-47.234	376.812	-51.523
18	54	20	60	90	65	450	166.66	-44.436	271.053	-48.661
19	65	0	40	90	75	600	175.00	-44.860	163.768	-44.285
20	65	0	50	30	85	300	390.00	-51.821	359.420	-51.112
21	65	0	60	60	65	450	322.22	-50.163	443.712	-52.942
22	65	10	40	30	85	450	344.44	-50.742	202.899	-46.146
23	65	10	50	60	65	600	325.00	-50.237	161.739	-44.176
24	65	10	60	90	75	300	340.00	-50.629	142.973	-43.105
25	65	20	40	60	65	300	390.00	-51.821	144.928	-43.223
26	65	20	50	90	75	450	166.66	-44.436	284.058	-49.068
27	65	20	60	30	85	600	312.50	-49.897	293.158	-49.342

Note: Er (b): Erosion rate of bamboo-epoxy composites;
Er (g): Erosion rate of glass-epoxy composites

Analysis of the results leads to the conclusion that factor combination A_1, B_1, C_1, D_3, E_1 and F_2 gives minimum erosion rate for alumina filled bamboo-epoxy composites (Figure 6.24). Similarly, analysis of the result further leads to the conclusion that factor combination A_3, B_2, C_1, D_3, E_1 and F_1 gives minimum erosion rate for alumina filled glass-epoxy composites (Figure 6.25). The respective interaction graphs are shown in the Figures 6.26 and 6.27 for bamboo-epoxy and glass-epoxy composites respectively.

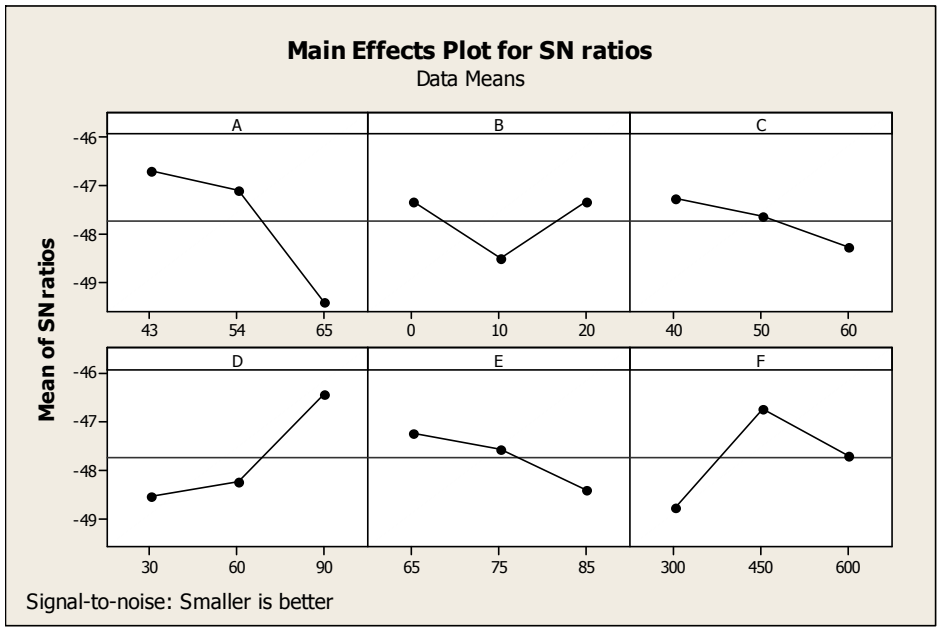

Figure 6.24 Effect of control factors on erosion rate
(For alumina filled bamboo-epoxy composites)

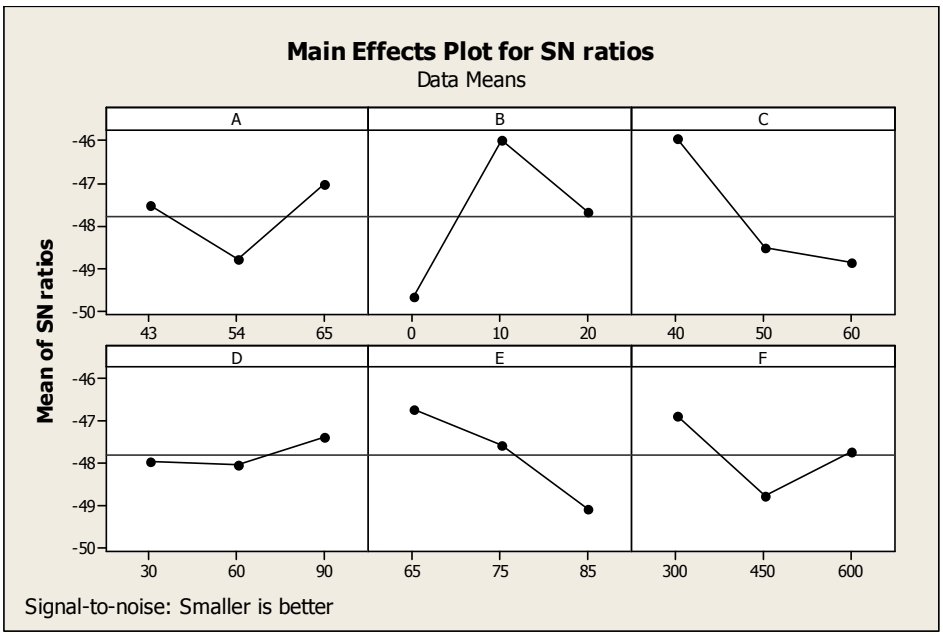

Figure 6.25 Effect of control factors on erosion rate
(For alumina filled glass-epoxy composites)

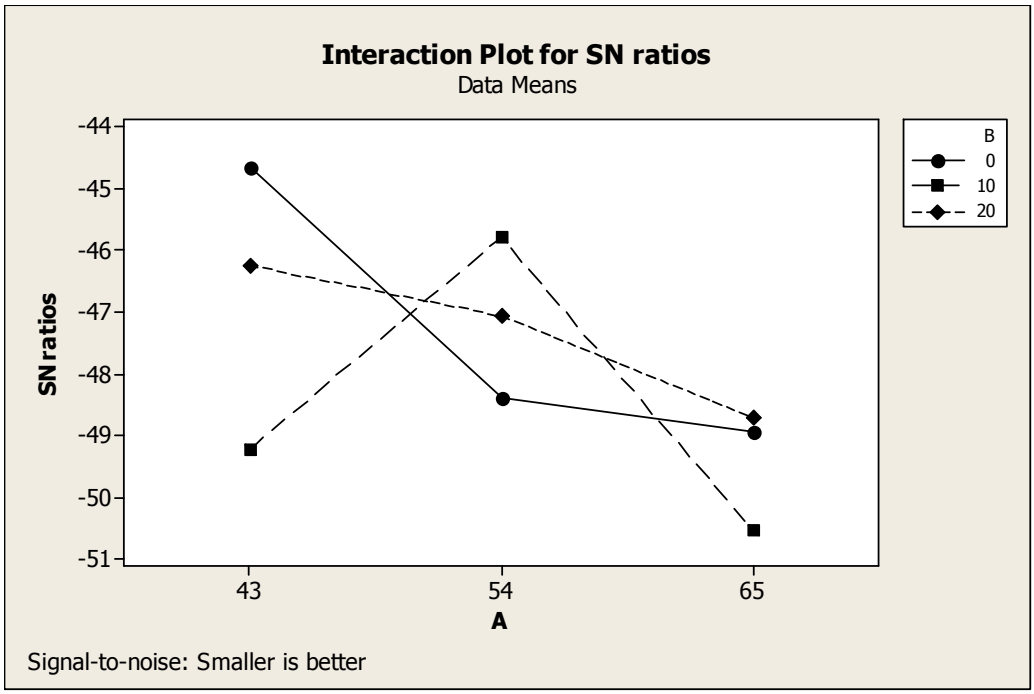

Figure 6.26 Interaction graph between impact velocity and filler content (A×B) for erosion rate (For alumina filled bamboo-epoxy composites)

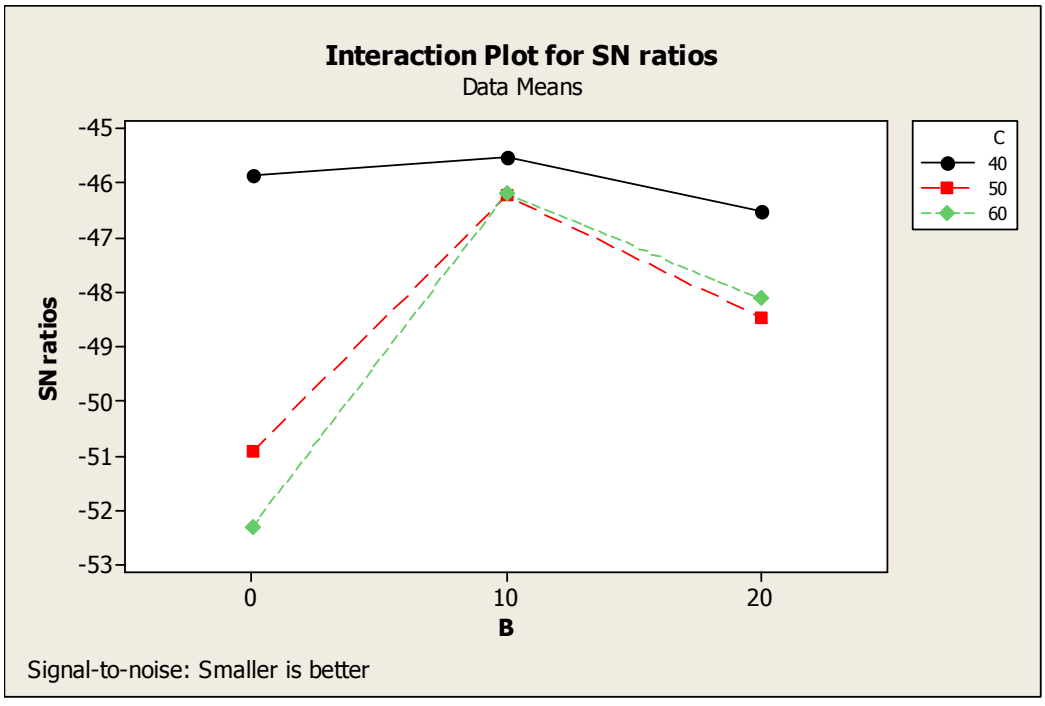

Figure 6.27 Interaction graph between filler content and erodent temperature (B×C) for erosion rate (For alumina filled glass-epoxy composites)

6.3.2 ANOVA and the Effects of Factors

Table 6.16 and Table 6.17 show the ANOVA results for the erosion rate of bamboo-epoxy and glass-epoxy composites respectively. The last column of the table indicates percentage contribution of the control factors and their interactions on the performance output i.e erosion rate [224]. From Table 6.16, it can be observed for the alumina filled bamboo-epoxy composites that impact velocity (p =0.366), erodent temperature (p = 0.481), erodent size (p = 0.537) and alumina content (p = 0.725) have considerable influence on erosion rate. The interaction of impact velocity and alumina content (p = 0.586) as well as alumina content and erodent temperature (p=0.657) show significant contribution on the erosion rate. The remaining factor and interactions have relatively less significant contribution.

Table 6.16 ANOVA table for erosion rate
(For alumina filled bamboo- epoxy composites)

Source	DF	Seq SS	Adj SS	Adj MS	F	P
A	2	38.19	38.19	19.09	1.73	0.366
B	2	8.35	8.35	4.18	0.38	0.725
C	2	4.66	4.66	2.33	0.21	0.481
D	2	23.81	23.81	11.91	1.08	0.825
E	2	6.69	6.69	3.35	0.30	0.767
F	2	18.98	18.98	9.49	0.86	0.537
A×B	4	39.83	39.83	9.96	0.90	0.586
A×C	4	18.26	18.26	4.56	0.41	0.795
B×C	4	31.18	31.18	7.80	0.71	0.657
Error	2	22.05	22.05	11.03		
Total	26	212.02				

[**]DF: degree of freedom, [##]Seq SS: sequential sum of squares, [$]Adj. SS: extra sum of squares[$$] Seq MS: sequential mean squares, [***]F: F-test, [###]P: percent contribution.

Similarly, from Table 6.17, it can be observed for the alumina filled glass-epoxy composites that alumina content (p =0.044), erodent temperature (p = 0.059), stand-off distance (p = 0.102), erodent size (p = 0.152) and impact velocity (p = 0.159) have considerable influence on erosion rate. The interaction of alumina

content and erodent temperature (p = 0.163) as well as impact velocity and erodent temperature (p = 0.205) show significant contribution on the erosion rate. The remaining factor and interactions have relatively less significant contribution on erosion rate.

Table 6.17 ANOVA table for erosion rate
(For alumina filled glass-epoxy composites)

Source	DF	Seq SS	Adj SS	Adj MS	F	P
A	2	15.170	15.170	7.585	5.27	0.159
B	2	62.209	62.209	31.104	21.62	0.044
C	2	45.522	45.522	22.761	15.82	0.059
D	2	2.255	2.255	1.127	0.78	0.561
E	2	25.464	25.464	12.732	8.85	0.102
F	2	16.073	16.073	8.036	5.59	0.152
A×B	4	7.449	7.449	1.862	1.29	0.480
A×C	4	23.668	23.668	5.917	4.11	0.205
B×C	4	31.027	31.027	7.757	5.39	0.163
Error	2	2.877	2.877	1.438		
Total	26	231.713				

[**]DF: degree of freedom, [##]Seq SS: sequential sum of squares, [$]Adj. SS: extra sum of squares[$$] Seq MS: sequential mean squares, [***]F: F-test, [###]P: percent contribution.

6.3.3 Confirmation Experiment

The confirmation experiment is performed by taking an arbitrary set of factor combination $A_3B_2C_2E_3F_1$ for bamboo-epoxy composites and $A_2B_3C_2E_3F_2$ for glass-epoxy composites, but factor D has been omitted in both bamboo and glass fiber reinforced epoxy composites as it has the least effect on performance characteristics. The estimated S/N ratio for the composites with alumina filler, the erosion rate can be calculated with the help of following prediction equations:

$$\bar{\eta}_{\text{BF-alumina}} = \bar{T} + (\bar{A}_3 - \bar{T}) + (\bar{B}_2 - \bar{T}) + [(\bar{A}_3\bar{B}_2 - \bar{T}) - (\bar{A}_3 - \bar{T}) - (\bar{B}_2 - \bar{T})] + (\bar{C}_2 - \bar{T}) + [(\bar{B}_2\bar{C}_2 - T) - (\bar{B}_2 - \bar{T}) - (\bar{C}_2 - \bar{T})] + (\bar{E}_3 - \bar{T}) + (\bar{F}_1 - \bar{T}) \quad (6.9)$$

$$\bar{\eta}_{\text{GF-alumina}} = \bar{T} + (\bar{A}_2 - \bar{T}) + (\bar{B}_3 - \bar{T}) + [(\bar{A}_2\bar{B}_3 - \bar{T}) - (\bar{A}_2 - \bar{T}) - (\bar{B}_3 - \bar{T})] + (\bar{C}_2 - \bar{T}) + (\bar{B}_3\bar{C}_2 - T) - (\bar{B}_3 - \bar{T}) - (\bar{C}_2 - \bar{T})] + (\bar{E}_3 - \bar{T}) + (\bar{F}_2 - \bar{T}) \quad (6.10)$$

$\bar{\eta}_{\text{BF-alumina}}$, $\bar{\eta}_{\text{GF-alumina}}$: Predicted average of alumina filled bamboo-epoxy composites and glass-epoxy composites respectively.

$\overline{T}$: Overall experimental average

$\overline{A}_3, \overline{A}_2, \overline{B}_2, \overline{B}_3, \overline{C}_2, \overline{E}_3$ and $\overline{F}_1, \overline{F}_2$: Mean response for factors and interactions at designated levels.

By combining like terms, the Eq. (6.9) and Eq. (6.10) reduces to

$$\overline{\eta}_{\text{BF-alumina}} = \overline{A}_3\overline{B}_2 + \overline{B}_2\overline{C}_2 - \overline{B}_2 + \overline{E}_3 + \overline{F}_1 - 2\overline{T} \quad (6.11)$$

$$\overline{\eta}_{\text{GF-alumina}} = \overline{A}_2\overline{B}_3 + \overline{B}_3\overline{C}_2 - \overline{B}_2 + \overline{E}_3 + \overline{F}_2 - 2\overline{T} \quad (6.12)$$

A new combination of factor levels A_3, A_2, B_2, B_3, C_2, E_3, F_1 and F_2 is used to predict erosion rate through prediction equation and it is found to be $\overline{\eta}_{\text{BF-alumina}} = -53.4930$ dB and $\overline{\eta}_{\text{GF-alumina}} = -52.7645$ dB respectively.

For each performance measure, an experiment is conducted for the same set of factor combinations and the obtained S/N ratio value is compared with that obtained from the predictive equation as shown in Table 6.18. The resulting model seems to be capable of predicting erosion rate to a reasonable accuracy. An error of 5.45 % and 6.63 % for the S/N ratio of erosion rate is observed for bamboo-epoxy composites and glass-epoxy composites respectively. However, the error can be further reduced if the number of measurements is increased. This validates the mathematical model for predicting the measures of performance based on knowledge of the input parameters.

Table 6.18 Results of the confirmation experiments for erosion rate

	Optimal control parameters (For bamboo-epoxy composites)		Optimal control parameters (For glass-epoxy composites)	
	Prediction	Experimental	Prediction	Experimental
Level	$A_3B_2C_2E_2F_1$	$A_3B_2C_2E_2F_1$	$A_2B_3C_2E_3F_2$	$A_2B_3C_2E_3F_2$
S/N ratio for Erosion rate (db)	-53.4930	-50.5776	-52.7645	-49.2661

6.3.4 Effect of Impingement Angle and Erodent Temperature on Erosion

The erosion wear rates of alumina filled bamboo-epoxy and glass-epoxy composites as a function of impingement angle are shown and compared in Figure 6.28. The figure shows the peak erosion taking place at an impingement angle of 60° for the unfilled as well as the alumina filled bamboo-epoxy and glass-epoxy composites. This clearly indicates that these composites respond to

solid particle impact neither in a purely ductile nor in a purely brittle manner. This behaviour can be termed as semi-ductile in nature which may be attributed to the incorporation of bamboo/glass fibers and alumina particles within the epoxy body.

Similarly, the variation of erosion rate of unfilled and alumina filled composites with erodent temperature is shown in Figure 6.29. This figure also presents a comparison between the erosion of composites with bamboo fiber reinforcement against glass fiber reinforcement for different erodent temperatures. Erosion trials are conducted at seven different temperatures under normal impact condition. It is seen that for all the composite samples, the erosion rates remain almost unaffected or very marginally affected by the change in erodent temperature from ambient to 40°C. The effect of erodent temperature on erosion is significant above 40°C and the rate of increase in erosion rate is greater at higher temperatures. It also becomes evident from this figure that the alumina filled epoxy composites with bamboo fiber reinforcement exhibit better erosion wear resistance as compared to glass reinforced composites under similar operating environment.

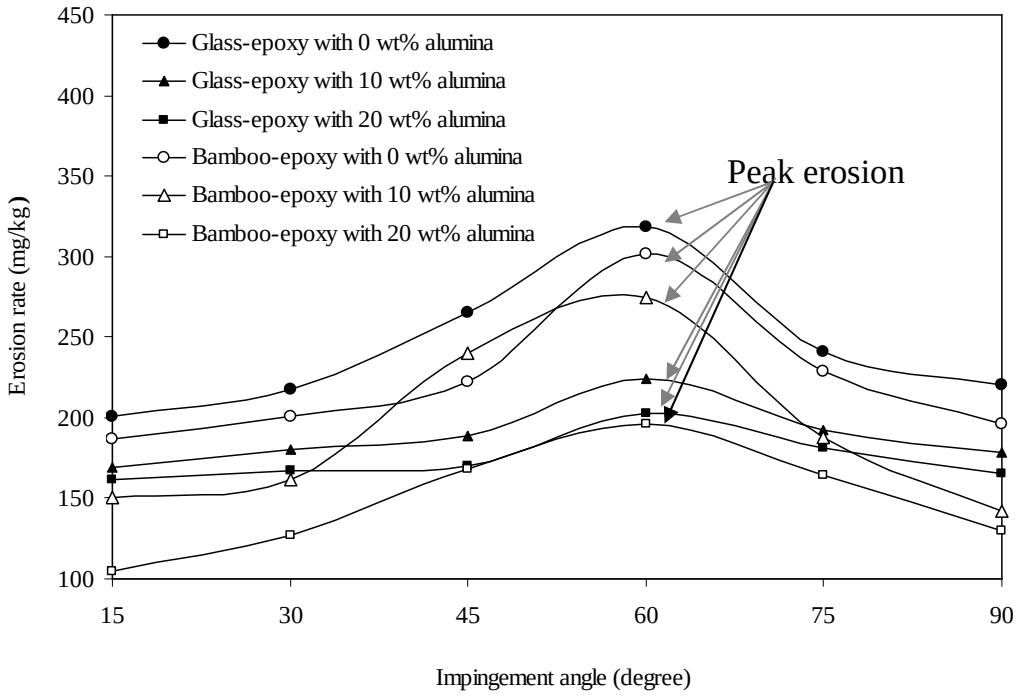

Figure 6.28 Effect of impingement angle on the erosion wear rate of the composites

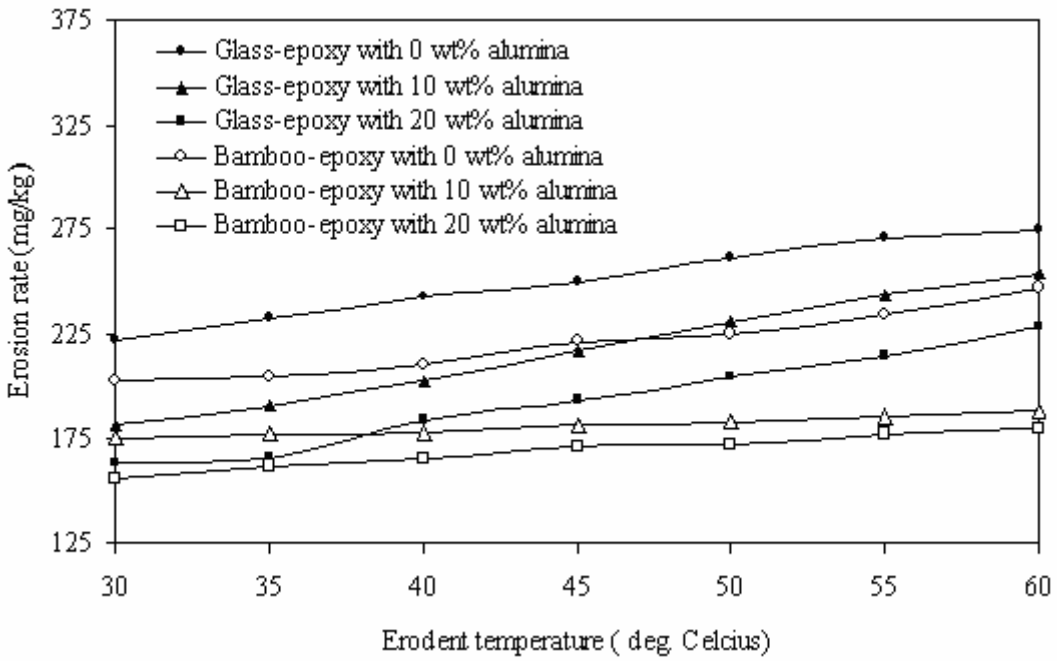

Figure 6.29 Effect of erodent temperature on the erosion rate of the composites

6.3.5 Erosion Efficiency

The values of erosion efficiencies of these composites calculated using Eq. (5.2) are given in Table 6.19 for bamboo based composites and in Table 6.20 for glass based composites. The erosion efficiencies of these composites under normal impact (η_{normal}) vary from 3-6%, 6-9% and 9-12% for impact velocities 65m/sec, 54m/sec and 43m/sec respectively. The erosion efficiencies of the composites under the present study indicate that at low impact speed the erosion response is semi-ductile (η=10-100%). On the other hand at relatively higher impact velocity the composites exhibit ductile (η < 10%) erosion behavior. The theoretical erosion wear rate (E_{rth}) of the alumina filled glass-epoxy composites $E_{rth}(g)$ and bamboo-epoxy composites $E_{rth}(b)$ are calculated using Eq. (5.13).These values are compared with the corresponding values $E_{rexpt}(g)$ and $E_{rexpt}(b)$ respectively obtained from experiments conducted under similar operating conditions. Table 6.21 presents a comparison between the theoretical and experimental results and the associated percentage errors for both alumina filled bamboo-epoxy as well as glass-epoxy composites. The errors in

experimental results with respect to the theoretical ones for the entire set of composites lie in the range 0-14%.

Table 6.19 Erosion efficiency of alumina filled bamboo-epoxy composites

Expt. No.	Impact Velocity (U) (m/sec)	Density of eroding material (ρ) (kg/m^3)	Hardness of eroding material (H_v)	Erosion rate (Er) (mg/kg)	Erosion efficiency (η)(%)
1	43	1243	33.13	150.00	16.9641
2	43	1243	33.13	133.33	5.026569
3	43	1243	33.13	250.00	7.068375
4	43	1348	38.63	275.00	11.14708
5	43	1348	38.63	360.00	10.94376
6	43	1348	38.63	244.44	29.72325
7	43	1723	42.37	144.44	3.767818
8	43	1723	42.37	200.00	20.86856
9	43	1723	42.37	300.00	10.43489
10	54	1243	33.13	277.77	6.64016
11	54	1243	33.13	225.00	4.033773
12	54	1243	33.13	290.00	20.79634
13	54	1348	38.63	160.00	3.084135
14	54	1348	38.63	264.44	20.38953
15	54	1348	38.63	175.00	4.497961
16	54	1723	42.37	300.00	19.84875
17	54	1723	42.37	230.00	5.072755
18	54	1723	42.37	166.66	2.75666
19	65	1243	33.13	175.00	2.165349
20	65	1243	33.13	390.00	19.30254
21	65	1243	33.13	322.22	5.316263
22	65	1348	38.63	344.44	12.72874
23	65	1348	38.63	325.00	5.765299
24	65	1348	38.63	340.00	4.523277
25	65	1723	42.37	390.00	5.93665
26	65	1723	42.37	166.66	1.902585
27	65	1723	42.37	312.50	14.26996

Table 6.20 Erosion efficiency of alumina filled glass-epoxy composites

Expt. No.	Impact Velocity (U) (m/sec)	Density of eroding material (ρ) (kg/m^3)	Hardness of eroding material (H_v)	Erosion rate (Er) (mg/kg)	Erosion efficiency (η) (%)
1	43	1530	24.80	204.348	14.05465
2	43	1530	24.80	342.029	7.841816
3	43	1530	24.80	413.720	7.113708
4	43	1627	39.92	220.290	7.645242
5	43	1627	39.92	183.333	4.771697
6	43	1627	39.92	197.134	20.52361
7	43	1800	47.46	289.855	8.107095
8	43	1800	47.46	173.913	19.45703
9	43	1800	47.46	207.891	7.753261
10	54	1530	24.80	226.087	3.286841
11	54	1530	24.80	353.623	3.855488
12	54	1530	24.80	382.147	16.66592
13	54	1627	39.92	150.725	2.487522
14	54	1627	39.92	289.855	19.13473
15	54	1627	39.92	301.159	6.627377
16	54	1800	47.46	226.087	16.03871
17	54	1800	47.46	376.812	8.910926
18	54	1800	47.46	271.053	4.807155
19	65	1530	24.80	163.768	1.232335
20	65	1530	24.80	359.420	10.81837
21	65	1530	24.80	443.712	4.452102
22	65	1627	39.92	202.899	6.419776
23	65	1627	39.92	161.739	2.456526
24	65	1627	39.92	142.973	1.628533
25	65	1800	47.46	144.928	2.365436
26	65	1800	47.46	284.058	3.476976
27	65	1800	47.46	293.158	14.35345

Table 6.21 Comparison of theoretical and experimental erosion rates along with the percentage errors for alumina filled bamboo-epoxy and glass-epoxy composites

Expt. No.	E_{rbth} (b) (mg/kg)	$E_{rbexpt.}$(b) (mg/kg)	Error (b) (%)	E_{rth} (g) (mg/kg)	$E_{rexpt.}$(g) (mg/kg)	Error (g) (%)
1	170.087	150.00	11.8096	231.712	204.348	11.8096
2	151.193	133.33	11.8144	387.851	342.029	11.8144
3	280.18	250.00	10.7717	479.506	413.720	13.7195
4	246.17	275.00	11.7115	198.058	220.290	11.2248
5	332.156	360.00	8.3828	168.967	183.333	8.5016
6	220.681	244.44	10.7662	185.092	197.134	6.5059
7	148.167	144.44	2.5157	296.660	289.855	2.2939
8	213.679	200.00	5.9338	168.416	173.913	3.2634
9	323.653	300.00	6.6902	183.665	207.891	13.1903
10	281.18	277.77	1.2126	206.075	226.087	9.7109
11	229.198	225.00	1.8314	333.054	353.623	6.1757
12	300.586	290.00	3.5218	378.521	382.147	0.9579
13	147.736	160.00	8.3015	135.548	150.725	11.1966
14	254.498	264.44	3.9080	277.781	289.855	4.3465
15	179.057	175.00	2.2655	339.767	301.159	11.3632
16	283.018	300.00	6.0003	208.071	226.087	8.6583
17	240.989	230.00	4.5601	380.134	376.812	0.8739
18	152.09	166.66	9.5801	247.356	271.053	9.5801
19	162.101	175.00	7.9576	160.040	163.768	2.3292
20	372.462	390.00	4.7088	327.574	359.420	9.7215
21	292.323	322.22	10.227	395.002	443.712	12.331
22	334.681	344.44	2.9158	179.336	202.899	13.138
23	293.47	325.00	10.7437	186.329	161.739	13.1971
24	321.168	340.00	5.8637	153.003	142.973	6.5553
25	366.722	390.00	6.3477	132.226	144.928	9.6057
26	169.491	166.66	1.6703	268.441	284.058	5.8174
27	350.616	312.50	10.8714	304.157	293.158	3.6163

6.3.6 Surface Morphology

The SEM image (Figure 6.30a) of the un-eroded surface of alumina filled bamboo-epoxy composite shows scattered alumina particles on the upper surface. Figure 6.30b showing the worn surface of the composite eroded at 90° reveals mainly the matrix fracture. The eroded surfaces exhibit sign of plastic deformation in the matrix regime at an impact velocity of 54 m/sec and erodent temperature of 60°C which indicate the initiation of surface damage as seen in

Figure 6.30c. Similarly, the most visible dominant features as noticed in Figure 6.30d are the fracture and cutting of fibers. Many fibers have cracked into small fragments and they are removed from their places partly with the surrounding matrix like spalled fragments. Subsequently under similar condition as mentioned above there is removal of matrix material from the surface resulting in exposure of broken fibers to erosive environment (Figure 6.30e). In this micrograph, the fibers are still held firmly in place by the matrix surrounding them. Repeated impacts gradually cause fiber-matrix debonding, brittle fracture of matrix and pulverization of fibers. The fibers are broken by means of shearing action that can be seen from the micrograph due to impingement of particles at higher impact velocity (Figure 6.30f).

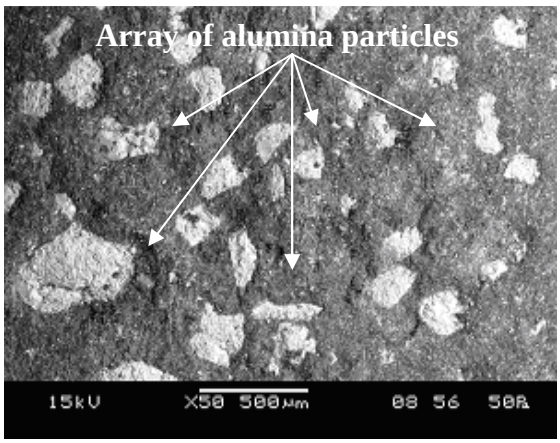

(a)

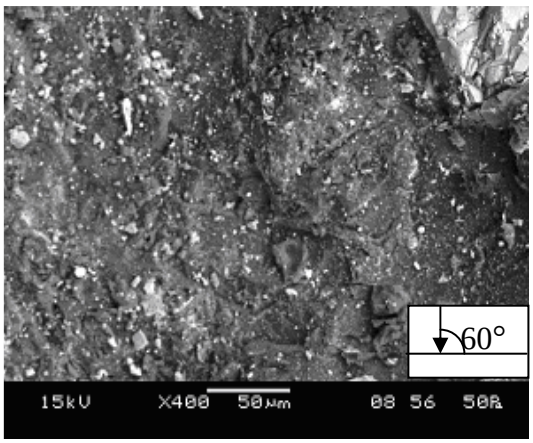

(b)

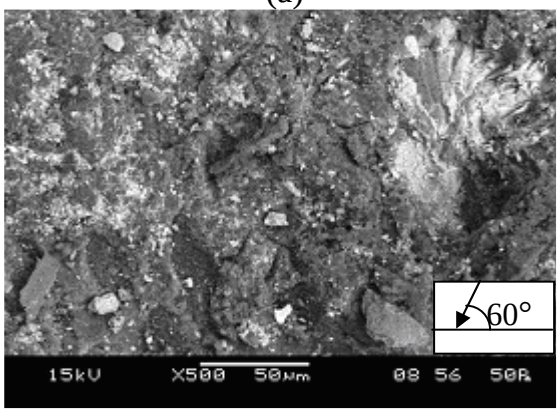

(c)

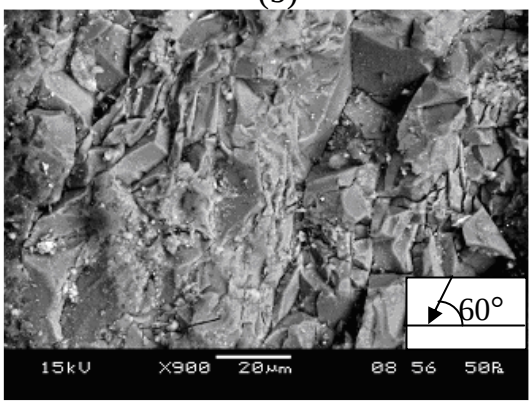

(d)

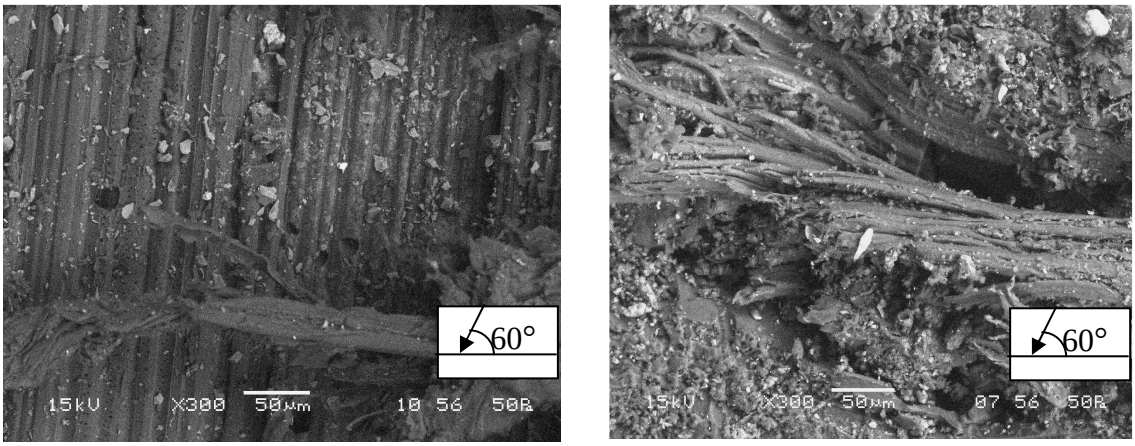

(e) (f)

Fig. 6.30. SEM images of eroded surfaces of alumina filled bamboo-epoxy composites.

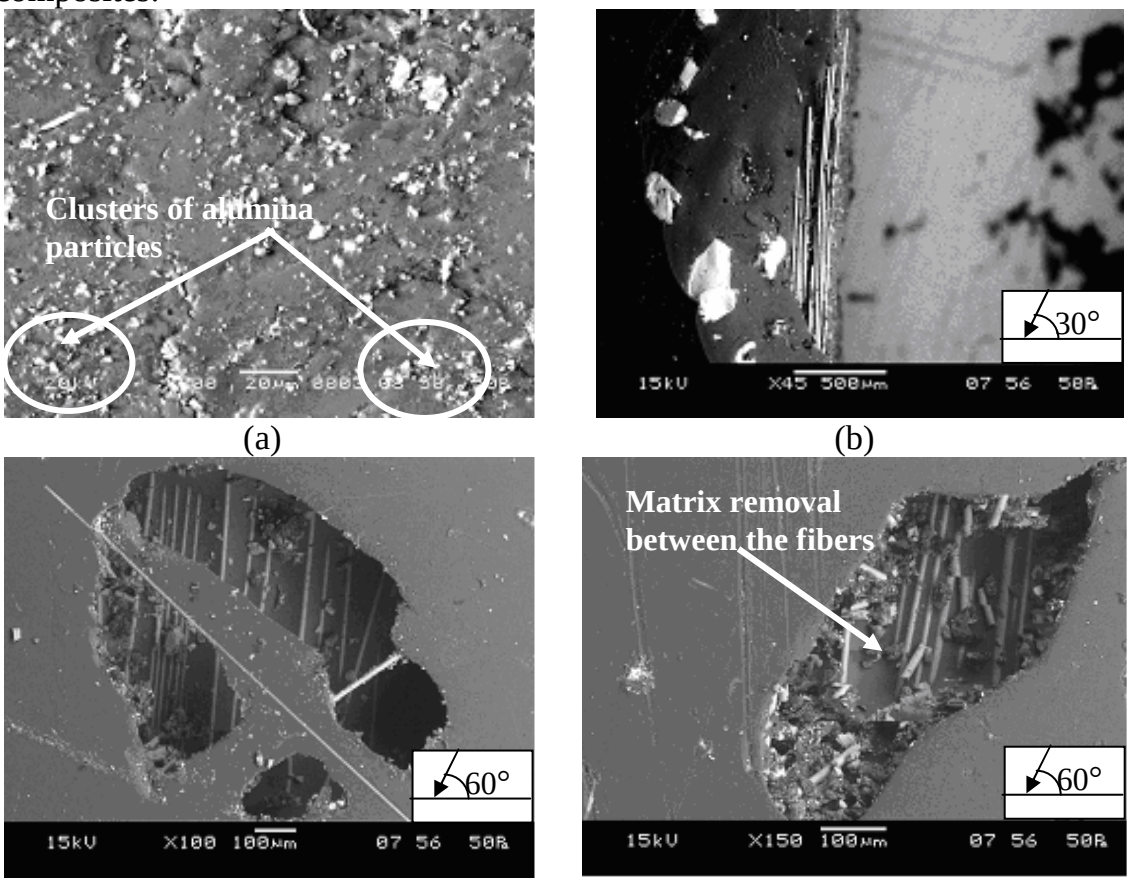

(a) (b)

(c) (d)

Fig. 6.31 Scanning electron micrograph of alumina filled glass fiber epoxy matrix composite surfaces erodent at impact velocity 43m/sec, impingement angle 30°, filler content 10wt%, erodent temperature 60°C, erodent size 450µm and S.O.D 65mm.

Figure 6.31a shows a portion of the alumina filled glass-epoxy composite surface before the erosion has occurred. Small and big clusters of alumina particles are observed on the upper surface of the composite. The SEM image of the eroded surface of the composite at impingement angle of 30° is seen in Figure 6.31b. Here, the erodent particles are at an elevated temperature of 60°C impacting the composite surface with a speed of 43 m/s. Because of the smaller normal component of the erodent impact velocity at this low impingement angle, the fibers resist to cracking and as expected not much fiber cracking is seen to have occurred. At higher impingement angle of 60° (Figures 6.31c and 6.31d), however, large craters are noticed in the matrix indicating surface damage due to erosion.

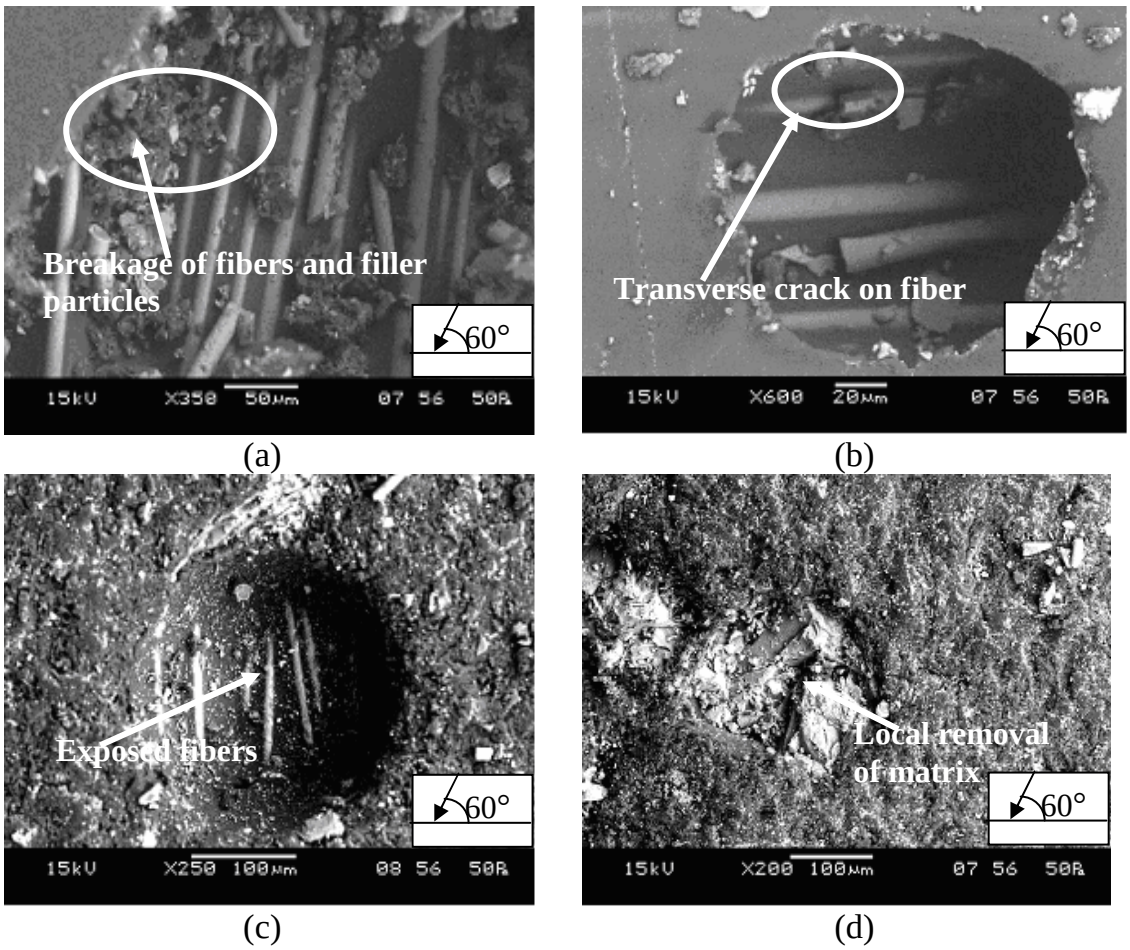

Fig. 6.32 Scanning electron micrograph of alumina filled glass fiber epoxy matrix composite surfaces eroded at impact velocity 43m/sec, impingement angle 60°, filler content 20wt%, erodent temperature 60°C, erodent size 300µm and S.O.D 75mm.

Figures 6.32a-d show SEM micrographs of alumina filled glass fiber reinforced epoxy composites eroded at 60^0 impingement angle where maximum wear rate is recorded. For transverse particle impact (Figs. 6.32a and 6.32b), the resistance to bending is lower and bundles of fibers get bent and break easily. Moreover, in case of transverse erosion, high interfacial tensile stresses are generated by particle impacts. This causes intensive fiber-matrix debonding and breakage of the fibers, which are not supported by the matrix. The continuous impact of sand particles on the composite surface breaks the fibers because of the formation of cracks. Figures 6.32c and 6.32d show features like indentation on the matrix body leading to local removal of resin material from the impacted surface which results in the exposure of the fibers.

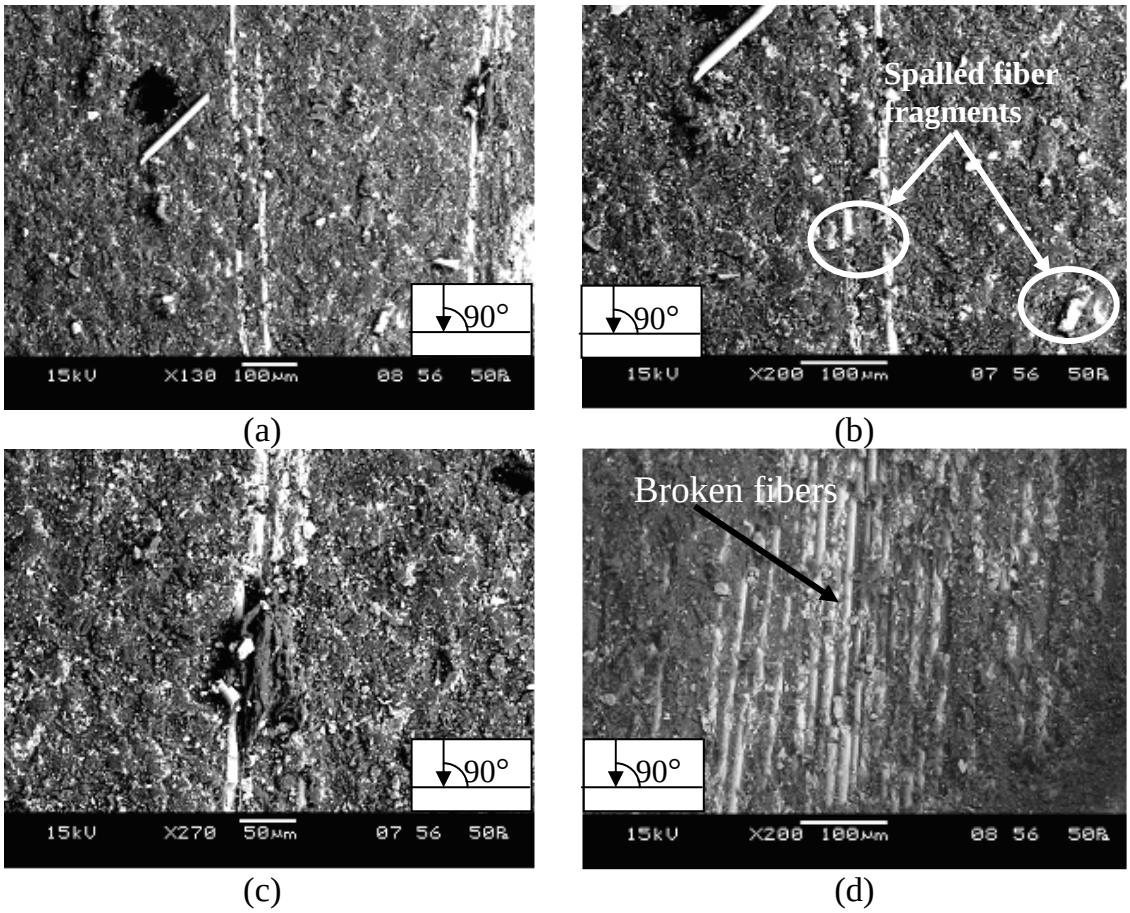

Fig. 6.33 Scanning electron micrograph of alumina filled glass fiber epoxy matrix composite surfaces erodent at impact velocity 54m/sec, impingement angle 90°, filler content 20wt%, erodent temperature 50°C, erodent size 300µm and S.O.D. 85mm.

As the impingement angle of the particles changes to larger values, the effects of normal force become dominant. Figures 6.33a-d illustrate the wear morphology of the material after erosion at normal impact with high impact velocity of 65 m/s. At this impingement angle there is no parallel component of impact force. Hence, no wear is likely to occur. Fibers are cracked into small fragments and they are removed from their places partly with the surrounding matrix like spalled fragments.

6.4 PART 4: SiC FILLED COMPOSITES

This part of the chapter presents the analysis and comparison of erosion response of bamboo-epoxy and glass-epoxy composites filled with silicon carbide (SiC).

6.4.1 Taguchi Experimental Analysis

The results of erosion experiments carried out according to the predetermined design on SiC filled bamboo-epoxy and glass-epoxy composites are presented in Table 6.22. The overall mean for the S/N ratio of the erosion rate is found to be -47.75 db for bamboo based composites and -48.51db for the glass based ones. Analysis of the results leads to the conclusion that factor combination A_1, B_2, C_2, D_3, E_3 and F_1 gives minimum erosion rate (Figure 6.34) for bamboo-epoxy composites and the factor combination A_1, B_2, C_1, D_3, E_1 and F_1 gives minimum erosion rate (Figure 6.35) for glass epoxy composites. The respective interaction graphs are shown in the Figures 6.36 and 6.37 for bamboo epoxy composites and Figures 6.38 and 6.39 for glass-epoxy composites.

Table 6.22 Comparison of erosion rates of SiC filled bamboo-epoxy against glass-epoxy composites under different test conditions as per L_{27} orthogonal array

Expt. No.	A (m/sec)	B (%)	C (^{0}C)	D (Degree)	E (mm)	F (µm)	E_r (b) (mg/kg)	S/N ratio (b) (db)	E_r (g) (mg/kg)	S/N ratio (g) (db)
1	43	0	40	30	65	300	150.00	-43.521	204.348	-46.207
2	43	0	50	60	75	450	133.33	-42.498	342.029	-50.681
3	43	0	60	90	85	600	250.00	-47.958	413.720	-52.334
4	43	10	40	60	75	600	300.00	-49.542	202.899	-46.145
5	43	10	50	90	85	300	130.00	-29.542	180.145	-45.112
6	43	10	60	30	65	450	200.00	-46.020	183.892	-45.291
7	43	20	40	90	85	450	211.11	-46.490	250.435	-47.973
8	43	20	50	30	65	600	325.00	-50.237	248.696	-47.913
9	43	20	60	60	75	300	390.00	-51.821	213.853	-46.602
10	54	0	40	60	85	450	277.77	-48.873	226.087	-47.085
11	54	0	50	90	65	600	225.00	-47.043	353.623	-50.970
12	54	0	60	30	75	300	290.00	-49.248	382.147	-51.644
13	54	10	40	90	65	300	140.00	-42.922	173.913	-44.806
14	54	10	50	30	75	450	233.33	-47.359	284.058	-49.068
15	54	10	60	60	85	600	487.50	-53.759	293.167	-49.342
16	54	20	40	30	75	600	312.50	-49.897	237.681	-47.519
17	54	20	50	60	85	300	220.00	-46.848	281.159	-48.979
18	54	20	60	90	65	450	200.00	-46.020	263.132	-48.403
19	65	0	40	90	75	600	175.00	-44.860	163.768	-44.284
20	65	0	50	30	85	300	390.00	-51.821	359.420	-51.112
21	65	0	60	60	65	450	322.22	-50.163	443.712	-52.942
22	65	10	40	30	85	450	244.44	-47.763	187.536	-45.461
23	65	10	50	60	65	600	425.00	-52.567	295.652	-49.415
24	65	10	60	90	75	300	360.00	-51.126	298.152	-49.488
25	65	20	40	60	65	300	430.00	-52.669	289.855	-49.243
26	65	20	50	90	75	450	233.33	-47.359	347.826	-50.827
27	65	20	60	30	85	600	362.50	-51.186	349.283	-50.863

Note: Er (b): Erosion rate of bamboo-epoxy composites
Er (g): Erosion rate of glass-epoxy composites

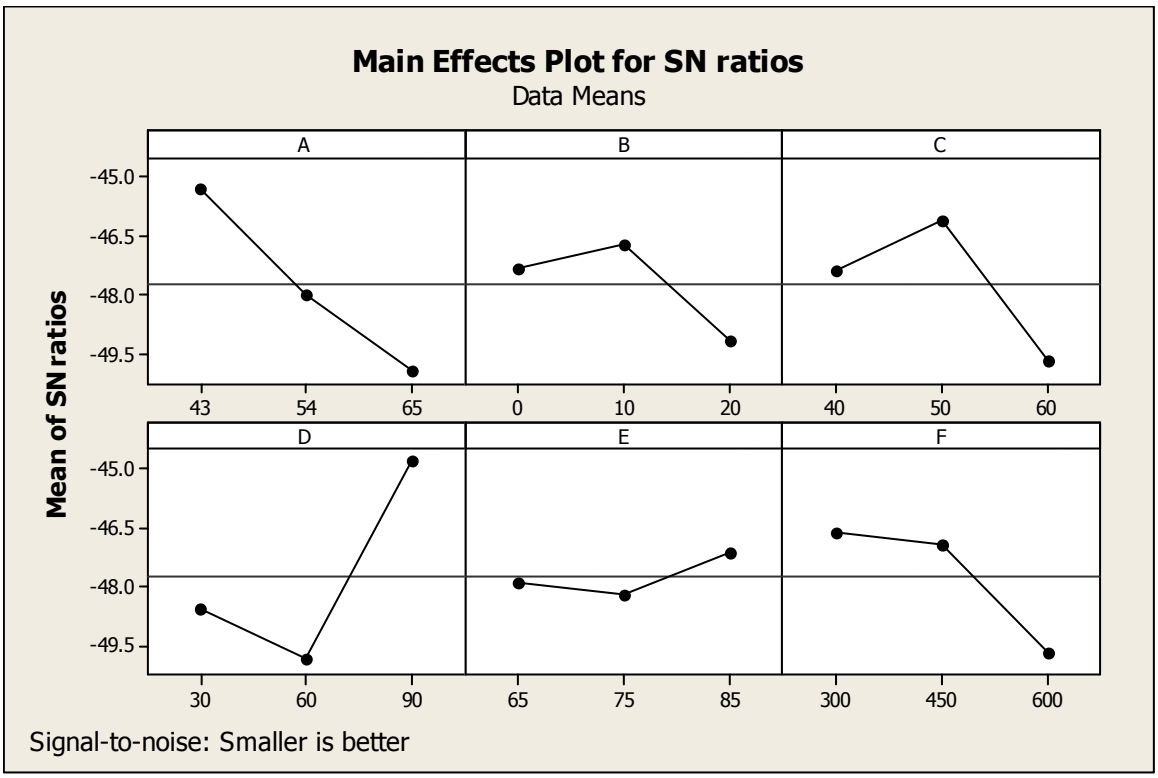

Figure 6.34 Effect of control factors on erosion rate (For SiC filled bamboo-epoxy composites)

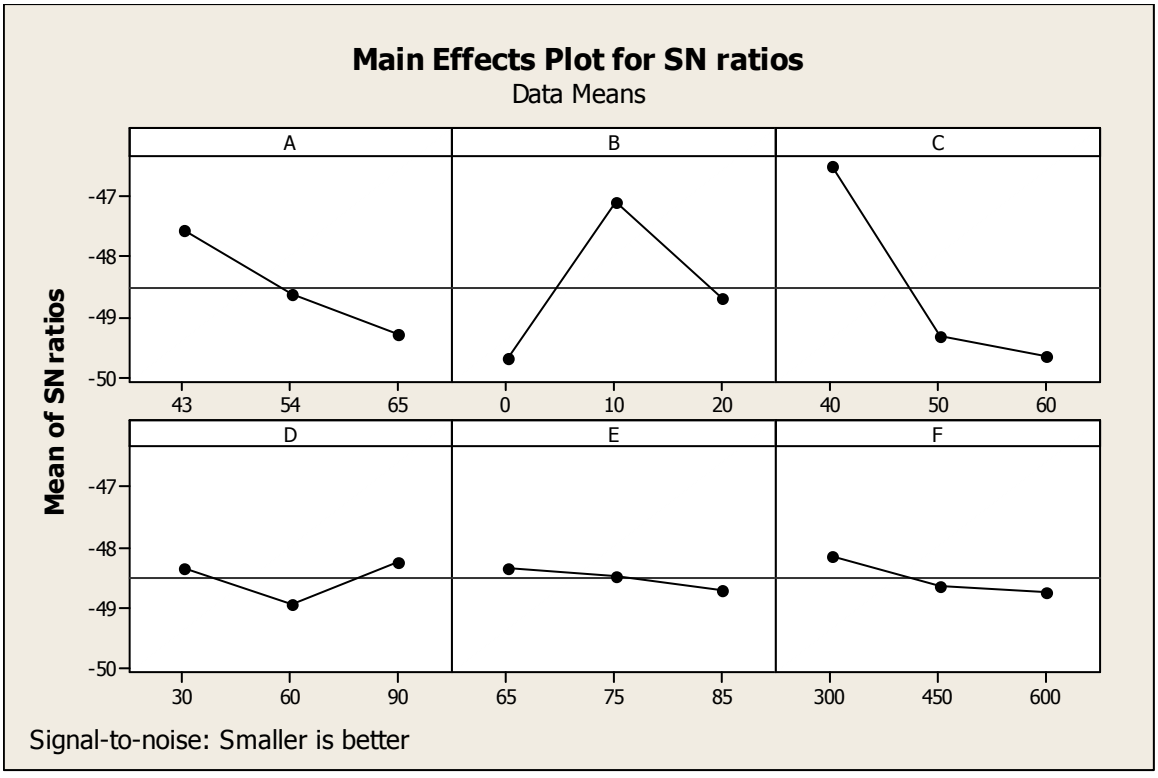

Figure 6.35 Effect of control factors on erosion rate (For SiC filled glass-epoxy composites)

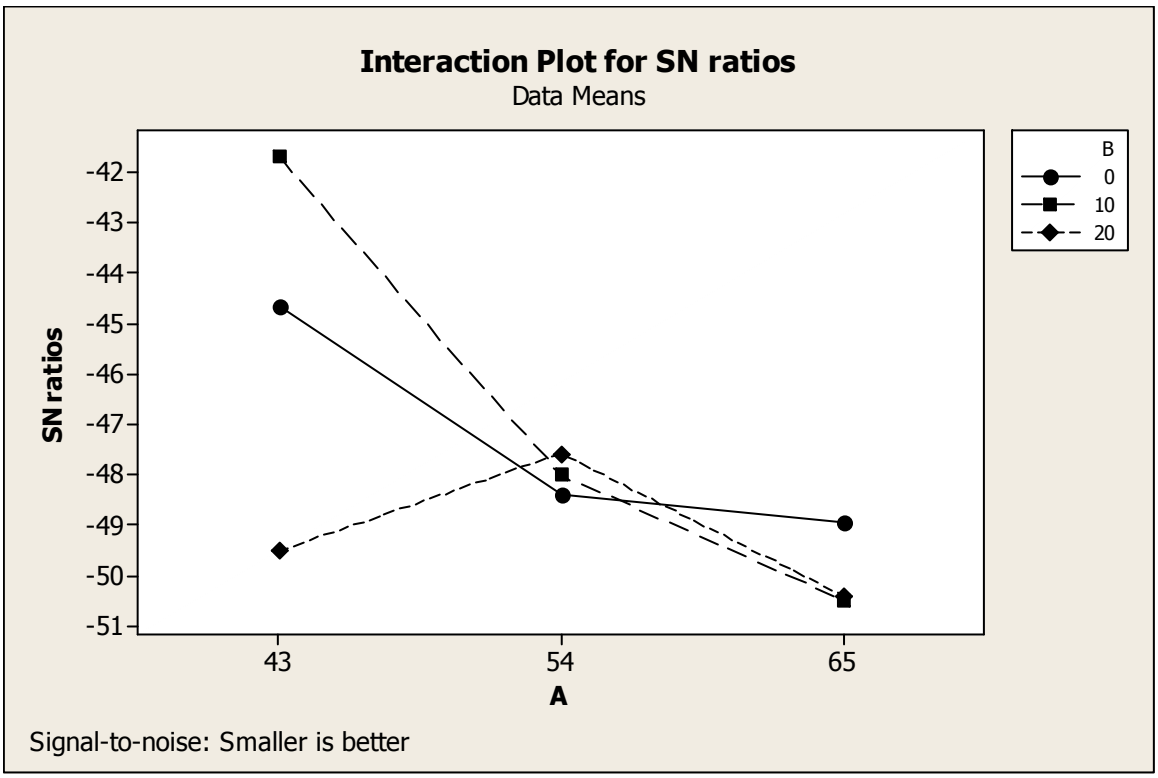

Figure 6.36 Interaction graph between impact velocity and filler content (A×B) for erosion rate (For SiC filled epoxy composites with bamboo-fiber reinforcement)

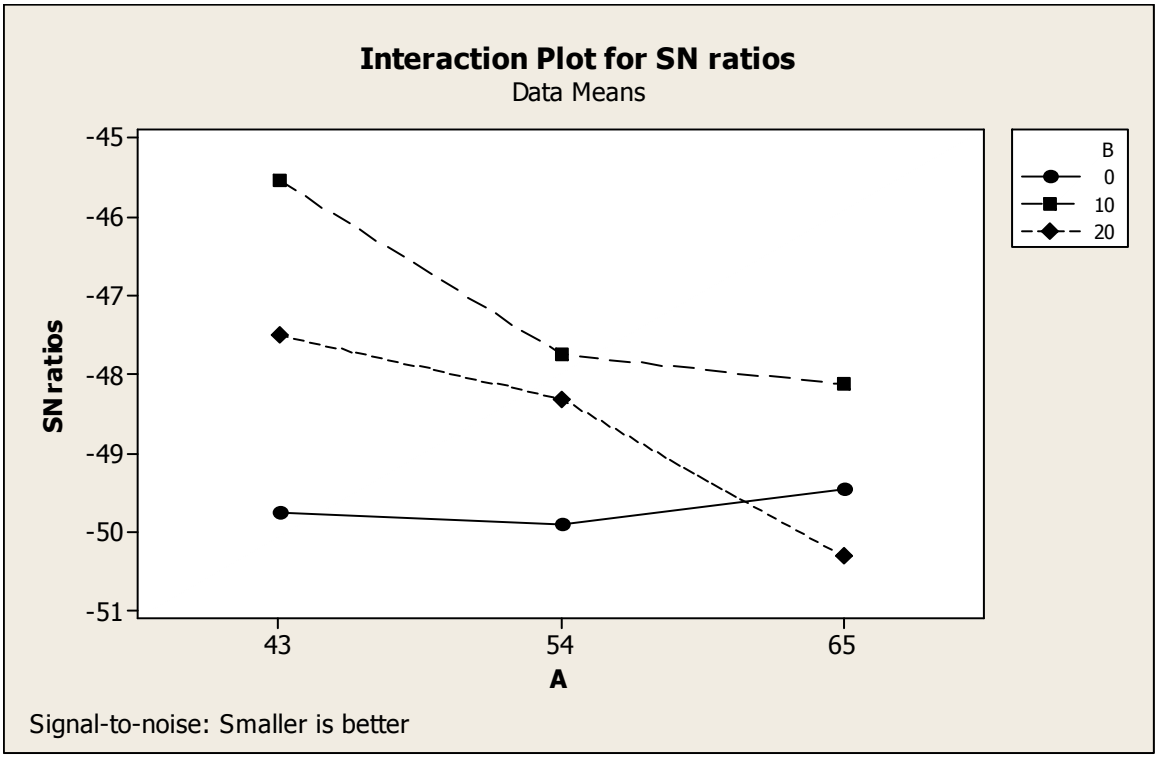

Figure 6.37 Interaction graph between impact velocity and filler content (A×B) for erosion rate (For SiC filled epoxy composites with glass-fiber reinforcement)

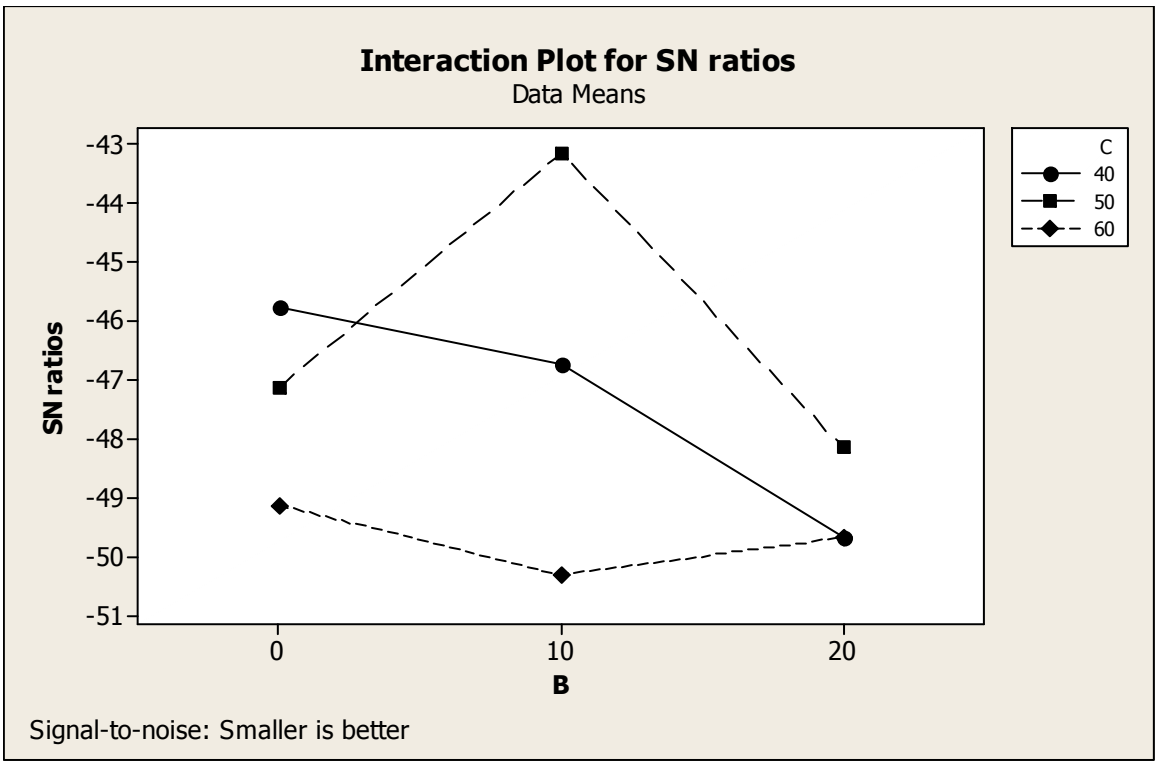

Figure 6.38 Interaction graph between filler content and erodent temperature (B×C) for erosion rate (For SiC filled epoxy composites with bamboo-fiber reinforcement)

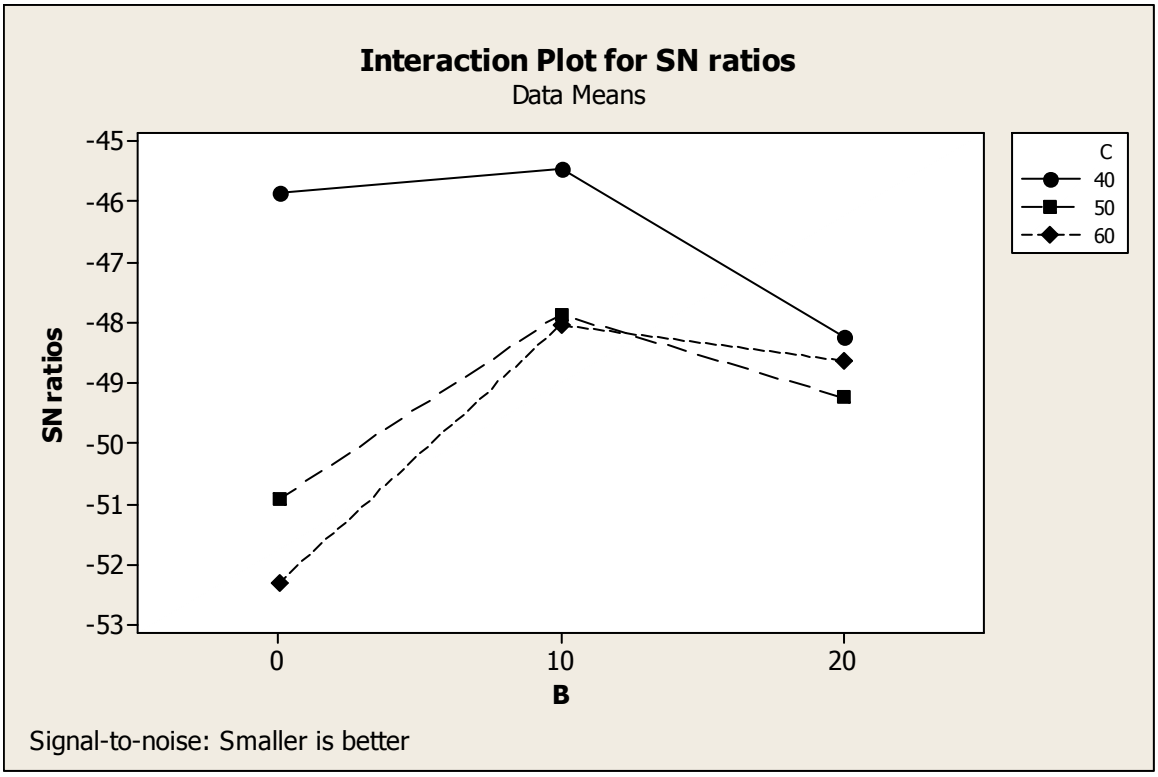

Figure 6.39 Interaction graph between filler content and erodent temperature (B×C) for erosion rate (For SiC filled epoxy composites with glass-fiber reinforcement)

6.4.2 ANOVA and the Effects of Factors

In order to find out statistical significance of various factors like impact velocity (A), SiC content (B), erodent temperature (C), impingement angle (D), stand-off distance (E) and erodent size (F) on erosion rate, analysis of variance (ANOVA) is performed on experimental data. Table 6.23 and Table 6.24 show the results of the ANOVA with the erosion rate of bamboo-epoxy and glass-epoxy based composites taken in this investigation. The last column of the table indicates percentage contribution of the control factors and their interactions on the performance output i.e erosion rate [224].

From Table 6.23, it can be observed for the SiC filled bamboo-epoxy composites that impingement angle (p=0.255), impact velocity (p = 0.301), erodent temperature (p = 0.419) and erodent size (p=0.455) have considerable influence on erosion rate. The interaction of impact velocity and SiC content (p=0.612) as well as impact velocity and erodent temperature (p=0.640) show significant contribution on the erosion rate. The remaining factors and interactions have relatively less significant contribution.

Table 6.23 ANOVA table for erosion rate
(For SiC filled bamboo-epoxy composites)

Source	DF	Seq SS	Adj SS	Adj MS	F	P
A	2	98.31	98.31	49.16	2.32	0.301
B	2	29.01	29.01	14.51	0.69	0.593
C	2	58.65	58.65	29.33	1.39	0.419
D	2	123.61	123.61	61.80	2.92	0.255
E	2	5.34	5.34	2.67	0.13	0.888
F	2	50.66	50.66	25.33	1.20	0.455
A×B	4	69.84	69.84	17.46	0.83	0.612
A×C	4	63.46	63.46	15.87	0.75	0.640
B×C	4	39.88	39.88	9.97	0.47	0.765
Error	2	42.32	42.32	21.16		
Total	26	581.07				

[**]DF: degree of freedom, [##]Seq SS: sequential sum of squares, [$]Adj. SS: extra sum of squares[$$] Seq MS: sequential mean squares, [***]F: F-test, [###]P: percent contribution

Similarly, from Table 6.24, it can be observed that erodent temperature (p = 0.054), SiC content (p=0.091), impact velocity (p = 0.184), impingement angle (p = 0.545) and erodent size (p = 0.607) have considerable influence on erosion rate. The interaction of SiC content and erodent temperature (p = 0.178) as well as impact velocity and SiC content (p = 0.376) show significant contribution on the erosion rate while the remaining factor and interactions have relatively less significant contribution.

Table 6.24 ANOVA table for erosion rate
(For SiC filled glass-epoxy composites)

Source	DF	Seq SS	Adj SS	Adj MS	F	P
A	2	13.396	13.396	6.698	4.42	0.184
B	2	30.234	30.234	15.117	9.98	0.091
C	2	53.519	53.519	26.760	17.66	0.054
D	2	2.531	2.531	1.265	0.84	0.545
E	2	0.540	0.540	0.270	0.18	0.849
F	2	1.962	1.962	0.981	0.65	0.607
A×B	4	11.412	11.412	2.853	1.88	0.376
A×C	4	10.944	10.944	2.736	1.81	0.387
B×C	4	29.476	29.476	7.369	4.86	0.178
Error	2	3.030	3.030	1.515		
Total	26	157.043				

[**]DF: degree of freedom, [##]Seq SS: sequential sum of squares, [$]Adj. SS: extra sum of squares [$$] Seq MS: sequential mean squares, [***]F: F-test, [###]P: percent contribution

6.4.3 Confirmation Experiment

The confirmation experiment is performed for bamboo-epoxy composites by taking an arbitrary set of factor combination $A_3B_3C_1D_2F_2$. Here, factor E has been omitted since it has the least effect on performance characteristic as evident from Table 6.23. Similarly, for the glass-epoxy composites, the confirmation experiment is performed by taking another arbitrary set of factor combination $A_2B_3C_2D_3F_2$. Here also, factor E has been omitted for being the least significant (Table 6.24). The estimated S/N ratio for erosion rate can now be calculated with the help of following prediction equation:

$$\bar{\eta}_{\text{BF-SiC}} = \bar{T} + (\bar{A}_3 - \bar{T}) + (\bar{B}_3 - \bar{T}) + [(\bar{A}_3\bar{B}_3 - \bar{T}) - (\bar{A}_3 - \bar{T}) - (\bar{B}_3 - \bar{T})] + (\bar{C}_1 - \bar{T}) + [(\bar{B}_3\bar{C}_1 - T) - (\bar{B}_3 - \bar{T}) - (\bar{C}_1 - \bar{T})] + (\bar{D}_2 - \bar{T}) + (\bar{F}_2 - \bar{T}) \quad (6.13)$$

$$\bar{\eta}_{\text{GF-SiC}} = \bar{T} + (\bar{A}_2 - \bar{T}) + (\bar{B}_3 - \bar{T}) + [(\bar{A}_2\bar{B}_3 - \bar{T}) - (\bar{A}_2 - \bar{T}) - (\bar{B}_3 - \bar{T})] + (\bar{C}_2 - \bar{T}) + [(\bar{B}_3\bar{C}_2 - T) - (\bar{B}_3 - \bar{T}) - (\bar{C}_2 - \bar{T})] + (\bar{D}_3 - \bar{T}) + (\bar{F}_2 - \bar{T}) \quad (6.14)$$

$\bar{\eta}_{\text{BF-SiC}}, \bar{\eta}_{\text{GF-SiC}}$: Predicted average for SiC filled bamboo fiber based and glass fiber based composites respectively.

$\bar{T}$: Overall experimental average

$\bar{A}_2, \bar{A}_3\ \bar{B}_3, \bar{C}_1, \bar{C}_2, \bar{D}_2, \bar{D}_3$ and $\bar{F}_2$: Mean response for factors and interactions at designated levels.

By combining like terms, the equation reduces to

$$\bar{\eta}_{\text{BF-SiC}} = \bar{A}_3\bar{B}_3 + \bar{B}_3\bar{C}_1 - \bar{B}_3 + \bar{D}_2 + \bar{F}_2 - 2\bar{T} \quad (6.15)$$

$$\bar{\eta}_{\text{GF-SiC}} = \bar{A}_2\bar{B}_3 + \bar{B}_3\bar{C}_2 - \bar{B}_2 + \bar{D}_3 + \bar{F}_2 - 2\bar{T} \quad (6.16)$$

A new combination of factor levels A_2, A_3, B_3, C_1,C_2, D_2, D_3 and F_2 is used to predict erosion rate through prediction equation and it is found to be $\bar{\eta}_{\text{BF-SiC}} = -50.2095\,\text{dB}$ and $\bar{\eta}_{\text{GF-SiC}} = -48.7032\,\text{dB}$ respectively.

For each performance measure, an experiment is conducted for the same set of factor combinations and the obtained S/N ratio value is compared with that obtained from the predictive equation as shown in Table 6.25. The resulting model seems to be capable of predicting erosion rate to a reasonable accuracy. An error of 2.42% and 1.15 % for the S/N ratio of erosion rate is observed for bamboo-epoxy composites and glass epoxy composites respectively. However, the error can be further reduced if the number of measurements is increased. This validates the mathematical model for predicting the measures of performance based on knowledge of the input parameters.

Table 6.25 Results of the confirmation experiments for erosion rate

	Optimal control parameters (For bamboo-epoxy composites)		Optimal control parameters (For glass-epoxy composites)	
	Prediction	Experimental	Prediction	Experimental
Level	$A_3B_3C_1D_2F_2$	$A_3B_3C_1D_2F_2$	$A_2B_3C_2D_3F_2$	$A_2B_3C_2D_3F_2$
S/N ratio for Erosion rate(db)	-50.2095	-51.4269	-48.7032	-49.2661

6.4.4 Effect of Impingement Angle and Erodent Temperature on Erosion

The erosion wear rates of SiC filled bamboo-epoxy and glass-epoxy composites as a function of impingement angle are shown in Figure 6.40 at constant impact velocity (54m/sec), erodent temperature (50°C), stand-off distance (75mm) and erodent size (450μm). It can be seen that the presence of SiC reduces the wear rate of the composites quite significantly. Further, while the maximum erosion is noticed to be occurring at impingement angle of 60° for the unfilled bamboo-epoxy composite and it occurs at impingement angle of 75° for composites filled with SiC. This shift in the erosion behavior is an indication of loss of ductility and is obviously attributed to the brittle nature of bamboo fibers and SiC particulates embedded in the matrix body. Similar behaviour is also shown by glass fiber reinforced epoxy composites filled with SiC particles. It is also important to note that the composites with higher filler content exhibit better erosion resistance.

Similarly, the variation of erosion rate of unfilled and SiC filled composites with erodent temperature at constant impact velocity (54m/sec), impingement angle (90°), stand-off distance (75mm) and erodent size (450μm) is shown in Figure 6.41. Erosion trials are conducted for seven different erodent temperatures under normal impact condition. From this figure, it can be observed that for all the composite samples, the erosion rates remain almost unaffected by the change in erodent temperature from ambient to 40°C. The effect of erodent temperature on erosion is significant above 40°C and the rate of increase in erosion rate is greater at higher temperatures. The observations are similar as in the cases of red

mud, copper slag and alumina filled bamboo-epoxy as well as glass-epoxy composites.

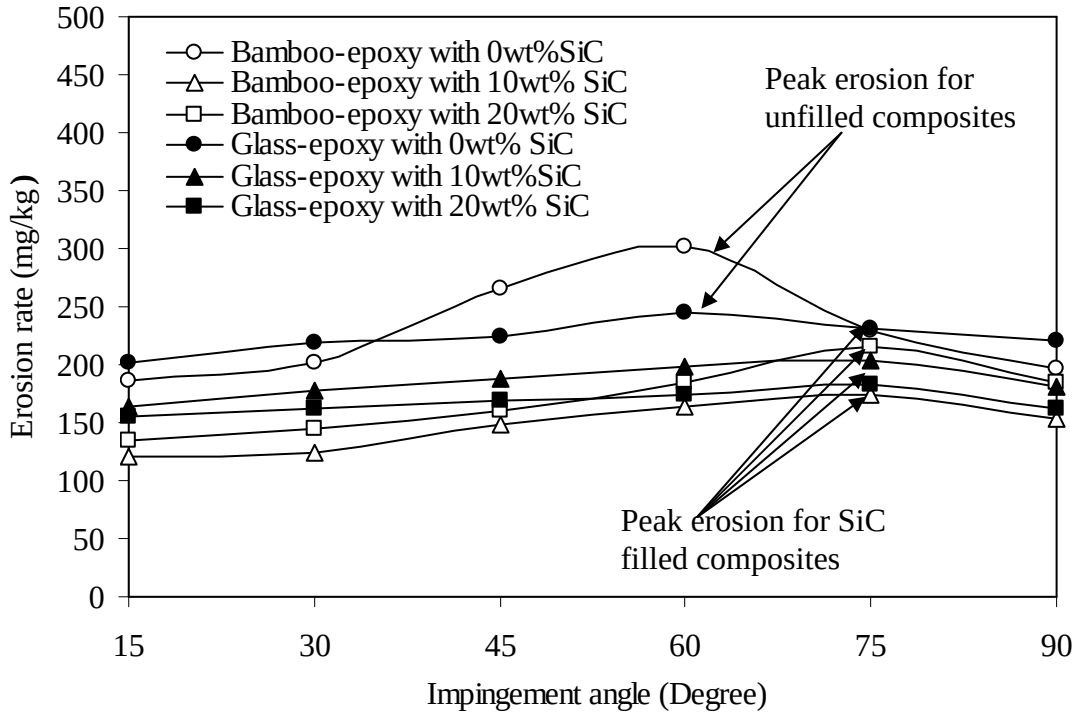

Fig. 6.40 Effect of impingement angle on the erosion wear rate of the composites

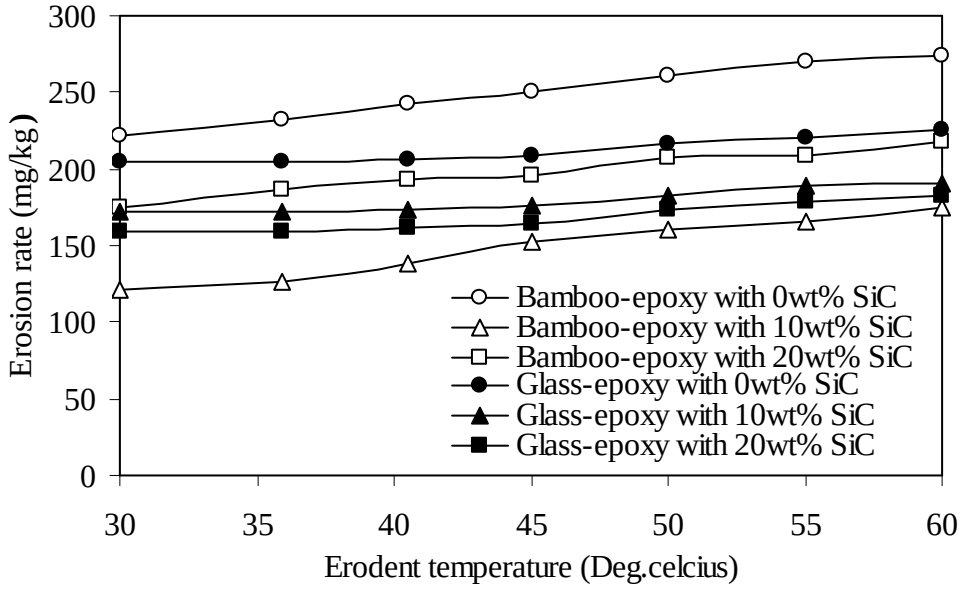

Fig. 6.41 Effect of erodent temperature on the erosion wear rate of the composites

6.4.5 Erosion Efficiency

The values of erosion efficiencies of these composites calculated using Eq. (5.2) is given in Table 6.26 for bamboo-epoxy composites and Table 6.27 for glass-epoxy composites along with their filler content and operating conditions. The erosion efficiencies of these composites under normal impact (η_{normal}) vary from 3 to 6%, 6-9% and 9-12% for impact velocities 65m/sec, 54m/sec and 43m/sec respectively.

Table 6.26 Erosion efficiency of SiC filled bamboo-epoxy composites

Expt. No.	Impact Velocity (U) m/sec	Density of eroding material (ρ) kg/m^3	Hardness of eroding material (H_v)	Erosion rate (Er) mg/kg	Erosion efficiency (η)%
1	43	1243	33.13	150.00	16.9641
2	43	1243	33.13	133.33	5.0265
3	43	1243	33.13	250.00	7.0683
4	43	1297	35.07	300.00	9.5108
5	43	1297	35.07	230.00	5.4684
6	43	1297	35.07	200.00	19.0206
7	43	1345	38.50	211.11	6.4102
8	43	1345	38.50	325.00	39.4739
9	43	1345	38.50	390.00	15.7905
10	54	1243	33.13	277.77	6.6401
11	54	1243	33.13	225.00	4.0337
12	54	1243	33.13	290.00	20.7963
13	54	1297	35.07	140.00	2.1106
14	54	1297	35.07	233.33	14.0706
15	54	1297	35.07	487.50	9.7999
16	54	1345	38.50	312.50	24.0672
17	54	1345	38.50	220.00	5.6481
18	54	1345	38.50	200.00	3.8507
19	65	1243	33.13	175.00	2.1653
20	65	1243	33.13	390.00	19.3025
21	65	1243	33.13	322.22	5.3162
22	65	1297	35.07	244.44	7.0650
23	65	1297	35.07	425.00	5.8965
24	65	1297	35.07	360.00	3.7458
25	65	1345	38.50	430.00	7.6192
26	65	1345	38.50	233.33	3.1006
27	65	1345	38.50	362.50	19.2684

Table 6.27 Erosion efficiency of SiC filled glass-epoxy composites

Expt. No.	Impact Velocity (U) m/sec	Density of eroding material (ρ) kg/m^3	Hardness of eroding material (H_v)	Erosion rate (Er)mg/kg	Erosion efficiency (η)%
1	43	1530	24.80	204.348	14.054
2	43	1530	24.80	342.029	7.841
3	43	1530	24.80	413.720	7.113
4	43	1620	38.07	202.899	6.744
5	43	1620	38.07	180.145	4.490
6	43	1620	38.07	183.892	18.336
7	43	1742	46.19	250.435	7.044
8	43	1742	46.19	248.696	27.980
9	43	1742	46.19	213.853	8.020
10	54	1530	24.80	226.087	3.286
11	54	1530	24.80	353.623	3.855
12	54	1530	24.80	382.147	16.665
13	54	1620	38.07	173.913	2.749
14	54	1620	38.07	284.058	17.960
15	54	1620	38.07	293.167	6.179
16	54	1742	46.19	237.681	16.956
17	54	1742	46.19	281.159	6.686
18	54	1742	46.19	263.132	4.693
19	65	1530	24.80	163.768	1.232
20	65	1530	24.80	359.420	10.818
21	65	1530	24.80	443.712	4.452
22	65	1620	38.07	187.536	5.683
23	65	1620	38.07	295.652	4.300
24	65	1620	38.07	298.152	3.252
25	65	1742	46.19	289.855	4.757
26	65	1742	46.19	347.826	4.281
27	65	1742	46.19	349.283	17.197

The theoretical erosion wear rate (E_{rth}) of the SiC filled bamoo-epoxy composites are calculated using Eq. (5.13). These values are compared with those obtained from experiments (E_{rexpt}) conducted under similar operating conditions. Table 6.28 presents a comparison among the theoretical and experimental results and the associated percentage errors for both SiC filled bamboo-epoxy as well as glass-epoxy composites. The errors in experimental results with respect to the theoretical ones lie in the range 0-14%. The erosion efficiencies of the composites under the present study indicate that at low impact

speed the erosion response is semi-ductile (η=10-100%). On the other hand at relatively higher impact velocity the composites exhibit ductile (η < 10%) erosion behavior [225].

Table 6.28 Comparison of theoretical and experimental erosion rates along with the percentage errors for SiC filled bamboo-epoxy and glass-epoxy composites

Expt. No.	E_{rbth} (b) (mg/kg)	$E_{rbexpt.}$(b) (mg/kg)	Error (b) (%)	E_{rth} (g) (mg/kg)	$E_{rexpt.}$(g) (mg/kg)	Error (g) (%)
1	170.087	150.00	11.8096	231.712	204.348	11.809
2	151.193	133.33	11.8144	387.851	342.029	11.814
3	265.18	250.00	5.7245	479.506	413.720	13.719
4	326.731	300.00	8.1812	185.711	202.899	9.254
5	226.013	230.00	1.7640	166.203	180.145	8.388
6	180.577	200.00	10.7561	193.547	183.892	4.988
7	193.400	211.11	9.1569	283.514	250.435	11.667
8	362.229	325.00	10.2777	232.837	248.696	6.811
9	379.749	390.00	2.6994	244.667	213.853	12.594
10	281.180	277.77	1.2126	236.075	226.087	4.230
11	239.198	225.00	5.9354	323.054	353.623	9.462
12	286.586	290.00	1.1912	338.520	382.147	12.887
13	133.019	140.00	5.2483	161.017	173.913	8.009
14	239.257	233.33	2.4771	295.625	284.058	3.912
15	482.372	487.50	1.0630	310.220	293.167	5.497
16	332.310	312.50	5.9613	226.690	237.681	4.848
17	223.555	220.00	1.5902	279.022	281.159	0.765
18	182.515	200.00	9.5801	240.127	263.132	9.580
19	162.101	175.00	7.9576	160.040	163.768	2.329
20	372.462	390.00	4.7088	327.574	359.420	9.721
21	294.323	322.22	9.4781	395.002	443.712	12.331
22	235.580	244.44	3.7610	173.329	187.536	8.196
23	406.846	425.00	4.4621	267.805	295.652	10.397
24	334.178	360.00	7.7271	293.945	298.152	1.430
25	395.616	430.00	8.6912	264.453	289.855	9.605
26	227.29	233.33	2.6574	345.030	347.826	0.810
27	370.715	362.50	2.2159	338.968	349.283	3.043

6.4.6 Surface Morphology

Figure 6.42 shows scanning electron micrographs of SiC filled bamboo-epoxy composite surface eroded at impact velocity of 54 m/sec. It is evident from the micrographs (Figures 6.42a and 6.42b) that the material removal in bamboo-

epoxy composite with 10wt% SiC is dominated by plastic deformation. Formation of micro-cracks and embedment of fragments of sand particles is evident from the micrograph in Figure 6.42c showing the erosion at 60° impingement angle.

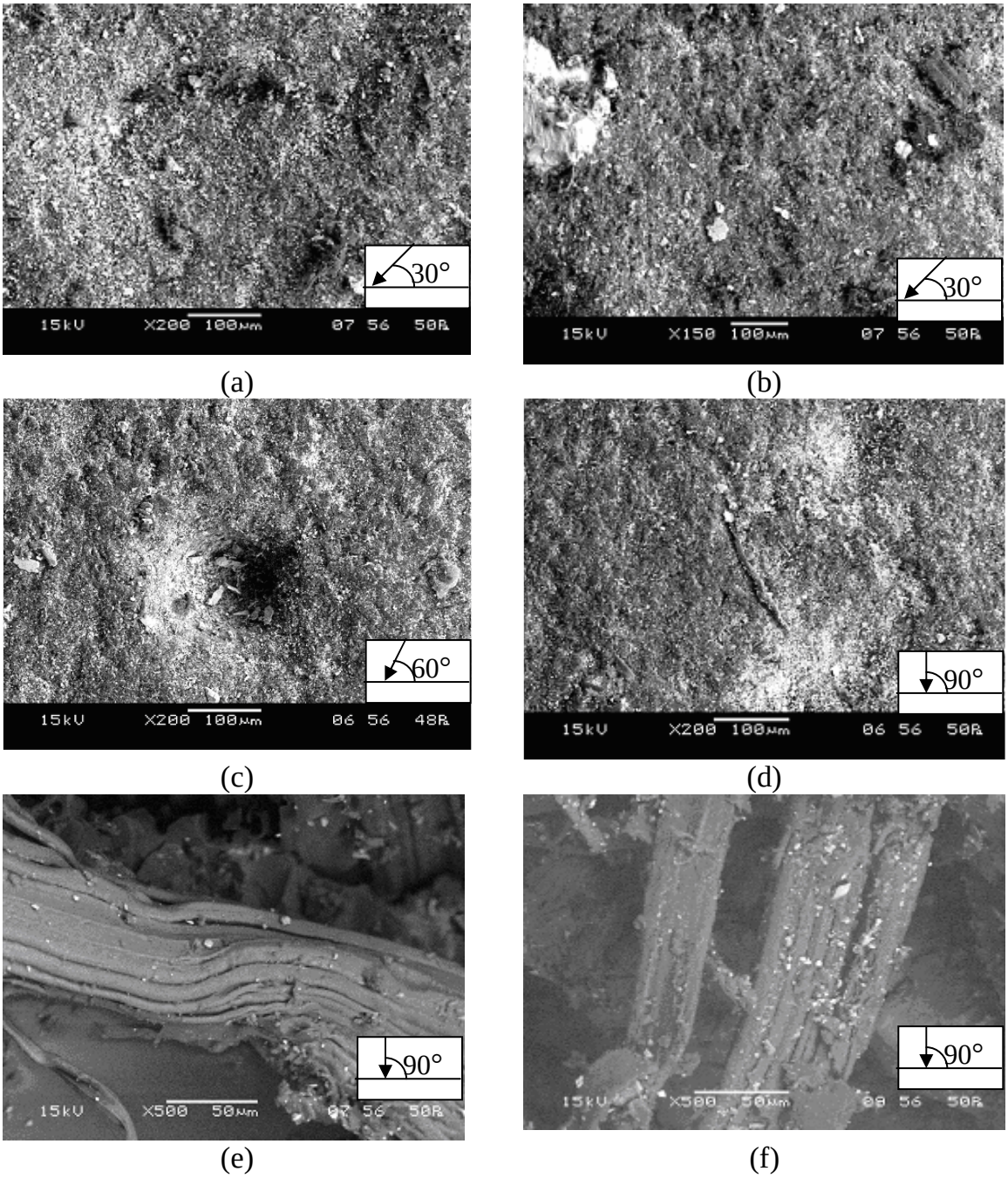

Fig. 6.42 SEM micrographs of the eroded bamboo-epoxy composites filled with SiC

However, during the normal impact the largest part of the initial energy of the erodent is converted into heat and hence matrix is softened which resulted in

embedment of sand particles (Figure 6.42d). These particles control further erosion of the target surface. Figures 6.42e and 6.42f show micrographs of eroded surfaces of composites with 20 wt% SiC. At normal impingement angle, removal of matrix along the length of the fiber and subsequent exposure of fibers can be seen from the micrograph (Figure 6.42e) at an impact velocity of 54m/sec. At higher impact velocity (65m/sec), the erodent particles possess higher kinetic energy that results in increased plastic deformation and removal of matrix leading to protrusion of fibers out from the matrix (Figure 6.42f).

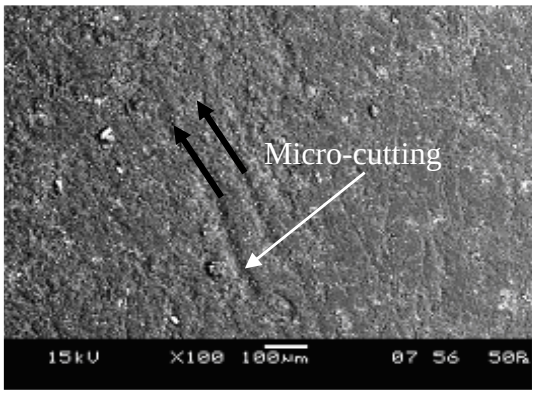

(a)

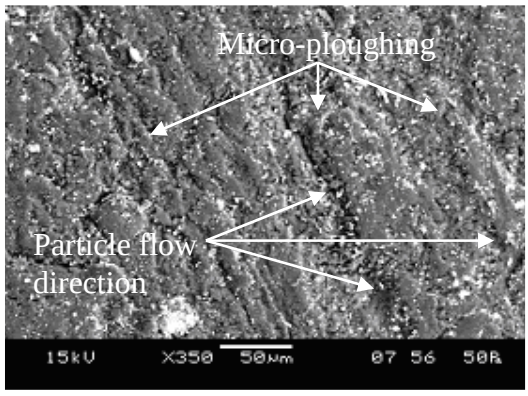

(b)

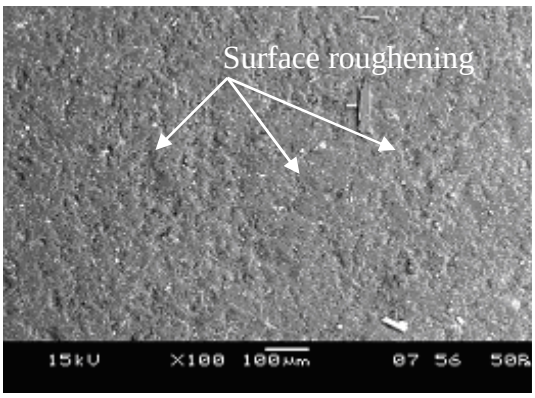

(c)

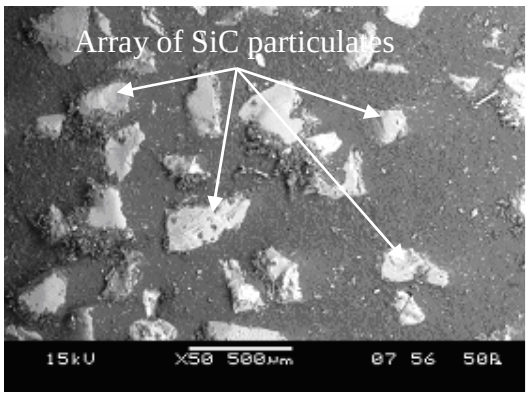

(d)

(e)

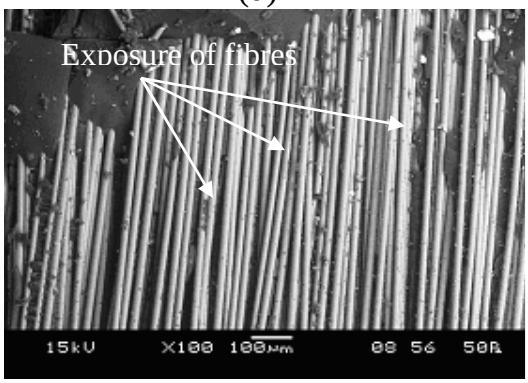

(f)

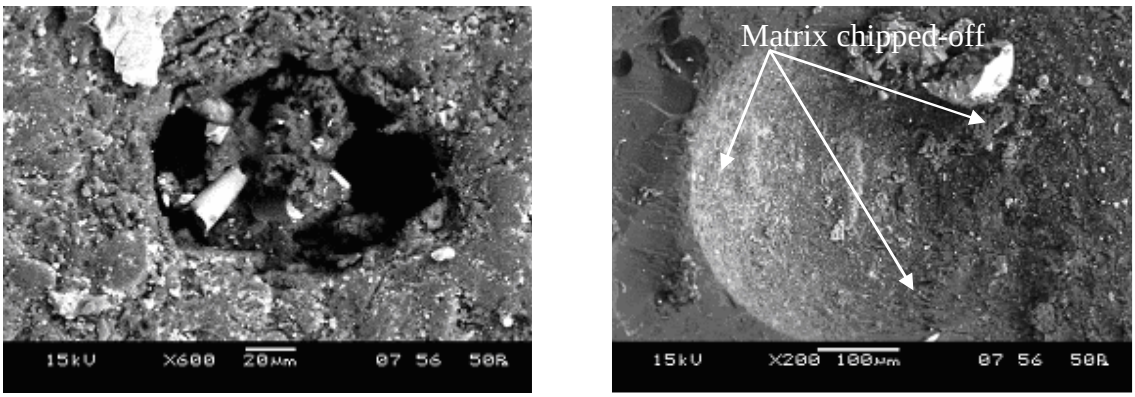

(g) (h)

Fig. 6.43 SEM micrographs of the eroded glass-epoxy composites filled with SiC.

Scanning electron micrographs of the worn surfaces of both unfilled and SiC filled glass-epoxy composites are shown in Figure 6.43. The SEM image of the composite without filler eroded at an impingement angle of 30° and an impact velocity of 43 m/sec is shown in Figure 6.43a. When impacting at low angles, the hard erodent particles penetrate the surface of the samples and cause material removal by micro-cutting and micro-ploughing (Figures 6.43a and 6.43b). And it is possible to investigate the particle flow direction easily from the wear trace of the particles, which are indicated by black arrows in the micrographs. Figures 6.43c and 6.43d illustrate the worn surfaces of SiC filled composites subjected to higher erodent impact velocity of 54 m/sec. These micrographs show the distribution of filler particles in the matrix and features like surface roughening. Figure 6.43e shows a portion of the eroded surface where matrix covering the fiber seems to be chipped off and the crater thus formed shows an array of almost intact fibres. Similarly, in Figure 6.43f, there is local removal of matrix material from the impacted surface resulting in exposure of fibers to the erosive environment. Figures 6.43g and 6.43h show the exposed fibres getting fragmented and dislodged from the matrix body leading to a greater degree of surface damage. This is a case of the erodent particles striking aggressively the composite surface at high impingement angle with high impact velocity. Due to repeated impact of the erodent carrying higher energy, the fibers beneath the matrix layer break and the SiC particles in the matrix body and along the matrix-fiber interface also undergo fragmentation resulting in loose debris. The matrix

shows multiple fractures and material removal. The exposed fibres are broken into fragments and thus can be easily removed from the worn surfaces.

6.5 Relative Effect of Different Fillers on Erosion Response

Table 6.29 provides the erosion wear rates for the bamboo-epoxy composites with the four different filler materials.

Table 6.29 Comparison of erosion rates of bamboo-epoxy composites with different fillers

Expt. No.	A (m/sec)	B (%)	C (°C)	D (Degree)	E (mm)	F (µm)	E_r (b) (mg/kg) Red mud	E_r (b) (mg/kg) Copper slag	E_r (b) (mg/kg) Alumina	E_r (b) (mg/kg) SiC
1	43	0	40	30	65	300	150.000	150.00	150.00	150.00
2	43	0	50	60	75	450	133.330	133.33	133.33	133.33
3	43	0	60	90	85	600	250.000	250.00	250.00	250.00
4	43	10	40	60	75	600	150.000	237.50	275.00	300.00
5	43	10	50	90	85	300	201.000	139.00	360.00	130.00
6	43	10	60	30	65	450	137.220	233.33	244.44	200.00
7	43	20	40	90	85	450	200.000	211.11	144.44	211.11
8	43	20	50	30	65	600	350.000	287.50	200.00	325.00
9	43	20	60	60	75	300	140.000	170.00	300.00	390.00
10	54	0	40	60	85	450	277.770	277.77	277.77	277.77
11	54	0	50	90	65	600	225.000	225.00	225.00	225.00
12	54	0	60	30	75	300	290.000	290.00	290.00	290.00
13	54	10	40	90	65	300	165.000	172.00	160.00	140.00
14	54	10	50	30	75	450	152.220	244.44	264.44	233.33
15	54	10	60	60	85	600	182.500	187.50	175.00	487.50
16	54	20	40	30	75	600	125.000	262.50	300.00	312.50
17	54	20	50	60	85	300	320.000	240.00	230.00	220.00
18	54	20	60	90	65	450	211.111	133.33	166.66	200.00
19	65	0	40	90	75	600	175.000	175.00	175.00	175.00
20	65	0	50	30	85	300	390.000	390.00	390.00	390.00
21	65	0	60	60	65	450	322.220	322.22	322.22	322.22
22	65	10	40	30	85	450	244.440	255.55	344.44	244.44
23	65	10	50	60	65	600	215.000	262.50	325.00	425.00
24	65	10	60	90	75	300	250.000	247.00	340.00	360.00
25	65	20	40	60	65	300	330.000	360.00	390.00	430.00
26	65	20	50	90	75	450	155.550	200.00	166.66	233.33
27	65	20	60	30	85	600	275.000	287.50	312.50	362.50
Mean erosion rate							**222.865**	225.817	243.403	261.40

Table 6.30 Comparison of erosion rates of glass-epoxy composites with different fillers

Expt. No.	A (m/sec)	B (%)	C (°C)	D (Degree)	E (mm)	F (µm)	E_r (b) (mg/kg) Red mud	E_r (b) (mg/kg) Copper slag	E_r (b) (mg/kg) Alumina	E_r (b) (mg/kg) SiC
1	43	0	40	30	65	300	204.348	204.348	204.348	204.348
2	43	0	50	60	75	450	342.029	342.029	342.029	342.029
3	43	0	60	90	85	600	413.720	413.720	413.720	413.720
4	43	10	40	60	75	600	256.522	273.913	220.290	202.899
5	43	10	50	90	85	300	376.124	284.058	183.333	180.145
6	43	10	60	30	65	450	266.667	389.247	197.134	183.892
7	43	20	40	90	85	450	222.663	163.768	289.855	250.435
8	43	20	50	30	65	600	121.739	234.319	173.913	248.696
9	43	20	60	60	75	300	175.362	239.192	207.891	213.853
10	54	0	40	60	85	450	226.087	226.087	226.087	226.087
11	54	0	50	90	65	600	353.623	353.623	353.623	353.623
12	54	0	60	30	75	300	382.147	382.147	382.147	382.147
13	54	10	40	90	65	300	139.130	307.246	150.725	173.913
14	54	10	50	30	75	450	157.342	156.522	289.855	284.058
15	54	10	60	60	85	600	191.304	200.197	301.159	293.167
16	54	20	40	30	75	600	140.192	204.348	226.087	237.681
17	54	20	50	60	85	300	274.638	214.493	376.812	281.159
18	54	20	60	90	65	450	226.087	276.371	271.053	263.132
19	65	0	40	90	75	600	163.768	163.768	163.768	163.768
20	65	0	50	30	85	300	359.420	359.420	359.420	359.420
21	65	0	60	60	65	450	443.712	443.712	443.712	443.712
22	65	10	40	30	85	450	173.913	121.739	202.899	187.536
23	65	10	50	60	65	600	198.193	197.101	161.739	295.652
24	65	10	60	90	75	300	168.116	221.890	142.973	298.152
25	65	20	40	60	65	300	318.152	144.928	144.928	289.855
26	65	20	50	90	75	450	214.493	202.899	284.058	347.826
27	65	20	60	30	85	600	295.652	167.892	293.158	349.283
Mean erosion rate							**252.042**	255.147	259.508	276.673

The values are obtained by conducting 27 erosion trials as per the pre-determined experimental scheme. The values of erosion rates for experiment numbers 1,2,3,10,11,12,19,20 and 21 in the Table 6.29 are same in the respective rows as they represent composites with out any particulate filler. The mean value of erosion rates of composites with each individual filler has been calculated. On comparing these mean values it is found that the composite with red mud gives the minimum erosion rate. Among the two conventional fillers, however, alumina is found to be better in this respect as the alumina filled bamboo-epoxy

composites exhibit a lower mean erosion rate as compared to the silicon carbide filled composites.

A similar comparison among the particulate fillers with respect to the erosion performance has been made for the glass-epoxy composites as well (Table 6.30). It is noted in this case also that the composites with red mud have minimum mean erosion rate. It is interesting to note that red mud and copper slag, in spite of being industrial wastes, show lower erosion rates as compared to the conventional fillers i.e. alumina and SiC.

Further, among the four filler materials considered for this study, red mud emerges as the best candidate to be used in epoxy based composites, irrespective of fiber type, as far as the resistance to solid particle erosion is concerned.

Chapter Summary

This chapter has provided:

1. The results of erosion tests for bamboo-epoxy and glass-epoxy composites with different particulate fillers and their comparison
2. The analysis of the experimental results using Taguchi method
3. The effect of impingement angle and erodent temperature on erosion response of composites
4. The surface morphologies of eroded composites using SEM
5. The comparison of different particulate fillers with regard to the erosion performance of composites under similar test conditions

The next chapter presents the summary of research findings and conclusions drawn from this investigation along with recommendations for potential applications and future work.

****

Chapter 7

SUMMARY AND CONCLUSIONS

The research reported in this thesis broadly consists of two parts:

- The first part has provided the description of the materials used, the experimental details and various mechanical characteristics of particulate filled bamboo-epoxy hybrid composites. An assessment of bamboo fiber as a potential reinforcing element has been made by comparing the properties and performance of bamboo based composites with those of a similar set of glass fiber reinforced composites.

- The second part has reported the effect of four different particulate fillers i.e. red mud, copper slag, alumina and silicon carbide on the solid particle erosion characteristics of these composites. While the primary focus of this research has remained on erosion wear performance of bamboo based hybrid composites, it has also attempted, at the same time to open up a new avenue for value added utilisation of the two industrial wastes (red mud and copper slag).

7.1 Summary of Research Findings

The performance of an engineering material is judged by its properties and behaviour under tensile, compressive, shear and other static or dynamic loading conditions in both normal and adverse test environments. This information becomes essential for selecting the proper material in a given application as well as for designing a composite structure with the selected material. To this end, the present work has reported the performance of a new class of polymer based hybrid composites with emphasis on the general trends observed in their properties and behaviour. A wealth of property data has been generated for a series of bamboo-epoxy and glass-epoxy composites filled with four distinctly different kinds of particulates. These material properties have been determined

by conducting physical and mechanical tests under controlled laboratory conditions.

By incorporating the chosen particulate fillers into the bamboo/glass-fiber reinforced epoxy, synergistic effects, as expected are achieved in the form of modified mechanical properties and improved erosion wear resistance. Inclusion of fiber in neat epoxy improved the load bearing capacity (tensile strength) and the ability to withstand bending (flexural strength) of the composites. But with the incorporation of particulate fillers, the tensile strengths of the composites are found to be decreasing in most of the cases. This decline in strength may be attributed to two reasons: one possibility is that the due to the presence of pores at the interface between the filler particles and the matrix, the interfacial adhesion may be too weak to transfer the tensile stress; the other is that the corner points of the irregular shaped particulates result in stress concentration in the matrix body.

Hardness values have been found to have improved invariably for all the composites on addition of particulate fillers, irrespective of the type of filler. The reduction in tensile strength and the improvement in hardness with the incorporation of fillers can be explained as follows: under the action of a tensile force, the filler-matrix interface is vulnerable to debonding depending on interfacial bond strength and this may lead to a break in the composite. But in case of hardness test, a compression or pressing stress is in action. So the polymeric matrix phase and the solid filler phase would be pressed together and touch each other more tightly. Thus, the interface can transfer pressure more effectively although the interfacial bond may be poor. This might have resulted in an enhancement of hardness.

In the present investigation, it is noticed that the composites with particulate fillers have higher void fraction compared to the unfilled composites. Among the particulate filled bamboo-epoxy composites, least value of void content is recorded for the composites with silicon carbide filler. However, for the glass-

epoxy composites, minimum void fraction is noted for the composites with red mud filler. The presence of pores and voids in the composite structure significantly affect some of the mechanical properties and even the performance of the composites. Higher void contents usually mean lower fatigue resistance, greater susceptibility to water penetration and weathering. However, presence of void is unavoidable in composite making particularly through hand-lay-up route.

The erosion wear rates of particulate filled bamboo-epoxy composites are found to be lower than those of the unfilled composites under similar test conditions. This has led to the conclusion that the presence of particulate fillers improves the erosion wear resistance of fiber reinforced epoxy composites. The reduction in material loss in these particulate filled composites can be attributed to two reasons. One is the improvement in the bulk hardness of the composite with addition of these hard filler particles. Secondly, during the erosion process, the filler particles absorb a good part of the kinetic and thermal energy associated with the erodent. This results in less amount of energy being available to be absorbed by the matrix body and the reinforcing fiber phase. These two factors together lead to the enhancement of erosion wear resistance of the composites. Similar trend in the erosion behaviour is noticed also for the glass-epoxy composites although bamboo based composites exhibit superior erosion resistance as compared to composites with glass fibers under identical test conditions.

The erosion wear rates of the composites are found to be dependent on the impingement angle. The findings of this research further suggest that, this dependency is also influenced by the nature of the filler material. In fact, the angle of impact determines the relative magnitude of the two components of the impact velocity namely, the component normal to the surface and parallel to the surface. The normal component will determine how long the impact will last (i.e. contact time) and the load. The product of this contact time and the tangential (parallel) velocity component determines the amount of sliding that takes place.

The tangential velocity component also provides a shear loading to the surface, which is in addition to the normal load that the normal velocity component causes. Hence, as this angle changes the amount of sliding that takes place also changes the nature and magnitude of the stress system. Both of these aspects influence the way a composite wears out. This study therefore implies that composites with fillers of different type and content would exhibit different angular dependency.

7.2 Conclusions

This analytical and experimental investigation on particulate filled bamboo/glass-epoxy composites has led to the following specific conclusions:

1. Successful fabrication of multi-component hybrid bamboo/glass-epoxy composites with reinforcement of conventional ceramic fillers such as Al_2O_3 and SiC is possible. Industrial wastes like red mud and copper slag can also be gainfully utilized as fillers in composite making.
2. Incorporation of these fillers modifies the tensile, flexural, impact and inter-laminar shear strengths of the composites both for bamboo as well as for glass fiber reinforcement. The tensile modulus, micro-hardness and density of the composites are also greatly influenced by the type and content of fillers. The particulate filled bamboo-epoxy composites possess higher hardness values compared to the glass-epoxy composites irrespective of the filler type. However, their strength properties are not found as good as those of the glass fiber reinforced composites. This suggests that bamboo fiber has the potential to replace glass fiber in some applications that do not require very high load bearing capabilities. However, while fabricating a composite of specific requirements, there is a need for the choice of appropriate fiber and filler material for optimizing the composite system.
3. A theoretical model based on conservation of particle kinetic energy and thermal energy during multiple impact erosion process has been developed. To overcome the shortcomings of the existing theoretical models an

'erosion efficiency' term has been introduced. It is demonstrated that if supported by an appropriate magnitude of erosion efficiency, the proposed model can perform well for polymer based hybrid composites for normal as well as oblique impacts.

4. Erosion characteristics of these composites can be successfully analyzed using Taguchi experimental design scheme. Taguchi method provides a simple, systematic and efficient methodology for the analysis of the control factors. Significant factors affecting the erosion rate of composites are identified through successful implementation of ANOVA. It is found that impact velocity and impingement angle are the two most significant factors for all bamboo-epoxy composites except the red mud filled ones for which impact velocity and stand-off-distance are the parameters most significantly influencing the erosion rate. Similarly, the analysis reveals that for all the glass-epoxy composites considered in this investigation, irrespective of the filler type, the two most significant factors contributing to the erosion are filler content and erodent temperature. It is noteworthy that while the factors (impact velocity, impingement angle, stand-off-distance) identified as significant for bamboo-epoxy composites are operating variables, the significant factors (filler content, erodent temperature) obtained for the glass-epoxy composites are material variables.
5. This study reveals the semi-ductile response for most of these particulate filled bamboo/glass-epoxy composites with respect to erosion wear. The peak erosion rate is found to be occurring at 60° impingement angle for the unfilled composites as well as for red mud and alumina filled composites with both bamboo as well as glass reinforcement. The impingement angles corresponding to peak erosion for SiC and copper slag filled composites are 75° and 45° respectively. The erosion rate of all these composites is also affected by the erodent temperature.
6. The erosion efficiency (η), in general, characterizes the wear mechanism of composites. The particulate filled composites under this study mostly exhibit semi-ductile erosion response (η = 3 - 48%) for low impact

velocities and (η = 1 - 20%) for relatively high impact velocity irrespective of the fiber type.

7. Several wear mechanisms have been observed microscopically which explained the way bamboo and glass fibers respond to erosion. For bamboo fiber composites, severe deterioration of both fiber and matrix, micro-ploughing in the matrix, transverse shearing, stripping and fibrillation of fiber are identified as the predominant damage mechanisms. Whereas fiber-matrix debonding, fiber-pulling and fracture are the characteristic features of damage in glass fiber based composites.
8. The presence of particulate fillers in these composites improves their erosion wear resistance and this improvement depends on the type and content of the fillers. It is interesting to note that red mud and copper slag, in spite of being industrial wastes, show lower erosion rates as compared to the conventional fillers i.e. alumina and SiC. Further, among the four filler materials considered in this study, red mud emerges as the best candidate to be used in epoxy based composites, irrespective of fiber type, as far as the resistance to solid particle erosion is concerned.

7.3 Recommendations for Potential Applications

The particulate filled bamboo/ glass-fiber reinforced hybrid composites fabricated and experimented upon in this investigation are found to have adequate potential for a wide variety of applications particularly in erosive environment. When solid particle erosion is not the predominant degrading factor, only bamboo-epoxy or glass-epoxy composites without any particulate filler can be recommended. Manufacturing of light weight sports goods such as: cricket bat, tennis racquets etc. are few such examples. Of course, the weight fraction of fiber in the composite is to be decided from the view point of required strength.

If the place of use is erosive in nature then particulate filled bamboo-fiber reinforced composites are to be preferred due to their reasonably high erosion

resistance. The present study has established that red mud and copper slag can be excellent candidates as particulate fillers in hybrid composites. When cost reduction is the prime consideration, industrial wastes like red mud and copper slag can effectively replace the conventional and relatively expensive materials like Al_2O_3 and SiC. Their use may be suggested in applications like engineering structures in dusty environment and low cost building materials in deserts. However, the type and content of fillers are to be decided judiciously keeping the strength and intensity of erosion attack in mind. Use of these composites, in general, may also be recommended for applications like partition boards, false ceilings, pipe lines carrying coal dust, exhaust fan blades, nozzles and diffusers, light weight vehicles etc.

7.4 Scope for Future Work

The present research work leaves a wide scope for future investigators to explore many other aspects of such hybrid composites. Some recommendations for future research include:

- Study on the response of these composites to other wear modes such as sliding and abrasion.
- Possible use of other ceramic/metallic fillers, polymeric resins and natural fibers in the development of new hybrid composites.
- Cost analysis of these composites to assess their economic viability in industrial applications.

****

REFERENCES

1. Agarwal B. D and Broutman L. J, (1990). Analysis and performance of fiber composites, Second edition, John wiley & Sfons, Inc, pp.2-16.
2. Lakkad S. C and Patel J. M, (1981). Mechanical properties of bamboo, a natural composite, Fibre Science and Technology, 14 (3), pp. 319-322.
3. Jang B. Z, (1994). Advanced Polymer composites: Principles and Applications, ASM International.
4. Kuljanin J, Vuckovic M, Comor M. I, Bibic N, Djokovic V and Nedeljkovic J. M, (2002). Influence of CdS-filler on the thermal properties of polystyrene, European Polymer Journal, 38(8), PP. 1659-1662.
5. Weidenfeller B, Höfer M and Schilling F, (2004). Thermal conductivity, thermal diffusivity, and specific heat capacity of particle filled polypropylene, Composites Part A: Applied Science and Manufacturing, 35 (4), pp. 423-429
6. Stolarski T. A, (1990). Tribology in Machine Design, Heiman Newnes, UK.
7. Päivi Kivikytö-Reponen, (2006). Correlation of Material Characteristics and Wear of Powder Metallurgical Metal Matrix Composites, Doctoral Theses in Materials and Earth Sciences, Helsinki University of Technology, Laboratory of Materials Science, Espoo.
8. Budinski K. G, (1998). Surface Engineering for Wear Resistance, Prentice Hall, New Jersey.
9. Robinowicz E, (1965). Friction and wear of materials, John Willey, New York, USA.
10. Thomas H. Kosel, (1992). Solid Particle Erosion, ASM Handbook, ASM International, 18, 199-213. (T.H. Kosel. In: P.J. Blau, Editor, Friction, Lubrication and Wear Technology, ASM Handbook, 18, pp. 207).

11. John M. J and Anandjiwala R. D, (2008). Recent Developments in Chemical Modification and Characterization of Natural Fiber-Reinforced Composites, Polymer Composites, 29(2), pp.187-207.
12. Saheb D. N and Jog J. P, (1999). Natural Fiber Polymer Composites: A Review, Advances in Polymer Technology, 18(4), pp. 351-363.
13. Joseph S, Sreekala M. S, Oommen Z, Koshy P and Thomas S, (2002). A Comparison of Mechanical Properties of Phenol Formaldehyde Composites Reinforced with Banana Fibers and Glass Fibers, Composites Science and Technology, 62(14), pp. 1857-1868.
14. Li Q and Matuana L. M, (2003). Surface of cellulosic materials modified with functionalized polyethylene coupling agents, Journal of Applied Polymer Science, 88 (2) pp. 278–286
15. Lundquist L, Marque B, Hagstrand P. O, Leterrier Y and Manson J. A. E, (2003). Novel pulp fibre reinforced thermoplastic composites, Composites Science and Technology, 63(1), pp. 137-152.
16. Eichhorn S. J, Baillie C. A, Zafeiropoulos N, Mwaikambo L. Y, Ansell M. P, Dufresne A, Entwistle K. M, Herrera-Franco P. J, Escamilla G. C, Groom L, Hughes M, Hill C, Rials T. G and Wild P. M, (2001). Review: Current international research into cellulosic fibres and composites, Journal of Materials Science, 36 (9), pp. 2107-2131.
17. Bledzki A. K and Gassan J, (1999). Composites reinforced with cellulose based fibres, Progress in Polymer Science, 24, pp. 221-274.
18. Mohanty A. K, Khan M. A and Hinrichsen G, (2000). Influence of chemical surface modification on the properties of biodegradable jute fabrics-polyester amide composite, Composites Part A: Applied Science and Manufacturing, 31(2), pp.143-150.
19. Mohanty A. K, Khan M. A and Hinrichsen G, (2000). Surface modification of jute and its influence on performance of biodegradable jute-fabric/Biopol composites, Composites Science and Technology, 60(7), pp.1115-1124.

20. Li X. H, Meng Y. Z, Wang S. J, Rajulu A.V and Tjong S. C, (2004). Completely biodegradable composites of poly (propylene carbonate) and short, lignocellulose fabric hildegardia populifolia, Journal of Polymer Science Part B: Polymer Physics, 42 (4), pp. 666-675.
21. Shibata M, Takachiyo K, Ozawa K, Yosomiya R and Takeishi H, (2002). Biodegradable polyester composites reinforced with short abaca fiber, Journal of Applied Polymer Science, 2002, 85, pp. 129-138.
22. Iannace S, Nocilla G and Nicolais L, (1999). Biocomposites based on sea algae fibers and biodegradable thermoplastic matrices, Journal of Applied Polymer Science, 73, pp. 583-592.
23. Shibata M, Ozawa K, Teramoto N, Yosomiya R and Takeishi H, (2003). Biocomposites made from short abaca fiber and biodegradable polyester, Macromolecular Materials and Engineering, 288, pp. 35-43.
24. Luo S and Netravali A. N, (1999). Interfacial and mechanical properties of environment-friendly 'green' composites made from pineapple fibers and poly (hydyoxybutyrate-co-valerate) resin, Journal of Materials Science, (34): 3709-3719.
25. Rout J, Misra M, Tripathy S. S, Nayak S. K and Mohanty A. K, (2001). The influence of fibre treatment on the performance of coir-polyester composites, Composites Science and Technology, 61(9), pp.1303-1310.
26. Bisanda E. T. N, (2000). The effect of alkali treatment on the adhesion characteristics of sisal fibres, Applies Composite Materials, 7(5-6), pp.331-339.
27. Gassan J and Bledzki A. K, (1999). Possibilities for improving the mechanical properties of jute/epoxy composites by alkali treatment of fibres, Composites Science and Technology, 59(9), pp. 1303-1309.
28. Kozłowskiy R and Władyka-Przybylak M, (2008). Flammability and fire resistance of compositesreinforced by natural fibers, Polymers for Advanced Technologies, 19, pp. 446-453.
29. Kahraman R, Abbasi S and Abu-Sharkh B, (2005). Influence of Epolene G-3003 as a Coupling Agent on the Mechanical Behavior of Palm Fiber-

Polypropylene Composites, International Journal of Polymeric Materials, 54(6), pp. 483-503.

30. Satyanarayana K. G, Sukumaran K, Mukherjee P. S, Pavithran C and Pillai S. G. K, (1990). Natural Fiber-Polymer Composites, Cement and Concrete Composites, 12(2), pp. 117-136.
31. Satyanarayana K. G, Sukumaran K, Kulkarni A. G, Pillai S. G. K and Rohatgi P. K, (1986). Fabrication and Properties of Natural Fiber-Reinforced Polyester Composites, Composites, 17(4), pp. 329-333.
32. Gowda T. M, Naidu A. C. B, and Chhaya R, (1999). Some Mechanical Properties of Untreated Jute Fabric-Reinforced Polyester Composites, Composites Part A: Applied Science and Manufacturing, 30(3), pp. 277-284.
33. Pothan L. A, Oommen Z and Thomas S, (2003). Dynamic Mechanical Analysis of Banana Fiber Reinforced Polyester Composites, Composites Science and Technology, 63(2), pp. 283-293.
34. Corbière-Nicollier T, Laban B. G, Lundquist L, Leterrier Y, Månson J. - A. E and Jolliet O, (2001). Life Cycle Assessment of Biofibers Replacing Glass Fibers as Reinforcement in Plastics, Resources, Conservation and Recycling, 33(4), pp. 267-287.
35. Pothan L. A, Thomas S and Neelakantan N. R, (1997). Short Banana Fiber Reinforced Polyester Composites: Mechanical, Failure and Aging Characteristics, Journal of Reinforced Plastics and Composites, 16(8), pp. 744-765.
36. Joseph K, Thomas S, Pavithran C, (1992). Viscoelastic properties of short-sisal-fiber-filled low-density polyethylene composites: effect of fiber length and orientation, Materials Letters, 15, pp. 224-228.
37. George J, Bhagawan S. S and Thomas S, (1996). Thermogravimetric and dynamic, mechanical thermal analysis of pineapple fibre reinforced polyethylene composites, Journal of Thermal Analysis and Calorimetry, 47(4), pp. 1121-1140.

38. Amash A and Zugenmaier P, (2000). Morphology and properties of isotropic and oriented samples of cellulose fibre-polypropylene composites, Polymer, 41(4), pp.1589-1596.
39. Luo S and Netravali A. N, (1999). Mechanical and thermal properties of environmentally friendly green composites made from pineapple leaf fibres and poly (hydroxybutyrate-co-valerate) resin, Polymer Composites, 20(3), pp. 367-378.
40. Cazaurang-Martinez M. N, Herrera-Franco P. J, Gonzalez-Chi P. I and Aguilar-Vega M, (1991). Physical and mechanical properties of henequen fibers, Journal of Applied Polymer Science, 43(4), pp. 749-756.
41. Karmaker A. C and Schneider J. P, (1996). Mechanical Performance of Short Jute Fiber Reinforced Polypropylene, Journal of Materials Science Letters, 1996, 15(3), pp. 201-202.
42. Srivastav A. K, Behera M. K and Ray B. C, (2007). Loading Rate Sensitivity of Jute/Glass Hybrid Reinforced Epoxy Composites: Effect of Surface Modifications, Journal of Reinforced Plastics and Composites, 26(9), pp. 851-860.
43. Shibata S, Cao Y and Fukumoto I, (2005). Press forming of short natural-fiber reinforced biodegradable resin: effects of fiber volume and length on flexural properties, Polymer Testing, 24(8). pp. 1005-1011.
44. Sapuan S. M, Leenie A, Harimi M and Beng Y. K, (2006). Mechanical properties of woven banana fiber reinforced epoxy composites, Materials and Design, 27(8), pp. 689-693.
45. Chawla K. K and Bastos A. C, (1979), The mechanical properties of jute fibers and polyester/jute composites. In: Proceedings of the third international conference on mechanical behaviour of materials. Cambridge, UK: Pergamon Press, pp. 191-196.
46. Hepworth D. G, Hobson R. N, Bruce D. M and Farrent J. W, (2000). The use of unretted hemp fibre in composite manufacture, Composites Part A: Applied Science and Manufacturing, 31(11), pp. 1279-1283.

47. Harriette L. B, Jorg M and Van den Oever M. J. A, (2006). Mechanical properties of Short-flax-fiber reinforced compounds, Composites Part A: Applied Science and Manufacturing, 37(10), pp. 1591-1604.
48. 51Monteiro S. N, Terrones L. A. H and D'Almeida J. R. M, (2008), Mechanical performance of coir fiber/polyester composites, Polymer Testing, 27(5), pp. 591- 595.
49. Santulli C, (2001). Post-impact damage characterisation on natural fibre reinforced composites using acoustic emission. NDT & E International, 34(8), pp. 531-536.
50. Pavithran C, Mukherjee P. S, Brahmakumar M and Damodaran A. D, (1987) Impact properties of natural fibre composites, Journal of Materials Science Letters, 6(8), pp. 882-884.
51. Tobias B. C, (1993). Tensile and impact behaviour of natural fibre-reinforced composite materials, In Proceedings of Advanced Composites '93: International Conference on Advanced Composite Materials; Wollongong; Australia; 15-19 Feb. 1993. pp. 623-627.
52. Zhang J.Y, Yu T. X, Kim J. K and Sui G. X, (2000). Static indentation and impact behaviour of reformed bamboo/aluminium laminated composites, Composite Structures, 50(2), pp. 207-216.
53. Sharma, Y. M. L, (1980), Bamboo in Asia Pacific Region, In Bamboo Research in Asia G. Lessard and A. Chouiard (Eds.) World Publications, Singapore, pp. 99-120.
54. Zehui J, (Eds.) (2007). Bamboo and Rattan in the World, Beijing: China Forestry Publishing House.
55. Liese, W, (1987) Anatomy and properties of bamboo, In Rao, A.N.; Dhanarajan, G.; Sastry, C.B. ed., Recent Research on Bamboo. Proceedings of the International Bamboo Workshop, Hangzhou, China, 6-14 October 1985, Chinese Academy of Forestry, Beijing, China; International Development Research Centre, Ottawa, Canada, pp. 196-208.

56. Godbole V. S and Lakkad S. C, (1986). Effect of water absorption on the mechanical properties of bamboo, Journal of Materials Science Letters, 5(3), pp. 303-304.
57. Shin, F. G, Xian X. J and Yipp M. W, (1989). Development and Evaluation of Bamboo/Plastic Composites, Proceedings of VII International Conference on Composite Materials (ICCM-VII), 4, pp. 467-474.
58. Shin F. G, Xian X. J and Yipp M. W, (1991). Reinforcements Mechanism in Bamboo/Epoxy Composites, Composite Design, Manufacture and Application, SAMPLE, 1-M-1-10.
59. Xian X. J and Shin F. G, (1989). Evaluation of Mechanical Behaviour and Application of Bamboo Reinforced Plastic Composites, Advances in Mechanics, 19(4), pp. 515-519.
60. Chen X, (1996). Bamboo fiber reinforced polypropylene composites: structure, morphology, and properties, Thesis (M.Phil.), Hong Kong University of Science and Technology.
61. Xian F. G, Zheng W. P and Yipp M. W, (1989). Analysis of the mechanical properties and microstructure of bamboo-epoxy composites, Journal of Materials Science, 24(10), pp. 3483-3490.
62. Jain S, Kumar R and Jindal U. C, (1992). Mechanical behaviour of bamboo and bamboo composite, Journal of Materials Science, 27(17), pp. 4598-4604.
63. Jain S, Jindal U. C and Kumar R, (1993). Development and fracture mechanism of the bamboo/polyester resin composite, Journal of Materials Science Letters, 12(8), pp. 558-560.
64. Li S. H, Fu S. Y, Zhou B. L, Zeng Q. Y and Bao X. R, (1994). Reformed bamboo and reformed bamboo/aluminium composite, Journal of Materials Science, 29(22), pp. 5990-5996.
65. Rajulu A. V, Baksh S. A, Reddy G. R and Chary K. N, (1998). Chemical resistance and tensile properties of short bamboo fiber reinforced epoxy

composites, Journal of Reinforced Plastics and Composites, 17(17), pp. 1507-1511.

66. Chen X, Guo Q, Mi Y, (1998). Bamboo fiber-reinforced polypropylene composites: A study of the mechanical properties, Journal of Applied Polymer Science, 69(10), pp. 1891-1899.
67. Thwe M. M and Liao K, (2002). Effects of environmental aging on the mechanical properties of bamboo-glass fiber reinforced polymer matrix hybrid composites, Composites Part A: Applied Science and Manufacturing, 33(1), pp. 43-52.
68. Okubo K, Fujii T and Yamamoto Y, (2004). Development of bamboo-based polymer composites and their mechanical properties, Composites Part A: Applied Science and Manufacturing, 35(3), pp. 377-383.
69. Ismail H, Edyham M. R and Wirjosentono B, (2002). Bamboo fibre filled natural rubber composites: the effects of filler loading and bonding agent, Polymer Testing, 21(2), pp.139-144.
70. Wu Y and Li Z, (2003). Flexural behavior of bamboo-fibre-reinforced mortar laminates, Cement and Concrete Research, 33, pp. 15-19.
71. Rajulu A. V, Rao B. R, Reddy R. L and Sanjeevi R, (2001). Chemical resistance and tensile properties of epoxy/polycarbonate blend coated bamboo fibres, Journal of Reinforced Plastics and Composites, 20(4), pp. 335-340.
72. Saxena M and Gowri V. S, (2003). Studies on bamboo polymer composites with polyester amide polyol as interfacial agent, Polymer Composites, 24(3), pp. 428-436.
73. Kumar H and Siddaramaiah, (2005). Study of chemical and tensile properties of polyurethane and polyurethane/polyacrylonitrile coated bamboo fibers, Journal of Reinforced Plastics and Composites, 24(2), 209-213.
74. Kumar H, Siddaramaiah and Roopa S, (2005). Chemical and tensile properties of unsaturated polyester and polyacrylonitrile semi-

interpenetrating polymer network coated bamboo fibers, Journal of Reinforced Plastics and Composites, 24(2), 215-218.

75. Das M, Pal A and Chakraborty D, (2006). Effects of mercerization of bamboo strips on mechanical properties of unidirectional bamboo-novolac composites, Journal of Applied Polymer Science, 100(1), pp. 238-244.
76. Das M and Chakraborty D, (2007).Role of mercerization of the bamboo strips on the impact properties and morphology of unidirectional bamboo strips-novolac composites. Polymer Composites, 28(1), pp. 57-60.
77. Mi Y, Chen X and Guo Q, (1997). Bamboo fiber-reinforced polypropylene composites: crystallization and interfacial morphology, Journal of Applied Polymer Science, 64(7), pp. 1267-1273.
78. Das M and Chakraborty D, (2006). Influence of alkali treatment on the fine structure and morphology of bamboo fibers, Journal of Applied Polymer Science, 102(5), pp. 5050-5056.
79. Takagi H and Ichihara Y, (2004). Effect of fiber length on mechanical properties of ‘‘Green” composites using a starch-based resin and short bamboo fibers. JSME International Journal Series A: Solid Mechanics and Material Engineering, 47(4), pp. 551-555.
80. Rao K. M. M and Rao K. M, (2007). Extraction and tensile properties of natural fibers: vakka, date and bamboo, Composite Structures, 77(3), pp. 288-295.
81. Lee S. H and Wang S, (2006). Biodegradable polymers/bamboo fiber biocomposite with biobased coupling agent, Composites Part A: Applied Science and Manufacturing, 37(1), pp. 80-91.
82. Okubo K, Fujii T and Yamashita N, (2005). Improvement of interfacial adhesion in bamboo polymer composite enhanced with microfibrillated cellulose, JSME International Journal Series A: Solid Mechanics and Material Engineering, 48(4), pp. 199-204.

83. Fujii T, Okubo K and Yamashita N, (2004). Development of high performance bamboo composite using micro fibrillated cellulose, In: High performance structures and materials (HPSM) conference, pp. 421-431.
84. Thwe M. M and Liao K, (2003). Durability of bamboo-glass fiber reinforced polymer matrix hybrid composites, Composites Science and Technology, 63(3-4), pp. 375-387.
85. Bashar A. S, Khan M. A and Idriss Ali K. M, (1996). Bamboo-plastic composite with MMA, Polymer-Plastics Technology and Engineering, 35(4), pp. 581-590.
86. Chen H, Miao M and Ding X, (2009). Influence of moisture absorption on the interfacial strength of bamboo/vinyl ester composites, Composites Part A: Applied Science and Manufacturing, 40(12), pp. 2013-2019.
87. Takei T, Hatta H and Taya M, (1991). Thermal Expansion Behavior of Particulate-filled Composites h Single Reinforcing Phase, Materials Science and Engineering, A131, pp. 133-143.
88. Ranganath S, (1997). A Review on Particulate-reinforced titanium matrix composites, Journal of Materials Science, 32(1), pp. 1-16.
89. Sawyer W. G, Freudenberg K. D, Praveen B and Schadler L. S, (2003). A study on the friction and wear behavior of PTFE filled with alumina nanoparticles, Wear, 254(5-6), pp. 573-580.
90. Kim J, Kang P. H and Nho Y.C, (2004). Positive temperature coefficient behavior of polymer composites having a high melting temperature, Journal of Applied Polymer Science, 92(1), pp. 394-401.
91. Nikkeshi S, Kudo M and Masuko T, (1998). Dynamic viscoelastic properties and thermal properties of powder-epoxy resin composites, Journal of Applied Polymer Science, 69(13), pp. 2593-2598.
92. Nielsen L. E and Landel R. F, (1994). Mechanical properties of polymers and composites, 2nd ed. New York: Marcel Dekker, pp.557.
93. Peters S. T, (1998). Handbook of composites. 2nd ed. London: Chapman and Hall, pp. 242-243.

94. Sumita M, Shizuma T, Miyasaka K and Ishikawa K, (1983). Effect of reducible properties of temperature, rate of strain, and filler content on the tensile yield stress of nylon 6 composites filled with ultrafine particles, Journal of Macromolecular Science, Part B, 22(4), pp. 601-618.
95. Bartczak Z, Argon A. S, Cohen R. E and Weinberg M, (1999). Toughness mechanism in semi-crystalline polymer blends: II. High-density polyethylene toughened with calcium carbonate filler particles, Polymer, 40(9), pp. 2347-2365.
96. Radford K. C, (1971). The mechanical properties of an epoxy resin with a second phase dispersion, Journal of Materials Science, 6(10), pp. 1286-1291.
97. Young R. J and Beaumont P. W. R, (1977). Failure of brittle polymers by slow crack growth Part 3 Effect of composition upon the fracture of silica particle-filled epoxy resin composites, Journal of Materials Science, 12(4), pp. 684-692.
98. Kinloch A. J, Maxwell D. L and Young R. J, (1985). The fracture of hybrid particulate composites, Journal of Materials Science, 20(11), pp. 4169-4184.
99. Young R. J, Maxwell D. L and Kinloch A. J, (1986). The deformation of hybrid particulate composites, Journal of Materials Science, 21(2), pp. 380-388.
100. Koh S. W, Kim J. K and Mai Y. W, (1993). Fracture toughness and failure mechanisms in silica-filled epoxy resin composites: effects of temperature and loading rate, Polymer, 34(16), pp. 3446-3455.
101. Cantwell W. J and Moloney A. C, (1994). Fractography and failure mechanisms of polymers and composites, Elesvier, Amsterdam, 233.
102. Imanaka M, Takeuchi Y, Nakamura Y, Nishimura A and Lida T, (2001). Fracture toughness of spherical silica-filled epoxy adhesives, International Journal of Adhesion Adhesives, 21(5), pp. 389-396.
103. Wang H, Bai Y, Liu S, Wu J and Wong C. P, (2002). Combined effects of silica filler and its interface in epoxy resin, Acta Materialia, 50(17), pp. 4369-4377.
104. Yamamoto I, Higashihara T and Kobayashi T, (2003). Effect of silica-particle characteristics on impact/usual fatigue properties and evaluation

of mechanical characteristics of silica-particle epoxy resins, JSME International Journal-Series A: Solid Mechanics and Material Engineering, 46 (2), pp. 145-153.

105. Nakamura Y, Yamaguchi M, Kitayama A, Okubo M and Matsumoto T, (1991). Effect of particle size on fracture toughness of epoxy resin filled with angular-shaped silica, Polymer, 32(12), pp. 2221-2229.
106. Nakamura Y, Yamaguchi M, Okubo M and Matsumoto T, (1991). Effect of particle size on impact properties of epoxy resin filled with angular shaped silica particles, Polymer, 32(16), pp. 2976-2979.
107. Nakamura Y, Yamaguchi M, Okubo M and Matsumoto T, (1992). Effects of particle size on mechanical and impact properties of epoxy resin filled with spherical silica, Journal of Applied Polymer Science, 45(7), pp. 1281-1289.
108. Pukanszky B and Voros G, (1993). Mechanism of interfacial interactions in particulate filled composite, Composite Interfaces,1(5), pp. 411-427.
109. Nicolais L and Nicodemo L, (1974). The Effect of particles shape on tensile properties of glassy thermoplastic composites, International Journal of Polymeric Materials, 3(3), pp. 229-243.
110. Patnaik A, Satapathy A, Mahapatra S. S and Dash R. R, (2009). A Comparative Study on Different Ceramic Fillers affecting Mechanical Properties of Glass-Polyester Composites, Journal of Reinforced Plastics and Composites, 28 (11), 1305-1318.
111. Biswas A. K and Davenport W. G, (2002). Extractive metallurgy of copper, Pergamon Press, pp. 518.
112. Collins R. J and Ciesielski S. K, (1994). In: Recycling and use of waste materials and by-products in highway construction national cooperative highway research program synthesis of highway practice, no. 199.
113. Ayano T and Sakata K, (2000). Durability of concrete with copper slag fine aggregate. In: Proceedings of the fifth CANMET/ACI international conference on durability of concrete, SP-192, pp. 141-158.

114. Behnood A, (2005). Effects of high temperatures on high-strength concrete incorporating copper slag aggregates. In: Proceedings of seventh international symposium on high-performance concrete, SP-228-66, pp. 1063-1075.
115. Moura W, Masuero A, Dal Molin D and Vilela A, (1999). Concrete performance with admixtures of electrical steel slag and copper concerning mechanical properties. In: Proceedings of the 2nd CANMET/ACI international conference on high-performance concrete, SP-186, pp. 81-100.
116. Taeb A and Faghihi S, (2002). Utilization of copper slag in the cement industry. ZKGInternational, 55(4), pp.98-100.
117. Al-Jabri K. S, Taha R and Al-Ghassani M, (2002). Use of copper slag and cement by-pass dust as cementitious materials, cement. Concrete and Aggregates, 24(1), pp. 7-12.
118. Shi C and Qian J, (2000). High performance cementing materials from industrial slags-a review, Resources, Conservation and Recycling, 29, pp. 195-207.
119. Gorai B, Jana, R. K and Premchand M, (2003). Characteristics and utilization of copper slag-a review, Resources, Conservation and Recycling, 39, 299-313.
120. Shi C, Meyer C and Behnood A, (2008). Utilization of copper slag in cement and concrete Resources, Conservation and Recycling, 52, 1115-1120
121. Patel M., Padhi B. K, Vidyasagar P, Pattnaik A. K, (1992). Extraction of titanium dioxide and production of building bricks from red mud, Research and Industry, 37**(**3), pp. 154-157.
122. Pera J, Boumaza R and Ambroise J, (1997). Development of a pozzolanic pigment from red mud, Cement Concrete Research, 27(10), 1513-1522.

123. Summers R. N, Guise N. R and Smirk D. D, (1993). Bauxite residue (Red Mud) increases phosphorus retention in sandy soil catchments in Western Australia Fertilizer Research, 34(1), pp. 85-94.
124. Yalcin N and Sevinc V, (2000). Utilization of bauxite waste in ceramic glass, Ceramics International, 26(5), pp. 485-493.
125. Balasubramanian G, Nimje M. T and Kutumbarao V. V, (2000). Conversion of aluminium industry wastes into glass-ceramic products, Fourth International Symposium on Recycleing of Metals & Engineered Materials, Warrendale, USA, pp.1223-1228.
126. Mahata T, Sharma B. P, Nair S. R and Prakash D, (2000) Formation of aluminium titanatemullite composite from bauxite red mud, Material and Mat. Trans. B, 318, pp. 551 – 553.
127. Banvolgyi G and Siklosi P, (1998). The improved low temperature digestion (ILTD) process: an economic and environmentally sustainable way of processing gibbsitic bauxites, Light Metals, pp. 45-53.
128. Kovalenko E. P, (1998). Improvement of the process of alumina production at Nilolaev alumina plant, Light Metals, pp. 55-58.
129. Satapathy A, Mishra S. C, Ananthapadmanabhan P.V and Sreekumar K. P, (2007). Development of Ceramic Coatings using Red Mud : A Solid Waste of Alumina Plants, Journal of Solid Waste Technology and Management, 33(2), pp. 48-53.
130. Thakur R. S and Das S. N, (1994). Red mud-Analysis and utilization, Publication and Information Directorate, New Delhi: New Delhi and Wiley Eastern Limited, India.
131. Almen J. O, (1950). Surface deterioration of gear teeth. In: J.T. Burwell, Jr., Editor, Mechanical Wear, American Society for Metals, Metals Park, Ohio, pp. 229-288.
132. Organisation for Economic Co-operation and Development**,** Glossary of Terms and Definitions in the Field of Friction**,** Wear and Lubrication**,** Research Group on Wear of Engineering Materials of the European OECD**,** Paris**,** p. 53 (1969).

133. Standard terminology relating to wear and erosion, standard G-40-01, American Society for Testing and Materials, 2001.
134. Finnie I, (1995). Some reflections on the past and future of erosion, Wear, 1, 186/187, pp. 1-10.
135. Meng H. C and Ludema K. C, (1995). Wear models and predictive equations: their form and content, Wear, 181-183, pp. 443-457.
136. Thai C. M, Tsuda K and Hojo H, (1981). Erosion behaviour of polystyrene, Journal of Testing and Evaluation, 9, pp. 359-365.
137. Walley S. M, Field J. E and Yennadhiou P, (1984). Single solid particle impact erosion damage on polypropylene, Wear, 100(1-3), pp. 263-280.
138. Friedrich K, (1986). Erosive wear of polymer surfaces by steel ball blasting, Journal of Materials Science, 21(9), pp. 3317-3332.
139. Rajesh J. J, Bijwe J, Tewari U. S and Venkataraman B, Erosive wear of various polyamides, Wear, 249(8), pp. 702-714.
140. Walley S. M and Field J. E, (1987). The erosion and deformation of polyethylene by solid particle impact, Philosophical Transactions, The Royal Society, London, A 321(1558), pp. 277-303.
141. Wang Y. Q, Huang L. P, Liu W. L and Li J, (1998). The blast erosion behavior of ultrahigh molecular weight polyethylene, Wear, 218(1), pp. 128-133.
142. Walley S. M, Field J. E and Greengrass M, (1987). An impact and erosion study of polyetheretherketone, Wear, 114(1), pp. 59-72.
143. Rao P. V and Buckley D. H, (1986). Angular particle impingement studies of thermoplastic materials at normal incidence, Tribology Transactions, 29(3), pp. 283-298.
144. Tilly G. P and Sage W, (1970). The interaction of particle and material behaviour in erosion process, Wear, 16(6), PP. 447-465.
145. Brandsta¨dter A, Goretta K.C, Routbort J. L, Groppi D. P and Karasek K. R, (1991). Solid particle erosion of bismileimide polymers, Wear, 147(1), pp. 155-164.

146. Hutchings I. M, Deuchar D. W. T and Muhr A. H, (1987). Erosion of unfilled elastomers by solid particle impact, Journal of Materials Science, 22(11), pp. 407-4076.
147. Li J and Hutchings I. M, (1990). Resistance of cast polyurethane elastomers to solid particle erosion, Wear, 135(2), pp. 293-303.
148. Besztercey G, Karger-Kocsis J and Szaplonczay P, (1999). Solid particle erosion of electrically insulating silicone and EPDM rubber compounds, Polymer Bulletin, 42(6), pp. 717-724.
149. Barkoula N. M and Karger-Kocsis J, (2002). Review-processes and influencing parameters of the solid particle erosion of polymers and their composites, Journal of Materials Science, 37(18), pp. 3807-3820.
150. Miyazaki N and Takeda N, (1993). Solid Particle erosion of fiber reinforced plastics, Journal of Composite Materials, 27(1), pp. 21-31.
151. Miyazaki N and Hamao T, (1994). Solid particle erosion of thermoplastic resins reinforced by short fibers, Journal of Composite Materials, 28 (9), pp. 871-883.
152. Harsha A. P, Tewari U. S and Venkataraman B, (2003). Solid particle erosion behaviour of various polyaryletherketone composites, Wear, 254(7-8), pp. 693-712.
153. Barkoula N. M and Karger-Kocsis J, (2002). Effects of fiber content and relative fiber-orientation on the solid particle erosion of GF/PP composites, Wear, 252(1-2), pp. 80-87.
154. Tewari U. S, Harsha A. P, Ha¨ger A. M and Friedrich K, (2003). Solid particle erosion of carbon fiber and glass fiber-epoxy composites, Composites Science and Technology, 63(3), pp. 549-557.
155. Arjula S and Harsha A. P, (2006), Study of erosion efficiency of polymers and polymer composites, Polymer Testing, 25(2), pp. 188-196.
156. Patnaik A, Satapathy A, Mahapatra S. S and Dash R. R, (2008). A Taguchi Approach for Investigation of Erosion of Glass Fiber-Polyester

Composites, Journal of Reinforced Plastics and Composites, 27(8), pp. 871-888.

157. Patnaik A, Satapathy A, Mahapatra S. S and Dash R. R, (2008). Parametric Optimization of Erosion Wear of Polyester-GF-Alumina Hybrid Composites using Taguchi Method, Journal of Reinforced Plastics and Composites, 27(10), pp. 1039-1058.
158. Patnaik A, Satapathy A, Mahapatra S. S and Dash R. R, (2008). Implementation of Taguchi Design for Erosion of Fiber Reinforced Polyester Composite Systems with SiC Filler, Journal of Reinforced Plastics and Composites, 27(10), pp. 1093-1111.
159. Patnaik A, Satapathy A, Mahapatra S. S and Dash R. R, (2008). A Modeling Approach for Prediction of Erosion Behaviour of Glass Fiber-Polyester Composites, Journal of Polymer Research, 15(2), pp. 147-160.
160. Patnaik A, Satapathy A, Mahapatra S. S and Dash R. R, (2009). Tribo-Performance of Polyester Hybrid Composites: Damage Assessment and Parameter Optimization using Taguchi Design, Materials and Design, 30(1), pp. 57-67.
161. Tewari U.S, Harsha A.P, Häger A.M and Friedrich K, (2002). Solid particle erosion of unidirectional carbon fibre reinforced polyetheretherketone composites, Wear, 252, pp. 992–1000.
162. Harsha A.P, Tewari U. S and Venkatraman B, (2003). Solid particle erosion behaviour of various polyaryletherketone composites, Wear, 254, pp.693–712.
163. Hoff S.M, (1995). Applying Advanced Materials to Turboshaft Engines, Aerospace Engg, 15(2), pp. 27–30.
164. Zhou R, Lu D.H, Jiang Y.H and Q.N. Li, (2005). Mechanical properties and erosion wear resistance of polyurethane matrix composites, Wear, 259, pp. 676–683.
165. Tsuda K, (2006). Masatoshi Kubouchi, Tetsuya Sakai, Asep Handaya Saputra, Nobuo Mitomo, General method for predicting the sand erosion rate of GFRP, Wear, 260, pp.1045–1052.

166. Miyazaki N, (2007). Solid Particle Erosion Behavior of FRPs with Prior Impact Damage, Journal of Composite Materials, 41, pp. 703-712.
167. Srivastava V.K, Pawar A.G, (2006). Solid particle erosion of glass fibre reinforced flyash filled epoxy resin composites, Composites Science and Technology, 66, pp. 3021–3028.
168. Ivosevic M, Knight R, Kalidindi S.R, Palmese G.R and Sutter J.K, (2006). Solid particle erosion resistance of thermally sprayed functionally graded coatings for polymer matrix composites, Surface & Coatings Technology, 200, pp.5145– 5151.
169. Sınmazcelik T and Taskıran I, (2007). Erosive wear behaviour of polyphenylenesulphide (PPS) composites, Materials and Design, 28, pp. 2471–2477.
170. Yang N and Nayeb-Hashemi H, (2007). The Effect of Solid Particle Erosion on the Mechanical Properties and Fatigue Life of Fiber-reinforced Composites, Journal of Composite Materials, 41, pp. 559-574.
171. Rattan R and Bijwe J, (2007). Influence of impingement angle on solid particle erosion of carbon fabric reinforced polyetherimide composite, Wear, 262, pp. 568–574.
172. George K. Drensky, Experimental Investigation of Composite Material, Erosion Characteristics under Conditions Encountered in Turbofan Engines.Doctor of Philosophy, M.S. University of Cincinnati, Cincinnati, Ohio – 2002.
173. Sarı N and Sınmazcelik T, (2007). Erosive wear behaviour of carbon fibre/polyetherimide composites under low particle speed, Materials and Design, 28, pp.351–355.
174. Harsha A.P and Thakre A.A, (2007). Investigation on solid particle erosion behaviour of polyetherimide and its composites, Wear, 262, pp.807–818.

175. Sinmazcelik T, Fidan S and Günay V, (2008). Residual mechanical properties of carbon/polyphenylenesulphide composites after solid particle erosion, Materials and Design, 29, pp.1419–1426.
176. Arjula S, Harsha A. P and Ghosh M. K, (2008). Erosive wear of unidirectional carbon fibre reinforced polyetherimide composite, Materials letters, 62, pp. 3246–3249.
177. Yang N.H, Nayeb-Hashemi H and Vaziri A., (2008). Non-destructive evaluation of erosion damage on E-glass/epoxy composites, Composites: Part A, 39, pp. 56–66.
178. Harsha A.P and Jha S.K, (2008). Erosive wear studies of epoxy-based composites at normal incidence, Wear, 265, pp.1129–1135.
179. Rabinowicz E, (1979). The wear equation for erosion of metals by abrasive particles, Department of ME, MIT.
180. Finnie I., (1958). The mechanism of erosion of ductile metals, In: Proceedings of 3rd US national congress of applied mechanics, American Society of Mechanical Engineers, 527-532.
181. Nesic S, (1991). Computation of localized erosion-corrosion in disturbed two-phase flow, PhD thesis, University of Saskatchewan, Saskatoon, Canada.
182. Bitter J. G. A, (1963). A study of erosion phenomena part 1, Wear, 6(1), pp. 5-21.
183. Bitter J. G. A, (1963). A study of erosion phenomena part II, Wear, 6(3), pp. 169-190.
184. Laitone J.A., (1979). Erosion prediction near a stagnation point resulting from aerodynamically entrained solid particles, Journal of Aircraft, 16(12), pp. 809-814.
185. Salama M. M and Venkatesh E. S, (1983). Evaluation of erosion velocity limitations of offshore gas wells, 15th Annual OTC. Houston, TX: May 2-5, OTC no. 4485.
186. Bourgoyne A.T, (1989). Experimental study of erosion in diverter systems due to sand production, SPE/IADC Drilling Conference, 28

February-3 March 1989, New Orleans, Louisiana, SPE/IADC 18716, pp. 807-816.

187. Chase D. P, Rybicki E. F and Shadley J. R, (1992). A model for the effect of velocity on erosion of N80 steel tubing due to the normal impingement of solid particles, Journal of Energy Resources Technology, 114(1), pp. 54-64.
188. Mc Laury B. S, (1993). A model to predict solid particle erosion in oil field geometries. MS thesis, The University of Tulsa.
189. Svedeman S. J and Arnold K. E, (1994). Criteria for sizing Multiphase flow lines for erosive/corrosive services, SPE Production & Facilities, 9(1), pp. 74-80.
190. Jordan K. G, (1998). Erosion in multiphase production of oil and gas, CORROSION 98, March 22 - 27, San Diego Ca.
191. Shirazi S. A and McLaury B. S, (2000). Erosion modeling of elbows in multiphase flow, In: Proceedings of 2000 ASME fluids engineering summer meeting, June 11-15, Boston, MA: Paper no. FEDSM2000-11251.
192. Gomes-Ferreira C, Ciampini D and Papini M, (2004). The effect of inter-particle collisions in erosive streams on the distribution of energy flux incident to a flat surface, Tribology International, 37(10), pp. 791-807.
193. Papini M, Ciampini D, Krajac T and Spelt J. K, (2003). Computer modelling of interference effects in erosion testing: effect of plume shape, Wear, 255(1-6), pp. 85-97.
194. Gorham D. A, Kharaz A. H, (2000). The measurement of particle rebound characteristics, Powder Technology, 112(3), pp. 193-202.
195. Wu C, Li L and Thornton C, (2003). Rebound behaviour of spheres for plastic impacts, International Journal of Impact Engineering, 28, pp. 929-946.

196. Karaz A. H and Gorham D. A, (2000). A study of the restitution coefficient in elastic-plastic impact, Philosophical Magazine Letters, 80(8), pp. 549-559.
197. Molinari J. F and Ortiz M, (2002). A study of solid-particle erosion of metallic targets, International Journal of Impact Engineering, 27(4), pp. 347-358.
198. Kleis I and Hussainova I, (1999). Investigation of particle-wall impact process, Wear, 233-235, pp.168-173.
199. Hutchings I. M, Winter R. E and Field J. E, (1976). Solid particle erosion of metals: the removal of surface material by spherical projectiles, Proceedings of the Royal Society of London A, 348, pp. 379-392.
200. Sundararajan G and Shewmon P. G, (1987). The oblique impact of a hard ball against ductile, semi-infinite, target materials-experiment and analysis, International Journal of Impact Engineering, 6(1), pp. 3-22.
201. Tirupataiah Y, Venkataraman B and Sundararajan G, (1990). The nature of the elastic rebound of a hard ball impacting on ductile, metallic target materials, Materials Science and Engineering: A, 124(2), pp. 133-140.
202. Sundararajan G, (1991). The depth of the plastic deformation beneath eroded surfaces: the influence of impact angle and velocity, particle shape and material properties, Wear, 149(1-2), pp.129-153.
203. Hutchings I .M, (1981). A model for the erosion of metals by spherical particles at normal incidence, Wear, 70(3), pp. 269-281.
204. Gachon Y, Vannes A. B and Farges G, (1998). Study of sand particle erosion of magnetron sputtered multilayer coatings, in: Proceedings of the International Conference on Erosive and Abrasive Wear (ICEAW); 9th International Conference on Erosion by Liquid and Solid Impact (ELSI IX), Cambridge, UK.
205. Shimizu K, Noguchi T and Seitoh H, (1998). FEM analysis of the dependency on impact angle during erosive wear, in: Proceedings of the International Conference on Erosive and Abrasive Wear (ICEAW); 9th

International Conference on Erosion by Liquid and Solid Impact (ELSI IX), Cambridge, UK.

206. Tomassone M. S, Sokoloff J. B and Widom A., (1997). Dominance of phonon friction for a xenon film on a silver (111) surface, Physical Review Letters, 79(24), pp. 4798-4801.
207. Gumbsch P and Cannon R. M, (2000). Atomic aspects of brittle fracture, MRS Bulletin, 25, pp.15-20.
208. Zhong W and Tománek D, (1990). First-principles theory of atomic-scale friction, Physical Review Letters, 64 (25), pp. 3054-3057.
209. Li D.Y, Elalem K, Anderson M. J and Chiovelli S, (1999). A microscale dynamical model for wear simulation, Wear, 225-229 (1), pp. 380-386.
210. Elalem K, Li D.Y, Anderson M. J and Chiovelli S, (2001). Modeling of abrasive wear of homogenous and heterogeneous materials, hydraulic failure analysis: fluids, components and system effects, ASTM, STP, 1339, Totten G. E, Wills D. K and Feldmann D, Eds., American Society for Testing and Materials, West Conshohocken, PA.
211. Chen Q and Li D. Y, (2003). Computer simulation of solid particle erosion, Wear, 254(3-4), pp. 203-210.
212. Ratner S. N, Farberoua I. I, Radyukeuich O. V and Lure E. G, (1967). Correlation between wear resistance of plastics and other mechanical properties, in: D.I. James (Ed.), Abrasion of Rubber, MacLaren, London, pp.145-154.
213. Lancaster J. K., Friction and wear, (1972) in A. D. Jenkins (ed.), Polymer Science: A Materials Science Handbook, 2, North-Holland, London, pp. 959-1046.
214. Velten K, Reinicke R and Friedrich K, (2000). Wear volume prediction with artificial neural networks, Tribology International, 33(10), pp. 731-736.
215. Zhang Z, Friedrich K and Velten K, (2002). Prediction on tribological properties of short fiber composites is using artificial neural networks, Wear, 252(7-8), 668-675.

216. Zhang Z and Friedrich K, (2003). Artificial neural network applied to polymer composites: a review, Composites Science and Technology, 63(14), pp. 2029-2044.
217. Fernandez J. E, Fernandez M. D. R, Diaz R. V and Navarro R. T, (2003). Abrasive wear analysis using factorial experiment design, Wear, 255(1-6), pp. 38-43.
218. Spuzic S, Zec M, Abhary K, Ghomashchi R and Reid I, (1997). Fractional design of experiments applied to a wear simulation, Wear, 212, pp. 131-139.
219. Prasad B. K, (2002). Abrasive wear characteristics of a zinc-based alloy and zinc-alloy/SiC composite, Wear, 252(3-4), pp. 250-263.
220. Deuis R. L, Subramanian C and Yellup J. M, (1998). Three-body abrasive wear of composite coatings in dry and wet environments, Wear, 214(1), pp.112-130.
221. Banerjee A, Prasad S. V, Surappa M. K and Rohatgi P. K, (1982). Abrasive Wear of Cast Aluminum Alloy/Zircon Particle Composites, Wear, 82, pp. 141-151.
222. Mondal D. P, Das S, Jha A. K and Yegnesswaran A. H, (1998). Abrasive wear of Al alloy-Al_2O_3 particle composite: a study on the combined effect of load and size of abrasive, Wear, 223(1-2), pp. 131-138.
223. Taguchi G, Konishi S., (1987).Taguchi Methods: Orthogonal Arrays and Linear Graphs: Tools for Quality Engineering, American Supplier Institute Inc., Dearborn, MI.
224. Taguchi G, (1986). Introduction to Quality Engineering, White Plains, NY: Asian Productivity Organization, UNIPUB.
225. Phadke M. S, (1989). Quality Engineering using Robust Design, Prentice-Hall, Englewood Cliffs, NJ.
226. Wu Y and Moore W. H, (1986). Quality Engineering: Product & Process Design Optimization, American Supplier Institute Inc., Dearborn, MI.

227. Logothetis N. and Haigh A, (1987). The Statistical Flexibility of Taguchi Method in the Optimization of Multi-response Processes, Profess. Statist. 6(7), pp. 10-16.
228. Logothetis N and Haigh A, (1988). Characterizing and optimizing multi-response processes by the Taguchi method, Quality and Reliability Engineering International, 4(2), pp. 159-169.
229. Shoemaker A. C and Kackar R. N, (1988). A methodology for planning experiments in robust product and process design, Quality and Reliability Engineering International, 4(2), pp. 95-103.
230. Phadke M. S and Dehnad K, (1988). Optimization of Product and Process Design for Quality and Cost, Quality and Reliability Engineering International, 4(2), pp. 105-112.
231. Barbero Ever J, (1999), Introduction to Composite Materials Design, Taylor & Francis, Philadelphia, PA.
232. Ahmad M and Kamke F. A, (2005). Analysis of Calcutta bamboo for structural composite materials: physical and mechanical properties, Wood Science and Technology, 39(6), pp. 448-459.
233. Mahapatra B. K, Rao M. B. S, Rao R. B and Paul A. K, (2000). Characteristics of Red Mud Generated at NALCO Refinery, Damanjodi, India, Light Metals, pp. 161-165.
234. Gorai B, Jana R. K and Premchand (2003). Characteristics and utilisation of copper slag: a review, Resources, Conservation and Recycling, 39(4), pp. 299-313.
235. Aglan H. A and Chenock Jr T. A, (1993). Erosion damage features of polyimide thermoset composites. SAMPEQ, pp. 41-47.
236. Fu S. Y and Lauke B, (1998). Characterization of tensile behavior of hybrid short glass fiber/ calcite particles/ABS composites, Composites Part A: Applied Science and Manufacturing, 29(5-6), pp. 575-583.
237. Thomason J. L, Vlug M. A, Schipper G and Krikor H. G. L. T, (1996). Influence of fibre length and concentration on the properties of glass fibre reinforced polypropylene: Part 3. Strength and strain at failure,

Composites Part A: Applied Science and Manufacturing, 27(11), pp.1075-1084.

238. Gassan J and Cutowski V. S (2000). Effect of corona discharge and UV treatment on the properties of jute-fiber epoxy composites, Composites Science and Technology, 60(15), pp. 2857-1863.
239. Mishra P K, (1997). Nonconventional Machining, Narosa Publishing House, New Delhi.
240. Sundararajan G, Roy M and Venkataraman B, (1990). Erosion Efficiency- A New parameter to Characterize the Dominant Erosion Micro-mechanism, Wear, 140(2), pp. 369-381.
241. Ruff A. W and Ives L. K, (1975). Measurement of solid particle velocity in erosive wear, Wear 1975, 35 (1), pp.195-199.
242. Montgomery D. C, (2005). Design and Analysis of Experiments, Fifth Ed. John Wiley & Sons, Inc. pp. 363-382.
243. Roy M, Vishwanathan B and Sundararajan G, (1994). Solid particle erosion of polymer matrix composites, Wear, 171(1-2), pp. 149-161.

******

Appendix - A1

List of Publications from the Present Research Work

International Journals

1. **Sandhyarani Biswas** and Alok Satapathy, 2009, "Tribo-performance analysis of red mud filled glass-epoxy composites using Taguchi experimental design", Materials and Design, 30 (8), 2841-2853.
2. **Sandhyarani Biswas** and Alok Satapathy, "Use of copper slag in glass-epoxy composites for improved wear resistance" Waste Management and Research, 28 (7), 2010, pp. 615-625.
3. **Sandhyarani Biswas** and Alok Satapathy, "Erosion Wear Analysis of SiC Filled Glass-Epoxy Composites using Taguchi Technique", International Polymer Processing, 1, 2010, pp. 23-33.
4. **Sandhyarani Biswas** and Alok Satapathy, "A Review on Natural Fiber Composites and their Erosion Wear Characteristics" Journal of Reinforced Plastics and Composites, DOI: 10.1177/0731684409348348.
5. **Sandhyarani Biswas** and Alok Satapathy, 2010 "A Comparative Study on Erosion Characteristics of Red Mud Filled Bamboo-Epoxy and Glass-Epoxy Composites" Materials and Design, 31 (4), 1752-1767.
6. **Sandhyarani Biswas** and Alok Satapathy, "An Assessment of Erosion Wear Response of SiC Filled Epoxy Composites Reinforced with Glass and Bamboo Fibers" International Polymer Processing, 15 (3), 2010, pp. 205-222.
7. **Sandhyarani Biswas** and Alok Satapathy, "A Study on Tribological Behaviour of Alumina Filled Glass-Epoxy Composites using Taguchi Experimental Design" Tribology Transactions, 53, 2010, pp. 520-532.
8. **Sandhyarani Biswas,** Alok Satapathy and Amar Patnaik, (2010). Effect of Ceramic Fillers on Mechanical Properties of Bamboo Fiber Reinforced Epoxy Composites: A Comparative Study, Advanced Materials Research, 123-125, pp. 1031-1034.
9. **Sandhyarani Biswas**, Alok Satapathy and Amar Patnaik, 2009 "Erosion Wear Behaviour of Polymer Composites: A Review", Journal of Reinforced Plastics and Composites, DOI: 10.1177/0731684408097786.

10. **Sandhyarani Biswas**, Alok Satapathy and Amar Patnaik, "Effect of Ceramic Fillers on Mechanical Properties of GF Reinforced Epoxy Composites: A Comparative Study", Journal of Reinforced Plastics and Composites, DOI: 10.1177/0731684409352113.
11. Amar Patnaik, Alok Satapathy, Navin Chand, N.M. Barkoula and **Sandhyarani Biswas**, 2010, "Solid Particle Erosion Wear Characteristics of Fiber and Particulate Filled Polymer Composites: A Review", Wear, 268 (1-2), pp. 249-263.

Seminars/Conferences

1. **Sandhyarani Biswas** and Alok Satapathy, "Analysis of Erosion Wear Behavior of Red Mud Filled Glass-Epoxy Hybrid Composites Using Taguchi Method" National Conference on Mechanism Science and Technology: from Theory to Application, Nov. 13-14, 2008, National Institute of Technology, Hamirpur.
2. Alok Satapathy and **Sandhyarani Biswas**, "Parametric Appraisal and Damage Assessment during Erosion of Glass-Epoxy-Alumina hybrid composites", Seventh AIMS International Conference on Technology and Business Management, March 28-31, 2009, Dubai.
3. **Sandhyarani Biswas**, Alok Satapathy and Amar Patnaik, "Solid Particle Erosion Characteristics of SiC Filled Glass Fiber Reinforced Epoxy based Hybrid Composites", The Fourth Asian Particle Technology Symposium (APT 2009), September 14-16, 2009, New Delhi.
4. **Sandhyarani Biswas**, Alok Satapathy and Amar Patnaik, "Erosion Wear Behaviour of Bamboo Fiber Reinforced Composites Filled with Red mud Particulate" Polymer Congress APA-2009 on Polymer Science and Technology: Vision and Scenario, December 17-20, 2009, New Delhi, India.
5. **Sandhyarani Biswas** and Alok Satapathy "A Comparative Study on Erosion Wear Behavior of Copper Slag Filled Bamboo-Epoxy and Glass-Epoxy Composites" International Conference on Advancements in Polymeric Materials APM-2010, Trends & Technology, Feb. 20-22, 2010, CIPET, Bhubaneswar.
6. **Sandhyarani Biswas**, Alok Satapathy and Amar Patnaik, Effect of Impingement Angle and Erodent Temperature on Erosion Behaviour of Bamboo Fiber Reinforced Epoxy Composites, 3rd National Symposium for Materials Research Scholars (MR-10), 7-8 May 2010, IIT Mumbai.

******

Appendix - A2

Brief Bio-Data of the Author

The author, **Sandhyarani Biswas**, born on 19-03-1981 graduated in Manufacturing Science and Engineering from University College of Engineering, Burla in the year 2004. She did her postgraduate study in Mechanical Engineering with specialization in Production Engg. at the National Institute of Technology (NIT), Rourkela. Immediately after the completion of M.Tech. in 2006, she joined NIT, Rourkela as a Faculty in the Department of Mechanical Engineering.

The author has been engaged in active research in the field of composite materials and tribology for the last couple of years. She has 20 research papers to her credit which have been published in various national and international journals of repute. She has also presented 18 research papers related to composites and optimization techniques at various national and international conferences held in India and abroad.

She has been selected to receive financial support for her proposed research project under *SERC Fast Track Scheme for Young Scientist* by the Department of Science and Technology (DST), Govt. of India in 2009. She is also the recipient of *Orissa Young Scientists Award* for the year 2009 by the Orissa Bigyan Academy.

At present, she is working as Assistant Professor in the Department of Mechanical Engineering at the National Institute of Technology, Rourkela, Orissa, India.

******